PREPARED FOR
GULF OIL CHEMICALS COMPANY

A NUMERICALLY BASED DESIGN PROCEDURE FOR BURIED HIGH-DENSITY POLYETHYLENE PROFILE-WALL PIPES BURIED IN FINE-GRAINED IN-SITU SOILS

RESEARCH PROJECT RF 48800

a report

from the Texas A&M
RESEARCH FOUNDATION
College Station, Texas

SEPTEMBER 1984

TEXAS TRANSPORTATION INSTITUTE
THE TEXAS A&M UNIVERSITY SYSTEM
COLLEGE STATION, TEXAS

A REPORT
PREPARED FOR
GULF OIL CHEMICALS COMPANY

A NUMERICALLY BASED DESIGN PROCEDURE FOR BURIED HIGH-DENSITY POLYETHYLENE PROFILE-WALL PIPES BURIED IN FINE-GRAINED IN-SITU SOILS

RESEARCH PROJECT RF 48800

SEPTEMBER 1984

TEXAS TRANSPORTATION INSTITUTE
THE TEXAS A&M UNIVERSITY SYSTEM
COLLEGE STATION, TEXAS

A NUMERICALLY BASED DESIGN PROCEDURE FOR BURIED HIGH-DENSITY POLYETHYLENE PROFILE-WALL PIPES BURIED IN FINE-GRAINED IN-SITU SOILS

Prepared for

Gulf Oil Chemicals Company

by

F. A. Brown and R. L. Lytton

Texas Transportation Institute
Texas A&M University System
College Station, Texas

Texas A&M Research Foundation Project RF 48800

"Investigation of Large-Diameter Polyethylene Pipes
Under Backfill and Service Loads - Phase II"

September 1984

ABSTRACT

The bilinear stress-strain law developed by Katona (1,2) in the CANDE finite element program was expanded to incorporate yield behavior for a pipe cross-section that is not symmetrical about its neutral axis. An additional subroutine for nonsymmetric high density polyethylene pipe was added to the CANDE program. The new pipe model was used in conjunction with an existing hyperbolic stress-strain curve soil model to analyze the effects of trench width, in-situ soil type, depth of water table, pipe size, and depth of cover. A full factorial analysis was adopted in order to record pipe stress, displacement, and strain levels for each possible combination of the different variables. Pipe stiffness and backfill type were also analyzed and incorporated into the data base created from the full factorial analysis.

The reductions in soil and pipe strength with time were analyzed using the well-known viscoelastic power law formulation (3,4,5). This allowed the prediction of pipe stress, displacement, and strain levels for different design times. A ten-year period was used in the full factorial analysis; however, other time periods were also analyzed.

Output from the CANDE program was used to create a regression data base containing pipe stress, displacement, and strain levels associated with the combinations of design parameters. Regression analysis was used to find the best-fit equations for elastic pipe-wall

strain, deflection, and post-yield pipe-wall strain. The resulting design equations provide the engineer with a modern way to analyze and design flexible plastic pipes which incorporate all of the controlling design parameters. Predictions from the regression equations were verified with independent CANDE runs and with full scale test data. The close correlation between deflection predictions from the design equations and the time dependent full scale test data provides additional support for the overall model used in this study and verifies the assumptions which were made concerning soil and pipe creep behavior.

Interpretation of the results of the primary study combined with the additional parameter studies provides several significant conclusions. The ideal backfill configuration is one in which the pipe is completely surrounded by coarse-grained material for a distance of approximately 0.25 diameters. Live load does not appreciably affect pipe performance if a minimum of one foot of cover above the pipe is used. The buckling failure mode does not control in dry soil applications; however, buckling should be checked with empirical equations when a high water table is expected. Pipe strain was generally found to be the controlling criterion for the elastic design of polyethylene profile-wall pipe.

TABLE OF CONTENTS

TABLE OF CONTENTS (Cont'd)

TABLE OF CONTENTS (Cont'd)

LIST OF TABLES

LIST OF FIGURES

LIST OF FIGURES (Cont'd)

LIST OF FIGURES (Cont'd)

LIST OF FIGURES (Cont'd)

LIST OF FIGURES (Cont'd)

LIST OF FIGURES (Cont'd)

LIST OF FIGURES (Cont'd)

INTRODUCTION

In current practice, engineers commonly use overly conservative design procedures in order to insure safe designs. Most of the design methods currently being used by engineers to analyze buried conduits are either based on a limited amount of test data or derived from an elastic solution. These procedures, which often lead to erroneous conclusions, require high factors of safety.

Trying to analyze a soil-structure interaction problem with simple linear elastic theory can often produce large errors since real soils exhibit high degrees of nonlinearity and stress dependency. This fact has led many researchers into the use of full scale testing procedures when developing or updating design procedures. This approach has, however, lost some of its appeal in today's competitive economical environment. Testing the effect of just one additional design parameter requires a substantial budget, and developing a complete design procedure for a new pipe material from full scale tests is financially impossible. This study is an attempt to update the design of flexible high-density polyethylene profile-wall pipe buried in fine-grained soils with present state-of-the-art soil-structure interaction theory.

The widespread use of flexible plastic pipe as a buried conduit has been fostered by its excellent performance in a variety of soil conditions. In an attempt to explain the mechanics behind this performance, the soil-structure interaction of buried flexible pipes

was investigated and appropriate design equations were formulated.

When attempting to design a buried flexible pipe, it is essential to represent its actual performance, taking into account all of the governing parameters. The plastic pipes used today have smaller stiffnesses and much different material properties than those associated with the early types of rigid pipe. As lower stiffnesses of pipes are used, the strength and load-carrying properties of the soil surrounding the pipe become more important. In order to predict the response of these very flexible pipes, one must accurately model the nonlinear, time-dependent properties of the pipe and the surrounding soil, as well as the interaction at the pipe-soil interface. The complex material properties of soils, the nonlinear and nonsymmetric pipe cross sections found in many flexible pipes, and the complex boundary conditions encountered in this soil-structure interaction problem can be accurately modeled using the finite element method.

The finite element program used in this analysis was CANDE (1, 2) developed by M. G. Katona and modified for the purposes of this investigation. CANDE was chosen from available programs because of its automatic mesh generator, its various soil and pipe models, and an overall structure designed for easy modification and additions.

Additions were made to the existing CANDE program. The incremental plane-strain program was extended so that the nonlinear behavior of nonsymmetric pipe cross sections, found in many of the large diameter flexible pipes on the market, could be analyzed accurately. The basic nonlinear pipe model used by Katona was

expanded so that the plane-strain beam elements used to model the pipe can represent post-yield behavior for a cross section not symmetric about its neutral axis.

The modified CANDE program was then used to create a complete factorial data set in terms of several important design parameters: trench width, depth of water table, pipe size, in-situ soil type, and depth of cover. A nonlinear stress-strain model of soil behavior that was already in the program, after Duncan (2,6), was used in all runs together with a subroutine designed to model high-density polyethylene material with a nonsymmetric cross section. Regression analysis was then used to find the best-fit equations for maximum pipe strain and pipe deflection in terms of the basic design parameters used in the finite element runs. Alternate studies were also conducted in order to determine the effects of some of the additional design parameters which were held constant in the basic factorial analysis. The regression equations were also updated to encompass a wider range of application with some additional runs outside the bounds of the original factorial analysis.

The resulting design equations were programmed on a small hand-held calculator to facilitate their use. The necessary parameters for input into the design equations were summarized and tabulated in terms of easily accessible soil and pipe properties. The resulting design procedure was verified with additional computer runs and available full-scale test data.

RELATED BACKGROUND MATERIAL

The problems associated with the safe and economical design of underground conduits have been challenging man since he first began using buried pipe. Although pipeline structures may be one of the earliest examples of the practice of the engineering arts, only in the past few decades has it been possible to design conduits with a greater degree of rationality.

TRADITIONAL METHODS

Most of the design procedures which are being used today can be traced back to the pioneering work done at Iowa State University by Marston and Spangler during the first part of this century (7,8). The Marston-Spangler method is basically comprised of an estimate of the effective vertical load acting on the conduit and of an assumed pressure distribution around the pipe. The effective load transmitted to the pipe is taken as the weight of the trench-fill soil above the pipe plus or minus the shearing resistance along the sides of the trench wall. The sign and magnitude of this shearing resistance is dependent on the relative stiffness between the soil and the pipe.

If the pipe has a stiffness smaller than that of the surrounding soil (Flexible Pipe Concept), the soil above the pipe is partially supported by the shearing resistance along the trench wall. The low stiffness of the conduit induces a settling of the soil above the

pipe. This downward motion of the fill material relative to the trench wall mobilizes an upward shear force which helps to support the pipe.

If the conduit is stiffer than the surrounding soil (Rigid Pipe Concept), the reverse is true. The stiffer zone around the rigid pipe may actually produce the shear forces between the trench wall and the backfill material that push down on the pipe. According to the Marston Arching Theory, the load on stiff pipe may, in fact, be larger than the weight of the soil prism above it.

Rigid pipe design is generally based on the so called D-load test (1). The D-load test is a standard procedure (ASTM-C-497-65T) in which the unrestrained load capacity of a concrete pipe is measured. The American Concrete Pipe Association uses a procedure in which the Marston-Spangler approach is used to determine an equivalent D-load on the pipe. The pipe is then sized by finding the cross section which will safely handle this equivalent D-load.

For flexible pipe design, the Marston-Spangler approach is also used to predict the expected deflections of the conduit. In later work done by Spangler and Watkins (9), they re-examined the original Iowa formula and offered some improved methods for classifying soil stiffness.

In the 1960's, wall crust strength and elastic buckling were investigated. White and Lager (10) proposed treatment of the flexible conduit as a compression ring. They assumed that the wall thrust load is equal to the weight of the soil prism above the pipe. If the pipe-wall area is large enough to carry this load, a safe

design results.

Many theories and formulas have been derived for buried cylinders in an elastic confining medium with an assumed hydrostatic loading. These approaches were very well summarized by Leonards and Stetkar (11).

Although these original design equations have been modified, no major design advances have been made in pipe design since these general concepts were introduced. The problem with these traditional design approaches arises from their representation of the interaction between the soil and the pipe. The pipe is typically analyzed using loads determined from some semi-empirical load distributions which ignore the fact that the soil and pipe deform as a continuous body.

Although these formulas have been made conservative for rigid pipes by using empirical coefficients derived through experience, they are often very inaccurate when trying to analyze the newer flexible conduits. When analyzing the newer, more flexible pipe material, such as high density polyethylene, it is extremely important to analyze the conduit as a soil-pipe system and to accurately model the shear and stress transfer between the soil and the pipe.

In our competitive age, the engineer must use the most advanced technique available in order to insure a safe, yet economical, design. Instead of analyzing the arching found around a buried pipe simply as a shear force on the trench walls, we must determine an accurate stress distribution around the pipe and the effects of these loads on pipe performance.

For years, structural engineers have used a principle known

simply as "moment distribution" to analyze the fact that the stiffest member carries the majority of the load, yet in pipe design, where the same laws of physics apply, engineers use approximately the same equations to analyze a "rigid" concrete pipe or a very "flexible" polyethylene pipe. It is a most opportune time to update our design procedures using the advanced engineering knowledge of today.

PIPE DEFINITIONS AND BEHAVIOR

Although most design methods view the pipe as a plane-strain cylinder, in reality culverts are three-dimensional structures. The plane-strain assumption is very applicable to most culvert applications; however, it is important to emphasize the limitations associated with this assumption. Plane-strain models the pipe installation as a long prismatic configuration with no changes in the pipe-soil cross-section or the load distribution along the length of the pipe.

Most installation of pipe does not completely conform to this idealized configuration. However, by designing for the most severe conditions along the pipe, an adequate design results since the plane-strain assumption is conservative with respect to in-plane response. Non-uniform loads along the length of the pipe can cause longitudinal bending. This effect is minimized, however, by the corrugation found on most flexible pipe. Properly designed joints between the pipe segments can also minimize the moment transfer between adjoining pipes and reduce the distress due to differential settlement.

Since the majority of the load on a buried pipe is due to the dead load of the soil above it, the loading pattern is usually quite uniform, thus producing a plane-strain problem. Shallow-buried pipes, can also be analyzed with the plane-strain assumption by converting the given live loads to equivalent plane-strain load. In summary, the plane-strain approximation leads to an accurate analysis for most pipe installations. If extreme non-uniform loads exist, a three-dimensional or a simple beam on an elastic foundation analysis should be used in order to check the out-of-plane loads.

Although the buried conduit system is a definite soil-structure interaction problem, it is worthwhile to review some basic pipe definitions and the structural behavior of a pipe when it is loaded independently of the soil system. Figure 1 illustrates the different portions of the plane-strain pipe model and some of the different cross sections commonly used for buried conduits.

The pipe cross sections A-A shown in Figure 1 are some of the typical types presently being used by the pipe industry. The elastic design of these cross sections can be described by four section properties:

E = Young's Elastic Modulus

μ = Poisson's Ratio

I = Moment of inertia of the pipe wall per longitudinal unit length

A = Thrust area of the pipe wall per longitudinal unit length

The basic concepts controlling the structural behavior of an unconfined pipe, as outlined by Katona (1), can be illustrated by

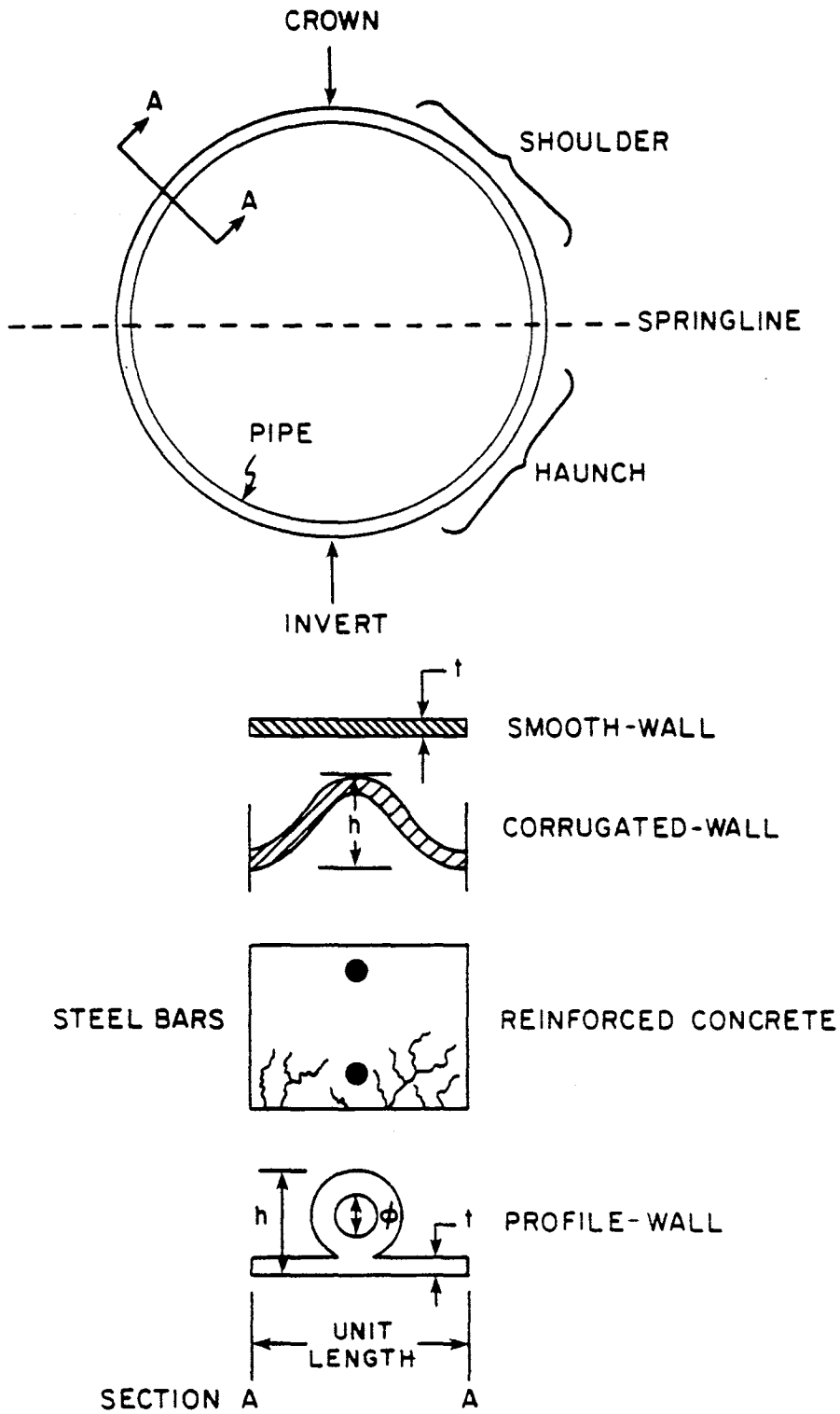

FIGURE 1. Pipe Definitions and Wall Types

considering two extreme load distributions, hydrostatic and concentrated (see Figure 2). For the hydrostatic case, only thrust load exists, no bending moment is produced, and the pipe deforms uniformly in the radial direction. The concentrated loading produces bending moment, thrust, and shear forces in the pipe wall and the deformation pattern is an oval shape. The equations for calculating the magnitudes of the loads and the deflections can be found in Roak (12).

Figure 2 illustrates the necessity of accurately predicting the load distribution around the pipe. For the hydrostatic case the load is evenly distributed through the cross section and the thrust area is fully utilized with a uniform compressive stress. The bending moments and deformations associated with the concentrated loading produce large tensile stresses in the outer fibers of the cross section. This tensile stress can cause premature failure if the pipe is constructed of a brittle material such as concrete.

In order to achieve an accurate, safe design without developing a costly rule-of-thumb design procedure through years of experience, it is clearly necessary to use modern techniques to analyze the soil-structure interaction problem. One of the modern alternatives available which permits an accurate representation of both the loading distributions around the conduit and the continuous deformation of the soil and the pipe together is the finite element method.

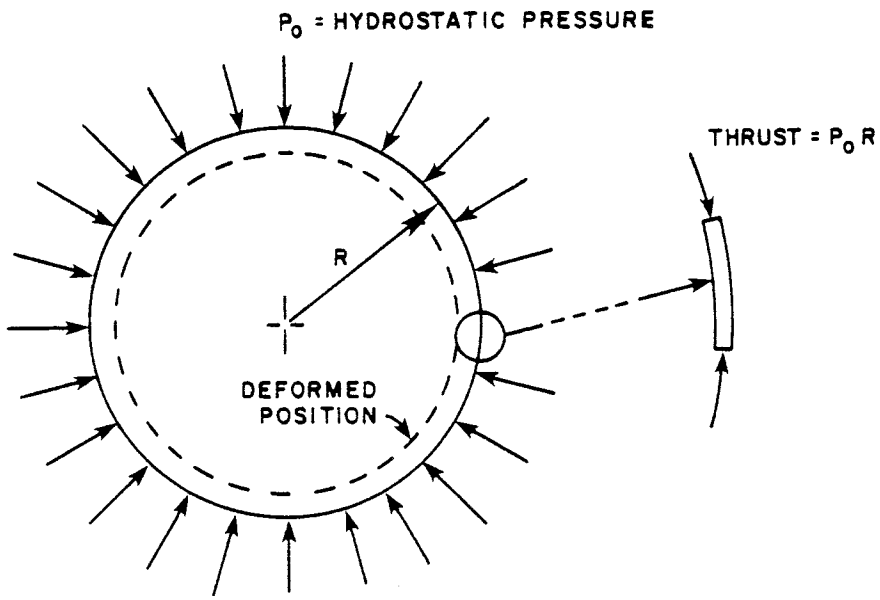

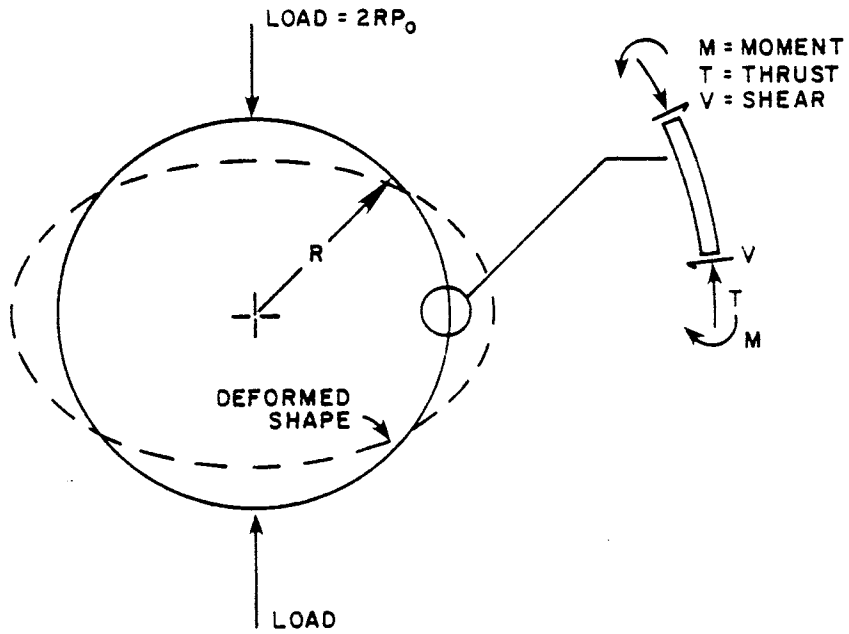

FIGURE 2. Concentrated Loading and Response After Katona (1)

COMPARISON OF AVAILABLE FINITE ELEMENT PROGRAMS

Several different finite element programs have been developed to analyze soil-structure interaction problems. Two of these programs, Culvert ANalysis and DEsign (CANDE) and Soil-STructure Interaction Program (SSTIPN), were selected for further review because of their immediate availability and direct application to the buried conduit problem. In order to make a selection of the appropriate program for the given flexible pipe analysis, it is necessary to outline the solution procedures and modeling options of each program.

SSTIPN Program

SSTIPN uses an incremental finite element method to calculate stresses and strains in the soil elements, displacements at the nodes and internal forces, and displacements in the structural element. Before these calculations can be made, the material properties within the elemental stiffness matrix must be defined for each material in the system.

The Duncan soil model, which is used in SSTIPN to characterize the nonlinear soil behavior, is probably the best model available today (1,6,13,14). The nonlinear nature of the stress-strain curve implies that the modulus of the soil varies with the state of strain in the soil. An iterative solution is used to converge on the correct modulus for each load increment. One of the weaknesses in the SSTIPN solution procedure is that no convergence check is made after each load step. Only two iterations are performed to approximate the

correct modulus for the calculated stress state during the load step. This can lead to large amounts of error if highly nonlinear soil properties are modeled or if the load steps are large.

The pipe model used in SSTIPN to characterize the pipe behavior assumes simple pipe geometry and linear elastic material properties. This greatly restricts the modeling capabilities of the program since no post-yield pipe behavior can be modeled. Using SSTIPN, it is not possible to investigate flexible pipe performance at high strain levels near failure or to even model small amounts of yielding in the outermost zones of the pipe cross section.

In order to account for the slippage and load transfer along the soil-conduit interface, SSTIPN also has an optional interface element. These elements, which have no physical size, model the load transfer capabilities on the interface using a set of shear and normal springs. The magnitude of the shear spring can be altered to model different amounts of interface friction.

For each analysis a complete set of soil properties must be obtained from previous investigations or hand calculated from triaxial soil test data. A finite element mesh must be constructed for each problem that is to be analyzed and labeled for use in the input data. The inability to generate its own finite element mesh makes this program very cumbersome to use when several different problems must be analyzed. The live loads, both symmetric and unsymmetric, acting on the system must be transformed to equivalent plane-strain loads. These loads can then be applied to the mesh at the appropriate points and load steps. When the above data is input into a data deck in the

proper form, a finite element analysis can be made and a solution is obtained.

CANDE Program

Unlike SSTIPN, CANDE was designed to use a variety of soil and pipe models. In fact, M. G. Katona, the author of CANDE, had the foresight to realize that new and better models would be developed. He therefore designed his program to be easily modified or expanded to incorporate new ideas. The program also has different solution levels which enables the user to bypass many of the time-consuming tasks normally associated with finite element analysis (see Table 1).

Level 1 Solution. Level 1 provides an elastic solution for a buried conduit system. This solution level is relatively simple and requires small amounts of computer time. It can be used for parametric studies such as interface slip, plastic hinging, etc; or to avoid convergence problems encountered when using nonlinear properties. However, soil seldom, if ever, behaves as a homogenous linear elastic material. Therefore, a more sophisticated model should be used whenever possible.

Level 2 Solution. Level 2 provides an automated finite element mesh generation and contains a variety of soil and pipe models. In addition to the Duncan soil model, CANDE has three other soil models which can be used in the finite element solution: the linear soil model, the overburden pressure dependent model, and the Extended

TABLE 1. Capabilities and Limitations of CANDE Solution Levels

Characteristics	Level 1 (Elasticity)	Level 2 (Finite Element With Auto Mesh)	Level 3 (Finite Element With User Mesh)
Pipe shapes	Round	Round; vertical ellipse horizontal ellipse; other[a]	Any open or closed pipe section
Soil zones	Homogenous throughout	In-situ; backfill; bedding; packing; other[a]	Up to ten different soil may be defined
Stress-strain models for soil zones	Linear; overburden dependent	Linear; overburden dependent; fully non-linear	Linear; overburden dependent; fully non-linear
Installation type represented	Embankment	Embankment; trench; other[a]	User defined configuration
Symmetry conditions	Double symmetry about vertical and horizontal axis	Symmetric about vertical axis	Arbitrary boundary conditions and symmetry
Load representations of soil	Incremented overburden	Incremented overburden; gravity load construction increments (5)	Incremented overburden; gravity load construction lifts; up to 10 max
Load representation of live loads	Equivalent overburden	Equivalent overburden; strip loading[a]	Equivalent overburden; strip loading
Pipe-soil interface	Slip; no slip	Slip; no slip; friction; separation	Slip; no slip; friction; separation[b]
Number of input cards[c]	5 to 10	6 to 11	50 to 500

[a]Level 2 is provided with a "porthole" that allows selective modifications and inputs to canned mesh.
[b]Interface model for Level 3 also applies to soil-soil interfaces.
[c]Computer execution time is typically 10 to 20 times longer for Levels 2 and 3 than for Level 1.

After Katona (1)

Hardin model.

The linear soil model, which assumes the soil behaves as an elastic medium, has many of the same limitations as the Level 1 closed form elastic solution. However, due to the nature of finite element modeling, each element can be assigned different elastic properties. This ability enables the user to create a system that more closely models the behavior of real soils by, for example, increasing the soil stiffness with depth.

The overburden pressure dependent model makes full use of the ability to assign different material properties to different elements within the finite element system. As each layer is applied in the incremental construction of the trench, the material properties of the layers are changed. This capability allows the soil to stiffen with increasing normal pressure.

The Extended-Hardin model uses a hyperbolic representation of the stress-strain characteristics of the soil which is similar to the Duncan model. The parameters needed to represent the soil properties must be determined from laboratory test data through curve fitting. Although this model has been verified with full scale tests, it has not been used extensively over as wide a range of soil types as has the Duncan model (6,14).

The Duncan soil model used in CANDE is an improved version of the one used in SSTIPN. Instead of making only two iterations at each load step to converge on the appropriate modulus, CANDE iterates until a user-specified tolerance is reached. This greatly improves the reliability of the results. A more complete description of the Duncan

soil model is given in the next section.

One strong point of the level two option is the automatic mesh generator. The program constructs a symmetric, efficient finite element mesh from the simple trench configuration input. This ability omits the time-consuming task of manually constructing a mesh for each analysis. This also greatly reduces the amount of input required (see Table 1). The level two option can be used to analyze most culvert installations, including trench and embankment conditions.

Level 3 Solution. Level 3 is a more general finite element solution scheme which requires the user to input the mesh geometry. It can be used to handle the problems which are beyond the capabilities of Level 2. Unsymmetric loading or peculiar trench geometry are examples of Level 3 applications.

Other Options. CANDE has an extensive pipe library which can be used to model most types of thin walled and corrugated pipes. There are separate subroutines within the program which model corrugated steel, corrugated aluminum, reinforced concrete and brittle plastic pipes. There is a design option within each of these subroutines which actually determines the most economical pipe size for the given soil types and trench geometry. This option is not applicable to all pipe materials. The CANDE code also has a typical set of hyperbolic parameters for standard soils (see Table 2). This also minimizes the amount of input necessary to make a finite element analysis. Hyperbolic parameters for other specific soils are available in the

TABLE 2. Standard Hyperbolic Parameters

Unified Classification	RC Stand. AASHTO	γ_m kip/ft^3	ϕ_o deg	$\Delta\phi$ deg	C kip ft^2	K	n	R_f	K_b	m
Coarse Aggregates										
GW, GP	105	0.150	42	9	0	600	0.4	0.7	175	0.2
SW, SP	95	0.140	36	5	0	300	0.4	0.7	75	0.2
	90	0.135	33	3	0	200	0.4	0.7	50	0.2
Silty Sand										
SM	100	0.135	36	8	0	600	0.25	0.7	450	0.0
	90	0.125	32	4	0	300	0.25	0.7	250	0.0
	85	0.120	30	2	0	150	0.25	0.7	150	0.0
Silty Clayey Sand										
SM-SC	100	0.135	33	0	0.5	400	0.6	0.7	200	0.5
	90	0.125	33	0	0.3	150	0.6	0.7	75	0.5
	85	0.120	33	0	0.2	100	0.6	0.7	50	0.5
Silty Clay										
CL	100	0.135	30	0	0.4	150	0.45	0.7	140	0.2
	90	0.125	30	0	0.2	90	0.45	0.7	80	0.2
	85	0.120	30	0	0.1	60	0.45	0.7	50	0.2

RC = Relative compaction
γ_m = Weight density

After Katona (1)

literature (6,13).

Interface behavior in CANDE is modeled by the Method of Constraints. Each interface element has a 6x6 element stiffness matrix which controls the strength of the interface in the normal and tangential direction. For a given load increment, the correct interface stiffness is determined by a trial-and-error process. This method of handling interface behavior has been shown to yield more realistic answers than the normal and shear spring concept used in SSTIPN (2,14).

Application to High-Density Polyethylene Profile-Wall Pipe.

Both programs, CANDE (1,2,11,13,15) and SSTIPN (6,11), have been verified by full-scale test data. The Duncan hyperbolic soil model is contained in both programs; however, CANDE uses an updated model. The simple elastic pipe model used in SSTIPN is inadequate when investigating the polyethylene profile-wall pipe. Linear elastic theory only allows investigation of pipe performances for stress levels below the yield value. This limitation neglects the high ductility and large strain capacity of the polyethylene material. The hollow reinforcing ribs, which are continuously wound around the thin-walled pipe shaft, give the profile-wall pipe a unique cross section (see Figure 3). Approximating this pipe-wall section with the thin walled or corrugated pipe models currently available with CANDE or SSTIPN would mean neglecting the added strength of the Spirolite design. Assuming that the Spirolite cross section is symmetric would also introduce large errors in the calculated bending stresses.

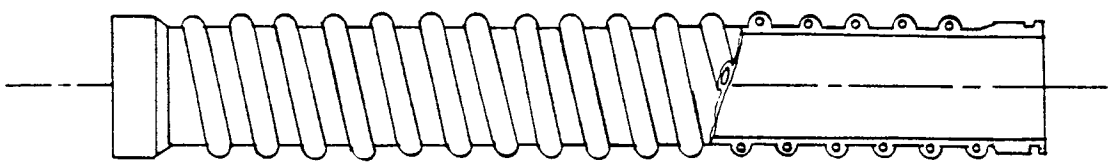

FIGURE 3. Profile-Wall Pipe With Nonsymmetric Cross-Section

The nonlinear pipe model in CANDE can, however, be modified to take into account the efficient hollow rib design. The bilinear approximation available with CANDE is capable of predicting the post-yield behavior of the polyethylene material. This permits engineers to fully utilize the strain capacity of the ductile material.

The Level 2 option in CANDE is a great time-saver for the user. With the large number of analyses required within this project, this is an especially important advantage.

One additional advantage to CANDE is that it computes factors of safety against wall crushing, excess deflection, and elastic buckling after each load step. This information, along with the standard stress, strain, and deflection information, fully describes the pipe response at each load step.

For these reasons, CANDE is the best program to use for this project.

THE DUNCAN SOIL MODEL

The majority of the computer analysis done in this project uses the Duncan Soil model developed by Duncan (6) and modified by Katona (2). This model was used since it produces a reasonable approximation of the nonlinear and stress dependent stress-strain behavior exhibited by most soil types. The general theory behind this numerical approach is outlined below in order to clarify later equations which are derived from this basic model.

Hyperbolic Stress-Strain Curves

The nonlinear properties of soils can be modeled by a hyperbolic stress-strain curve. Kondner and his coworkers (16,17) have shown that a simple hyperbolic curve (see Figure 4) can reasonably approximate the stress-strain behavior for most soils. This hyperbola can be represented by the following equation:

$$(\sigma_1-\sigma_3) = \frac{\varepsilon}{a + b\varepsilon} \tag{1}$$

where

σ_1 = major principal stress,

σ_3 = minor principal stress, and

ε = axial strain.

The soil constants a and b found in Equation (1) have physical significances. For a constant confining pressure, σ_3 = constant, a and b can be described as:

$$a = 1/E_i \tag{2}$$

$$b = 1/(\sigma_1-\sigma_3)_{ult} \tag{3}$$

where

E_i = the initial tangent modulus or the initial slope of the stress-strain curve and

$(\sigma_1-\sigma_3)_{ult}$ = the asymptotic value of the stress difference.

The values of a and b can easily be determined from a given stress-strain curve. The hyperbolic plot can be transformed, as shown in Figure 4, to produce a linear relationship between $\varepsilon/(\sigma_1-\sigma_3)$ and ε. A best-fit straight line can be used on the transformed plot to

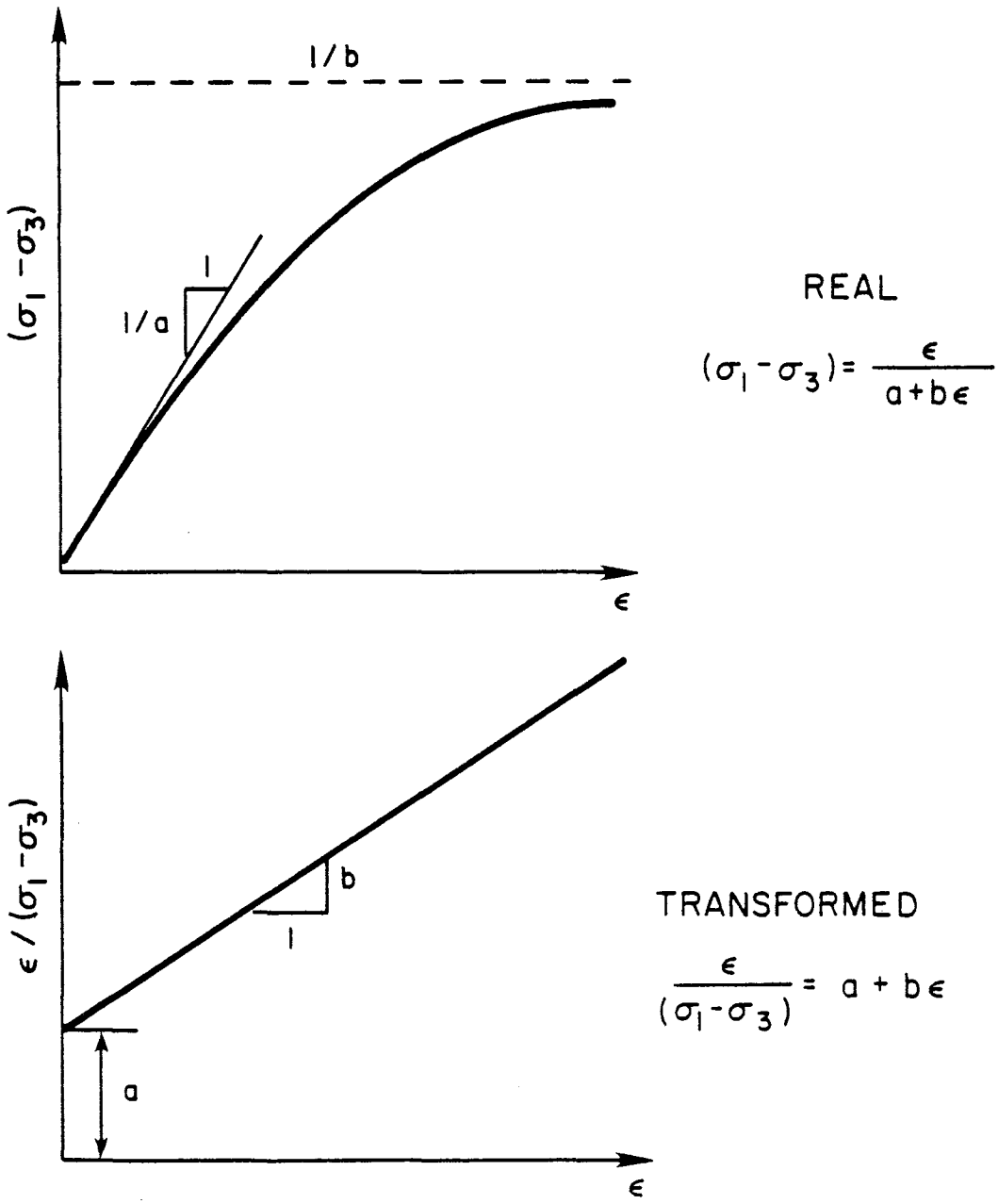

FIGURE 4. Hyperbolic Representation of a Stress-Strain Curve

estimate a and b.

Stress Dependency

All soils, except fully saturated soils tested under unconsolidated-undrained conditions, exhibit a steeper stress-strain curve (E_i) and a higher strength $(\sigma_1-\sigma_3)_f$ when the confining pressure is increased. To account for this fact, empirical equations have been established. The relation between E_i and confining pressure, σ_3, is of the following form:

$$E_i = Kp_a \left(\frac{\sigma_3}{p_a}\right)^n \tag{4}$$

where

K = modulus number

n = modulus exponent

p_a = atmospheric pressure

Both K and n are dimensionless numbers; therefore, they are valid in any set of units. To change from one system of units to another, you only need to change the units of p_a.

The variation of $(\sigma_1-\sigma_3)_{ult}$ with confining pressure is accounted for by first relating $(\sigma_1-\sigma_3)_{ult}$ to the compressive strength at failure, $(\sigma_1-\sigma_3)_f$:

$$(\sigma_1-\sigma_3)_f = R_f(\sigma_1-\sigma_3)_{ult} \tag{5}$$

where R_f is the failure ratio. Since the actual stress difference

at failure, $(\sigma_1-\sigma_3)_f$, is always smaller than the asymptotic value, $(\sigma_1-\sigma_3)_f$, the value of R_f varies between 0.5 and 0.9 for most soils.

The familiar Mohr-Coulomb strength relationship is used to estimate $(\sigma_1-\sigma_3)_f$ for a given σ_3. This relationship is shown graphically in Figure 5 and is expressed below:

$$(\sigma_1-\sigma_3)_f = \frac{2c \cos \phi + 2\ \sigma_3 \sin \phi}{(1 - \sin \phi)} \tag{6}$$

where

c = the cohesion intercept and

ϕ = the friction angle.

Tangent Modulus

The instantaneous slope for a given stress-strain curve is the tangent modulus, E_t. The expression for E_t can be derived by differentiating Equation (1) with respect to ε and making the necessary substitutions for a and b:

$$E_t = [1 - \frac{R_f\ (1-\sin \phi)(\sigma_1-\sigma_3)}{2c \cos \phi + 2\ \sigma_3 \sin \phi}]^2\ Kp_a\ (\frac{\sigma_3}{p_a})^N \tag{7}$$

This equation is used in the incremental approach to approximate

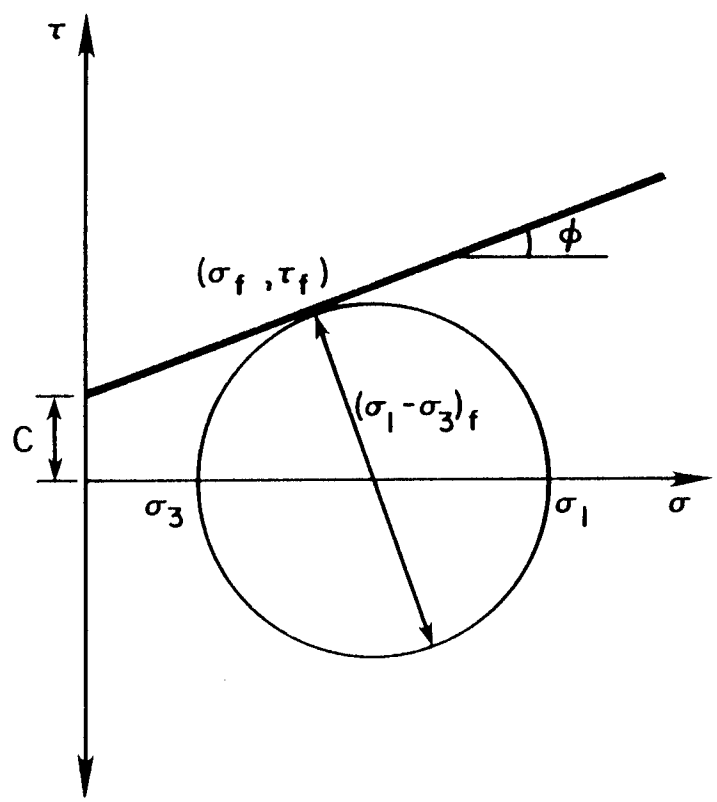

$$(\sigma_1 - \sigma_3)_f = \frac{2C \cos\phi + 2\sigma_3 \sin\phi}{1 - \sin\phi}$$

$$(\sigma_1 - \sigma_3)_f = R_f \, (\sigma_1 - \sigma_3)_{ult}$$

FIGURE 5. Mohr-Coulomb Failure Diagram

the elastic modulus of the soil elements. The load is applied in a series of steps so that the hyperbolic stress-strain curve can be modeled with a series of straight lines. The slope of the straight line during the load increment is found with an iterative solution technique. A value for E_t is estimated at the beginning of the load step and is used in the standard elastic stiffness matrix to generate a set of stress levels at the end of the load step. Equation 7 is then used to calculate a new E_t. If the calculated E_t is the same as the estimated value, convergence has been obtained and the next load step is applied. However, if the ratio of the estimated value to the calculated value is above a prescribed limit, a new value is estimated and another solution obtained.

Two elastic parameters are required to specify the material properties for an elastic solution. The second incrementally-elastic property, the bulk modulus of the soil, can also be modeled with a hyperbolic curve. Although this is a justifiable approach, it is not as widely accepted as the hyperbolic tangent modulus approach. Since the nonlinear bulk modulus approach requires more soils tests and because of the uncertainties with modeling certain fine-grained soils, a constant Poisson's ratio approach is sometimes adopted.

THE NONLINEAR PIPE MODEL

The modifications made to the CANDE program are based upon the general theory developed by Katona, which represents the basic bilinear approximation of a pipe beam element (1). An outline of that theory is presented here as an introduction to the modifications that were made.

KATONA'S BILINEAR SYMMETRIC BEAM ELEMENT

A general incremental stress-strain law can be written as:

$$\Delta\sigma = E'(\varepsilon)\Delta\varepsilon \tag{8}$$

and is shown graphically in Figure 6.

where

$$E'(\varepsilon) = E_e\,[1-\alpha(\varepsilon)] \tag{9}$$

$\alpha(\varepsilon)$ = dimensionless function of strain

$$= 1 - E'/E_e \tag{10}$$

$\Delta\sigma$ = increment of stress (circumferential)

$\Delta\varepsilon$ = increment of strain (circumferential)

$E'(\varepsilon)$ = tangent modulus

E_e = initial linear modulus

Since the tangent modulus $E'(\varepsilon)$ of each pipe element used for any load step during the incremental analysis is dependent on the strain level, an iteration procedure must be used to arrive at the proper

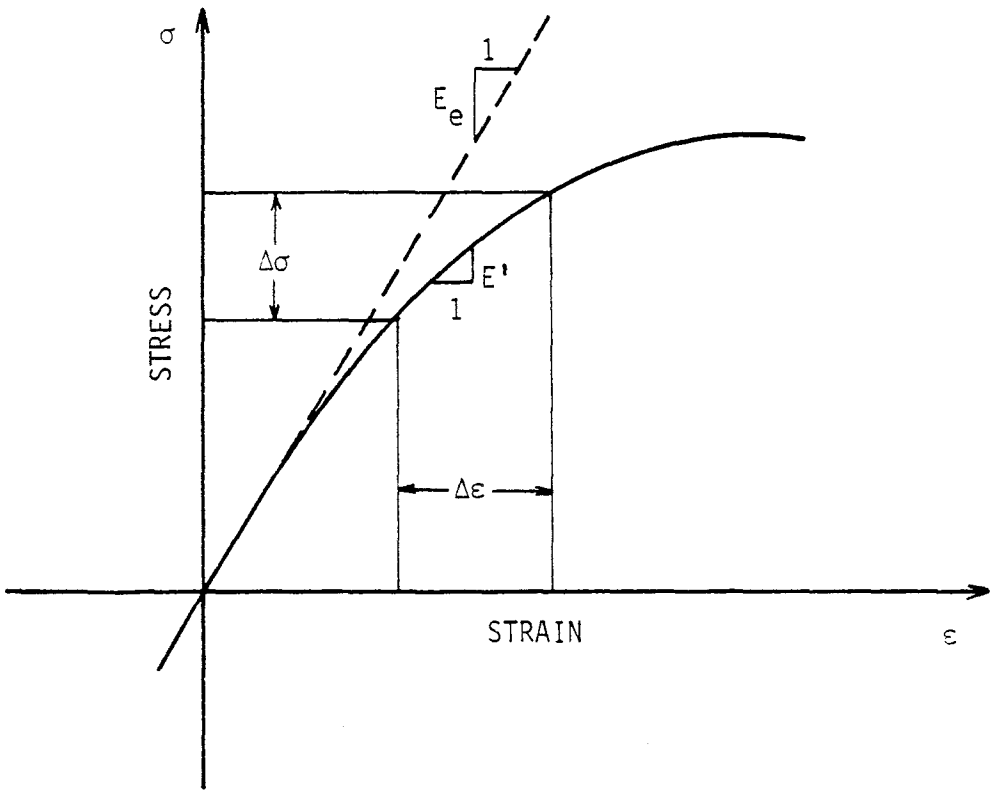

FIGURE 6. General Nonlinear Stress-Strain Curve
After Katona (1)

$E'(\varepsilon)$.

Three basic assumptions were made by Katona when establishing his nonlinear pipe model:

1) Circumferential strains are linear throughout the pipe wall section and can be decomposed into a constant thrust (ε_n) and flexural contribution (ε_m), as illustrated in Figure 7.

$$\varepsilon(y) = \varepsilon_n + \varepsilon_m(y) \tag{11}$$

where

$\varepsilon_m(y) = \phi(y-\bar{y})$, (12)

ϕ_m = curvature of the section,

y = spatial coordinate measuring section depth, and

$\bar{y}$ = the distance to the centroid of the section.

2) Incremental thrust or axial stress, $\Delta\sigma_n$, does not contribute to the moment:

$$\int_A \Delta\sigma_n(\bar{y}-y)\ dA = 0 \tag{13}$$

3) Incremental moment stress, $\Delta\sigma_n$, does not contribute to thrust forces:

$$\int_A \Delta\sigma_m\ dA = 0 \tag{14}$$

The incremental stress level at any point in the cross section is the sum of the flexural and thrust contributions:

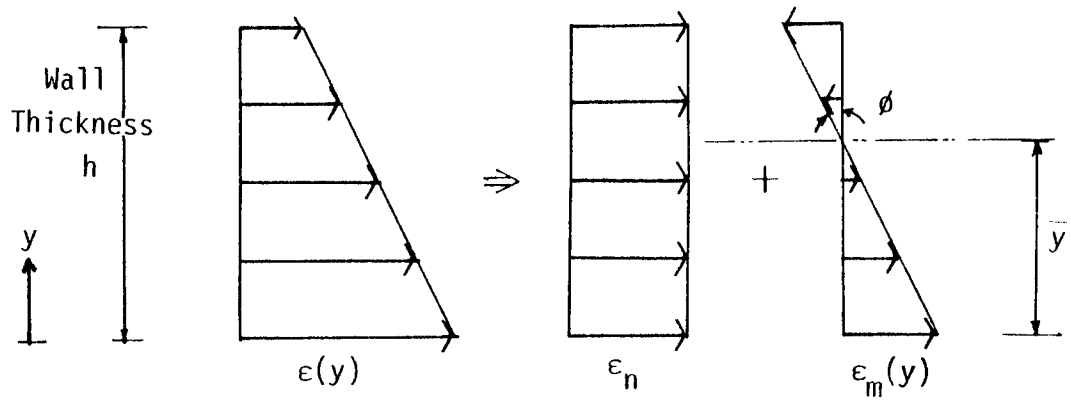

FIGURE 7. Linear Strain Distribution
After Katona (1)

$$\Delta\sigma = \Delta\sigma_n + \Delta\sigma_m \tag{15}$$

Applying the nonlinear stress-strain law, Equation 9, to each stress component, and substituting Equation 12 for $\varepsilon_m(y)$, one obtains the following equations for moment and thrust stress:

$$\Delta\sigma_n = E_e\,[1-\alpha(\varepsilon)]\,\Delta\varepsilon_n \tag{16}$$

$$\Delta\sigma_m = E_e\,[1-\alpha(\varepsilon)]\,\Delta\phi(\bar{y}-y) \tag{17}$$

The incremental thrust, N, and incremental moment, M, can be found by summing the forces across the section and finding the moments about the neutral axis, respectively.

$$\Delta N = \int_A \Delta\sigma\, dA = \int_A (\Delta\sigma_n+\Delta\sigma_m)\, dA \tag{18}$$

$$\Delta M = \int_A \Delta\sigma(\bar{y}-y)dA = \int_A (\Delta\sigma_n+\Delta\sigma_m)\,(\bar{y}-y)\, dA \tag{19}$$

By applying the above stress-strain relationships for incremental thrust and moment stress and using Assumptions 2 and 3, one arrives at the following relationship for incremental thrust and moment:

$$\Delta N = \int_A E_e\,[1-\alpha(\varepsilon)]\,\Delta\varepsilon_n\, dA \tag{20}$$

$$\Delta M = \int_A E_e\,[1-\alpha(\varepsilon)]\,(\bar{y}-y)^2\,\Delta\phi\, dA \tag{21}$$

The above equations can be simplified to:

$$\Delta N = E_e A^* \, \Delta\varepsilon_n \tag{22}$$

$$\Delta M = E_e I^* \, \Delta\phi \tag{23}$$

where

$$A^* = \int_A [1-\alpha(\varepsilon)] \, dA$$

$$I^* = \int_A [1-\alpha(\varepsilon)] \, (\bar{y}-y) \, dA.$$

The modified area, A^*, and the modified moment of inertia, I^*, differ from the standard linear form only by the $[1-\alpha(\varepsilon)]$ term. In fact, $E_e A^*$ and $E_e I^*$ are the effective nonlinear EA and EI of the pipe elements. These values can be used in the standard elastic element stiffness matrix during a given incremental load step.

The location of the bending axis, $\bar{y}$, is also a function of the stress state during plastic loading of the pipe cross section; however, the restrictions that the thrust stresses do not contribute to the section moment (Equation 12) and that the bending stresses across the cross section sum to zero (Equation 13) make it possible to solve for $\bar{y}$ during any load increment. The stress-strain relationship can be applied in the form of either Equation 15 or 16. By noting that the $\Delta\varepsilon_n$ and $\Delta\phi$ terms are constant during any load increment, the same equation for $\bar{y}$ is obtained with either stress-strain form:

$$y = \frac{\int_A E_e \, [1-\alpha(\varepsilon)] \, \bar{y} \, dA}{\int_A E_e \, [1-\alpha(\varepsilon)] \, dA} \tag{24}$$

A simple iteration procedure was adopted by Katona in the CANDE code to determine the correct values for A*, I*, and $\bar{y}$ during any incremental load step. Values for A*, I*, and $\bar{y}$ are assumed at the beginning of each load step. The global system of equations is then solved using these assumed values. New values are calculated from the resulting strain state. If the differences between the assumed values and the calculated values are greater than the prescribed limits, the new values of A* and I* are inserted into the element stiffness matrix, and the global equations are re-solved. When the differences are sufficiently small, convergence is obtained, and the next load increment is applied.

A complication occurs in evaluating the integrals for A*, I*, and $\bar{y}$. Since strain varies from point to point across the cross section, $\alpha(\varepsilon)$ varies also. The evaluation of these integrals are greatly simplified by a simple bilinear approximation for the stress-strain characteristics of the pipe material. Using the bilinear approximation, there are only three material states possible, elastic, plastic or transitional. They are illustrated in Figure 8 and defined as follows:

1) Elastic state - the material properties at a point in the section are below the elastic limit during the incremental load

where

$$E' = E_e \tag{25}$$

$$1 - \alpha(\varepsilon) = 1 \tag{26}$$

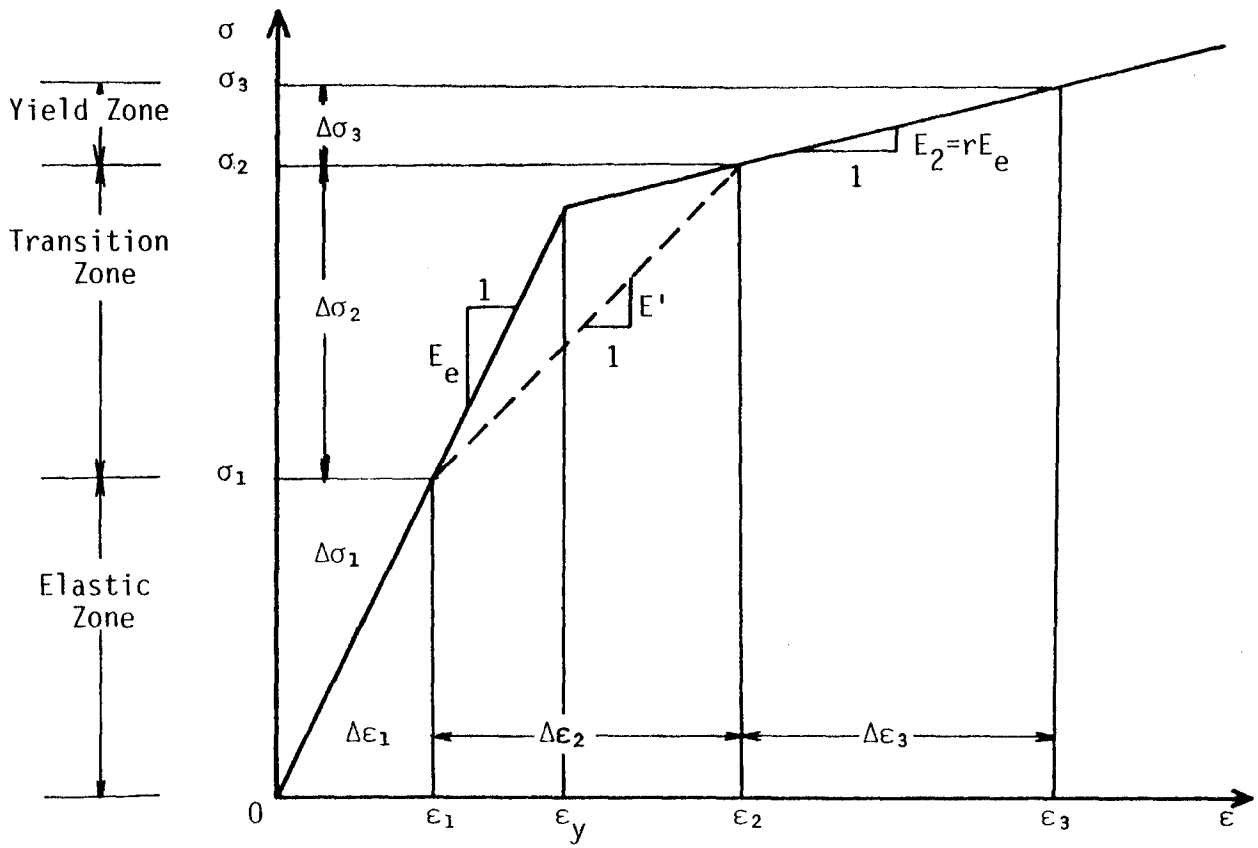

FIGURE 8. Bilinear Stress-Strain Curve After Katona (1)

2) Transitional state - a point in the cross section goes from an elastic to plastic response during the incremental load

where

$$E' = \Delta\sigma_2/\Delta\varepsilon_2 \tag{27}$$

$$= \frac{\sigma_2 - \sigma_1}{\varepsilon_2 - \varepsilon_1}$$

$$= \frac{\sigma_y + (\varepsilon_2-\varepsilon_y)r\ E_e - \sigma_1}{\varepsilon_2-\varepsilon_1}$$

$$= \frac{\varepsilon_y E_e + (\varepsilon_2-\varepsilon_y)r\ E_e - \varepsilon_1 E_e}{\varepsilon_2-\varepsilon_1}$$

$$1-\alpha(\varepsilon) = \frac{E'}{E_e} = \frac{(\varepsilon_y-\varepsilon_1) + (\varepsilon_2-\varepsilon_y)r}{\varepsilon_2-\varepsilon_1} \tag{28}$$

3) Yield state - the stress level at a point is greater than the yield strength during the complete load step

where

$$E' = E_2 = r\ E_e \tag{29}$$

$$1-\alpha(\varepsilon) = \frac{r\ E_e}{E_e} = r \tag{30}$$

where

$\Delta\varepsilon_1$ = an elastic state strain increment

$\Delta\varepsilon_2$ = a transitional state strain increment

$\Delta\varepsilon_3$ = a plastic state strain increment

E_2 = the post-yield modulus of the pipe material

ε_y = yield strain of the pipe material

E_e = the elastic modulus of the pipe material

THE NEW NONSYMMETRIC BEAM ELEMENT

High density polyethylene pipe is presently being manufactured with profile-walls. Profile-wall pipe is a flat wall pipe reinforced with a circular profile extrusion continuously wound around the mandrel during the manufacturing process (see Figure 3). The result is a pipe cross section that is not symmetric about the centroid of the wall cross section.

The evaluation of A^*, I^*, and $\bar{y}$ is more difficult in this case than for a thin-wall pipe or a standard corrugated pipe. For the flat-wall or corrugated pipe, the elemental unit area is constant for any point in the pipe cross section, and the integration involved to obtain A^*, I^*, and $\bar{y}$ is relatively simple. For the nonsymmetric beam element, the integration must be done over the peculiar cross section. To eliminate the necessity of performing a difficult integration over the circular portion of the unit cross section, a simplifying assumption was made. A cross section composed of four rectangles of different areas was equated with the actual profile (see Figure 9).

The dimensions of the simplified cross section are determined by requiring the assumed cross section to have the same total height, H, area, A, moment of inertia, I, and distance to the centroid, Z, as the actual profile. By setting the thickness of the upper and lower

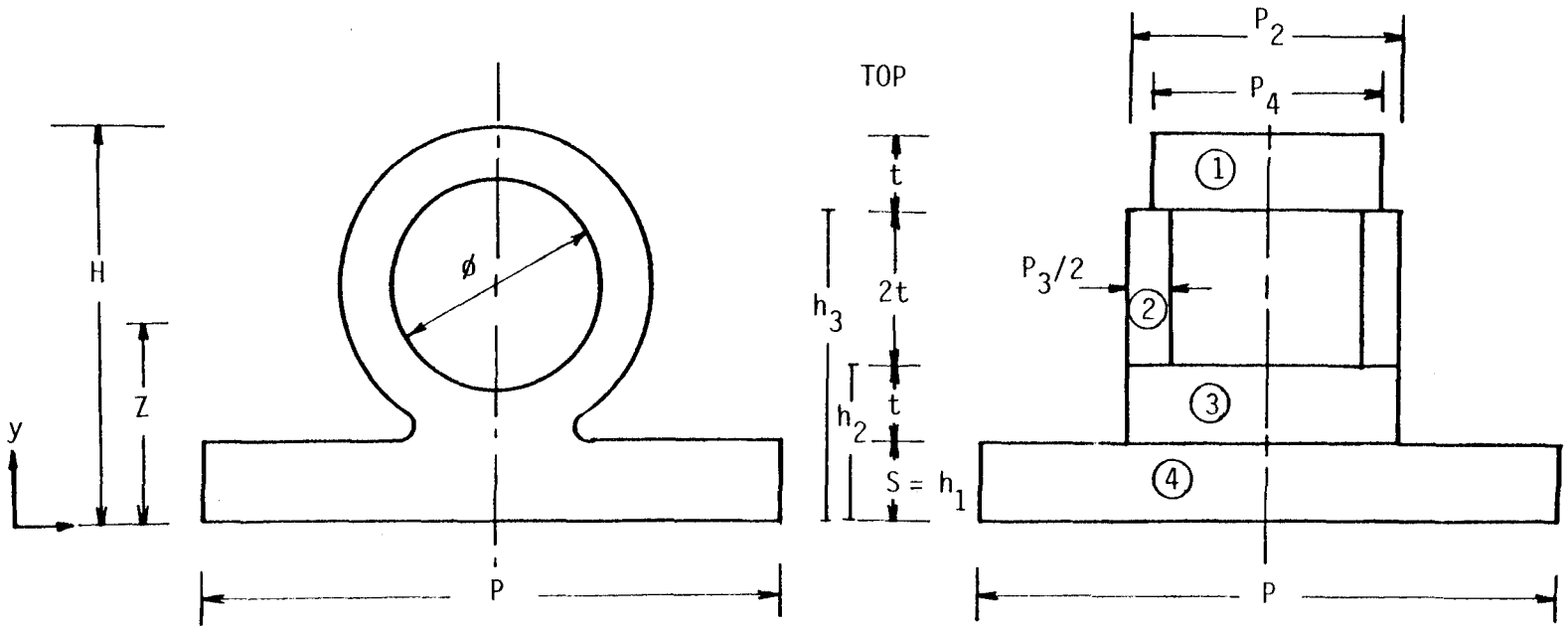

FIGURE 9. Actual and Transformed Cross-Section of the Profile-Wall Pipe

transformed areas equal to t and setting the height of the middle transformed area equal to 2t, it is possible to solve four equations and four unknowns to determine t, P_2, P_3 and P_4.

$$t = \frac{H - S}{4} \tag{31}$$

$$A = PS + tP_2 + 2tP_3 + tP_4 \tag{32}$$

$$\begin{aligned} I = {} & 1/12\ (PS^3 + P_2t^3 + 8P_3t^3 + P_4t^3) \\ & + PS\ (S/2 - Z)^2 + P_2\ t(S + t/2 - Z)^2 \\ & + P_3 2t\ (2t+S-Z)^2 + P_4 t\ (7/2t + S - Z)^2 \end{aligned} \tag{33}$$

$$Z = \frac{PS^2/2 + tP_2(S+t/2) + 2tP_3(S+2t) + tP_4(S+7t/2)}{PS + t(P_2 + 2P_3 + P_4)} \tag{34}$$

The solution of the above set of linear equations is straightforward but results in a long expression (see Appendix A).

These equations are programmed into the new CANDE subroutine so that the dimensions of the transformed cross section are automatically calculated from the input actual section properties S, P, H, I, A and Z.

The CANDE code is a plane-strain program, which analyzes a typical 1.0 inch section of the pipe. The total area, A, of a unit profile and the areas of each transformed rectangle; A1, A2, A3, and A4; must be divided by the unit profile length, P, in order to get the contributing area per longitudinal inch of the pipe. The integral

expressions for unit area, A*; unit moment of inertia, I*; and distance to the neutral axis, $\bar{y}$, can now be evaluated in four parts, one for each zone of the transformed pipe cross section. The width of each of the transformed areas is constant. The two-dimensional integral can therefore be reduced to a one-dimensional integral.

$$\begin{aligned} A^* &= \int_A [1-\alpha(\varepsilon)]dA \\ &= \frac{A1}{S}\int_0^{h_1}[1-\alpha(\varepsilon)]dy + \frac{A2}{t}\int_{h_1}^{h_2}[1-\alpha(\varepsilon)]dy \\ &\quad + \frac{A3}{2t}\int_{h_2}^{h_3}[1-\alpha(\varepsilon)]dy + \frac{A4}{t}\int_{h_3}^{H}[1-\alpha(\varepsilon)]dy \end{aligned} \tag{35}$$

$$\begin{aligned} I^* &= \int_A [1-\alpha(\varepsilon)](\bar{y}-y)\ dA \\ &= \frac{A1}{S}\int_0^{h_1}[1-\alpha(\varepsilon)](\bar{y}-y)\ dy + \frac{A2}{t}\int_{h_1}^{h_2}[1-\alpha(\varepsilon)](\bar{y}-y)\ dy \\ &\quad + \frac{A3}{2t}\int_{h_2}^{h_3}[1-\alpha(\varepsilon)](\bar{y}-y)\ dy + \frac{A4}{t}\int_{h_3}^{H}[1-\alpha(\varepsilon)](\bar{y}-y)\ dy \end{aligned} \tag{36}$$

$$\begin{aligned} \bar{y} &= \frac{1}{A^*}\int_A [1-\alpha(\varepsilon)]y\ dA \\ &= \frac{1}{A^*}\left[\frac{A1}{S}\int_0^{h_1}[1-\alpha(\varepsilon)]y\ dy + \frac{A2}{t}\int_{h_1}^{h_2}[1-\alpha(\varepsilon)]y\ dy \right. \\ &\quad \left. + \frac{A3}{2t}\int_{h_2}^{h_3}[1-\alpha(\varepsilon)]y\ dy + \frac{A4}{t}\int_{h_3}^{H}[1-\alpha(\varepsilon)]y\ dy\right] \end{aligned} \tag{37}$$

As outlined in the summary of Katona's bilinear stress-strain model, there are three possible strain states which can exist in the pipe cross section: Elastic, Plastic or Transitional. If the entire cross section is at a stress level below the elastic limit, the elastic values for area, moment of inertia, and distance to the neutral axis can be used in the elemental stiffness matrix. However, once some plastic deformation has occurred, the elastic, transition, and plastic zones must be determined for each iteration in order to

calculate the modified values for A^*, I^*, and $\bar{y}$.

After the first iteration during load step K, outer and inner fiber strains can be determined from the calculated moment and thrust force at each node using Equations 11, 22, and 23. Since the strains are assumed to be linear throughout the pipe section, determining the inner and outer fiber strain, determines the entire strain profile. If the maximum strains in the profile for both load step K-1 and the present load step K are below the yield strain, then no further iteration is required and the elastic solution is correct. However, if some yielding has occurred in load step K or K-1, the strain state of each zone in the transformed cross section must be determined (see Figure 10).

The linear strain profile is examined and values of ye_1, ye_2, yt_1, and yt_2 are determined. Once the strain state of the complete section has been determined, the integrals for A^*, I^* and $\bar{y}$ can be determined using Equations 28 and 30 to estimate the values of $[1-\alpha(\varepsilon)]$ corresponding to the existing strain. For the elastic and plastic strain states the $[1-\alpha(\varepsilon)]$ term is a constant and can be taken out of the integral, but for the transitional strain state each point in the zone has a different value of $[1-\alpha(\varepsilon)]$. To eliminate the necessity of evaluating the complete integral, an average value of $[1-\alpha(\varepsilon)]$ is used for the entire transitional zone found in each rectangular zone of the transformed cross section. The net result is that Equations 35, 36, and 37 can be evaluated directly and written in the following general form:

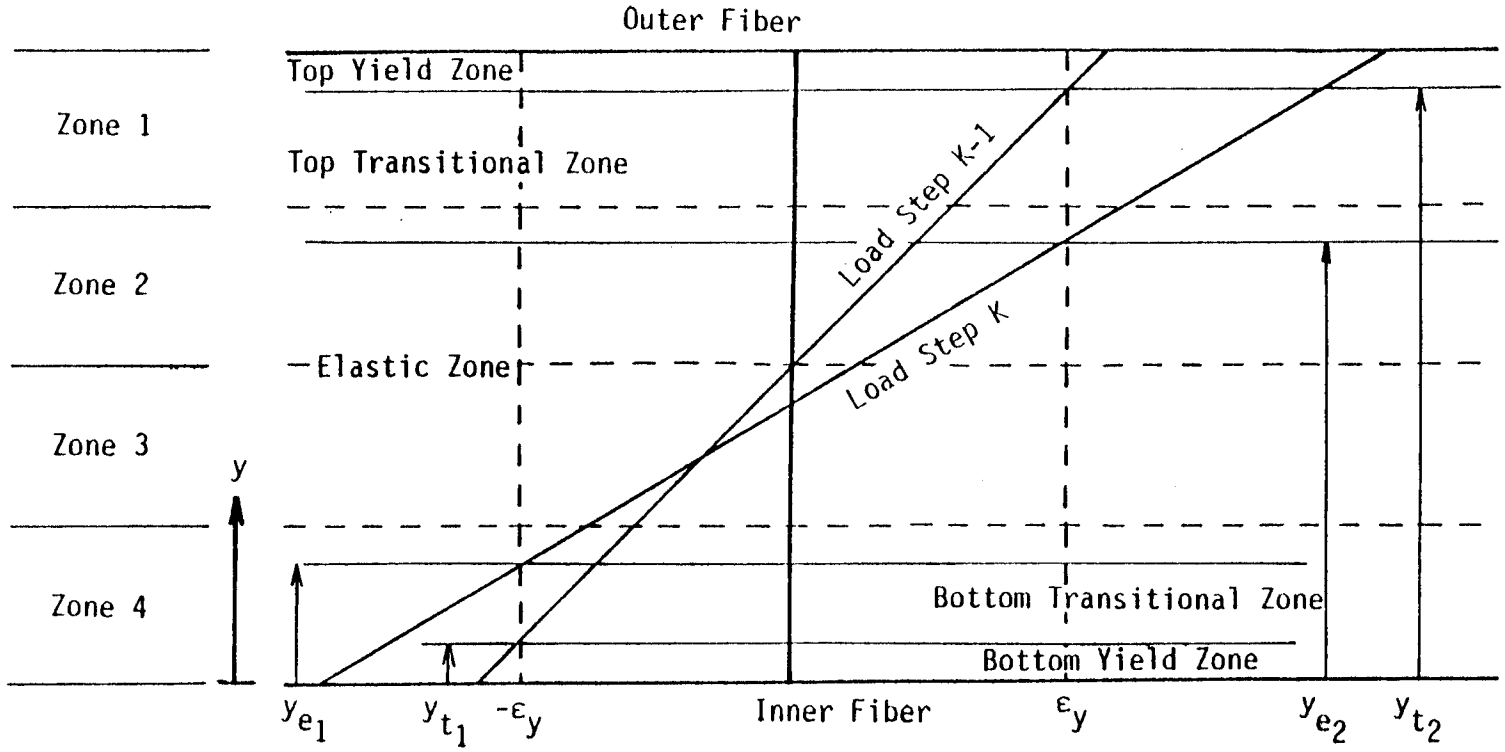

ye_1 = the distance to the bottom of the elastic zone for the present load step K

ye_2 = the distance to the top of the elastic zone for the present load step K

yt_1 = the distance to the bottom of the elastic zone for the last converged load step K-1

yt_2 = the distance to the top of the elastic zone for load step K-1

Figure 10. Strain Diagram for Load Step K-1 to Load Step K

$$A^* = \sum_{i=1}^{4} t_i \{A_{i1}-B_{i1} + WT1_i(A_{i2}-B_{i2}) + WT2_i(A_{i3}-B_{i3}) + r(A_{i4}-B_{i4}) + r(A_{i5}-B_{i5})\} \quad (38)$$

$$I^* = \sum_{i=1}^{4} \frac{-t_i}{3} \{[(\bar{y}-A_{i1})^3-(\bar{y}-B_{i1})^3] + WT1_i[(\bar{y}-A_{i2})^3-(\bar{y}-B_{i2})^3] + WT2_i[(\bar{y}-A_{i3})^3-(\bar{y}-B_{i3})^3] + r[(\bar{y}-A_{i4})^3-(\bar{y}-B_{i4})^3] + r\,[(\bar{y}-A_{i5})^3-(\bar{y}-B_{i5})^3]\} \quad (39)$$

$$\bar{y} = \sum_{i=1}^{4} \frac{t_i}{2A^*} \{(A_{i1}{}^2-B_{i1}{}^2) + WT1_i(A_{i2}{}^2-B_{i2}{}^2) + WT2_i(A_{i3}{}^2-B_{i3}{}^2) + r(A_{i4}{}^2-B_{i4}{}^2) + r(A_{i5}{}^2-B_{i5}{}^2)\} \quad (40)$$

where

i = the number of the rectangular zone in the transformed area,

t_i = the unit width of the zone (unit area of the zone/zone thickness),

A_{i1}, B_{i1} = the upper and lower limits of the elastic zone in layer i, respectively,

A_{i2}, B_{i2} = the upper and lower limits of the bottom transition zone,

A_{i3}, B_{i3} = the upper and lower limits of the top-transitional zone,

A_{i4}, B_{i4} = the upper and lower limits of the bottom-yield zone,

A_{i5}, B_{i5} = the upper and lower limits of the top-yield zone,

$WT1_i$ = the average value for $[1-\alpha(\varepsilon)]$ in the bottom transitional zone in layer i,

$WT2_i$ = the average value for $[1-\alpha(\varepsilon)]$ in the top transitional

zone in layer i, and

r = the ratio of the yield modulus to the elastic modulus.

It is apparent that all four of the zones in the transformed area cannot simultaneously have a yield, an elastic, and a transitional zone; however, the above general equation will handle all possible strain distributions. The values of the upper and lower limits, A_{ij} and B_{ij}, can be found by examining the linear strain profile in each of the material zones. Recording the correct numerical values of A_{ij} and B_{ij}, or setting them equal to zero if the particular strain state does not exist, is merely an exercise in numerical bookkeeping.

When the iteration process converges upon the appropriate values of A^*, I^*, and $\bar{y}$, correct values for nodal moments, thrust loads and shear loads are obtained. The resulting strain profiles, calculated for each node, are accurate representations of nonlinear response in a nonsymmetric pipe cross section. The total stresses at any point in the cross section can be calculated directly from the linear strain diagrams and the bilinear stress-strain curve.

The elastic modulus of the pipe material can be used to relate stress and strain for the portion of the cross section which has strains below the elastic limit. However, for any section of the strain diagram with strains above the elastic limit, the elastic and plastic stresses must be summed to arrive at the total stresses (see Figure 8). The post-yield stress, σ_3, corresponding to a post-yield strain, ε_3, can be expressed as follows:

$$\sigma_3 = \sigma_y + (\varepsilon_3 - \varepsilon_y)\ E_2 \tag{41}$$

The net result of the bilinear stress-strain approximation is that linear strains throughout the pipe cross section produce a realistic bilinear stress distribution as can be seen in Figure 11. Although the bilinear stress-strain model is an approximation for the actual stress-strain characteristics of high-density polyethylene, it permits the investigation of post yield behavior in which the user can adequately approximate high distress levels in the nonsymmetric profile-wall pipe.

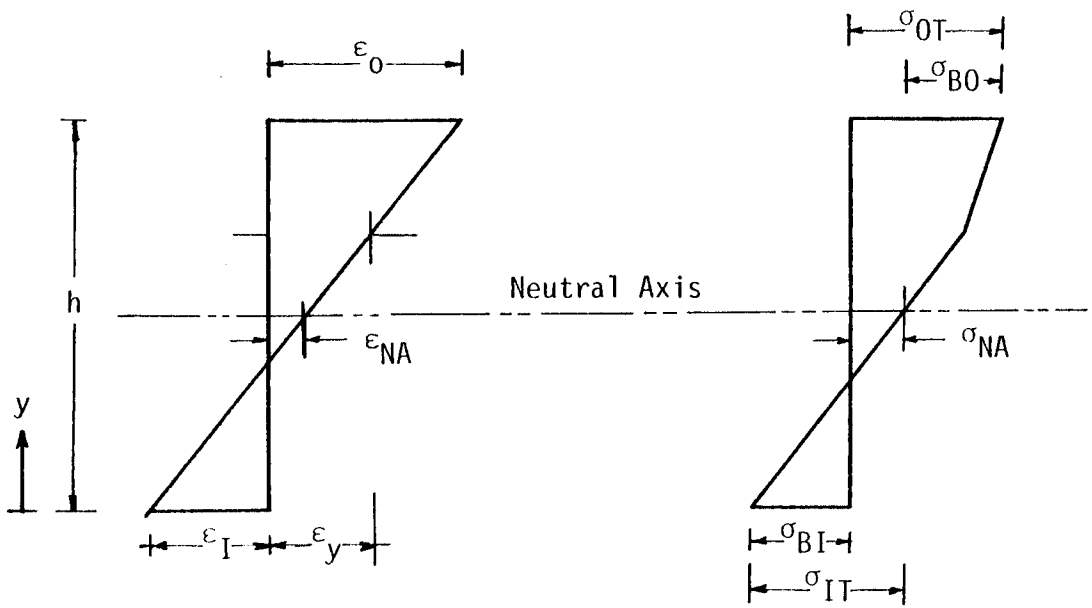

ε_o = outer fiber strain

ε_I = inner fiber strain

ε_{NA} = strain at the neutral axis (thrust strain)

σ_{OT} = total outer fiber stress

σ_{BO} = outer fiber bending stress

σ_{NA} = stress at the neutral axis (thrust stress)

σ_{BI} = inner fiber bending stress

σ_{IT} = inner fiber total stress

FIGURE 11. Bilinear Stress-Strain Relationship

DETERMINATION OF PIPE RESPONSE FOR A FACTORIAL SET OF DESIGN PARAMETERS

Although the modified CANDE program can be used to predict the response of a profile-wall pipe under almost any set of design conditions, the use of a large finite element program for a standard pipe design is somewhat impractical. Consequently, pipe responses were predetermined using a factorial set of design conditions, and the resulting data set was used as a basis for developing simple design equations which can be used effectively for common design problems.

DESIGN VARIABLES IN THE STUDY

A design engineer is typically faced with the problem of determining how well a pipe will respond when used at a particular site. The in-situ soil strength, water table depths, design period, and expected burial depth are all variables that are relatively fixed for each design. Pipe size, pipe stiffness, trench width, backfill material, and trench compaction are variables which can be specified by the engineer. In order to develop a useful design equation, each of the above variables was included in the set of analyses.

A factorial study was designed so that the effect of each variable could be studied under a variety of conditions. The number of individual values for each variable was limited based on a preliminary sensitivity analysis, information in the literature, available data, and communication with flexible pipe design engineers.

Properties of the Pipe Material and Soils Used

Since both high density polyethylene and fine-grained soils are time dependent materials, life expectancy is a necessary consideration. This study was limited to fine-grained in-situ soils.

As an introduction to time-dependent behavior of soils and pipe materials, a slight digression is useful here. Most engineers are familiar with the two stages of consolidation: primary and secondary. During primary consolidation, the load and total stresses in the soil do not change and settlement occurs because water is slowly squeezed out of the soil. During the so-called "secondary" consolidation, the total stresses and the water content of the soil remain unchanged but the soil continues to settle due to a phenomenon known as "creep."

Creep is the continuing strain of a material with time under constant stress. All materials creep, but some do more than others. It is known that a material such as concrete, which most people would regard as rigid, creeps so much that in order to estimate the long-term deflections of a concrete beam, one must use one-third of its short-term modulus (18). The same is generally true of high density polyethylene of which the pipe material is constructed and of the soil which surrounds it. The amount by which the modulus of each must be modified depends upon the time at which the desired pipe deflection or strain is to be calculated.

The Duncan soil model used in this study provides an accurate representation of the short-term stress-strain properties associated with different soil materials. Although this model does not account for the effects of soil creep behavior directly, the expected behavior

of a soil at some time, t, can be analyzed with the Duncan soil model by developing a relationship for the change in the Duncan soil parameters with time.

The elastic modulus versus time relationship (relaxation curve) of many materials (19,20,21) and of most soils (3,4,5, 22,23) can be represented by the simple power law equation:

$$E(t) = E_1 t^{-m} \tag{42}$$

where

$E(t)$ = the elastic modulus at time t, in seconds,

m = straight line slope of the logarithmic plot of the relaxation curve, and

E_1 = the elastic modulus for a time equal to 1 sec.

Because of Equation 42, the ratio of elastic modulus at some time, t, to the modulus at some other time, t_o, is proportional to the (t/t_o) ratio raised to the (-m) power. This makes it possible to calculate a long-term initial tangent modulus, $E_i(t)$, from the Duncan soil model for the short-term initial tangent modulus, E_i, shown in Equation 43.

$$E_i = P_a k \left(\frac{\sigma_3}{p_a}\right)^n \tag{43}$$

where

k, n = dimensionless soil parameters,

P_a = atmospheric pressure, and

σ_3 = confining pressure.

The short-term initial tangent modulus is taken from triaxial tests with $t_o \cong 100$ sec. and, as seen in Equation 43, is directly proportional to a dimensionless stiffness parameter, k. If one assumes that n is not affected by design time, the following relationship for a time dependent k(t) can be stated:

$$k(t) = k\left(\frac{t}{t_o}\right)^{-m} \tag{44}$$

The above equation makes it possible to use the Duncan soil model to approximate time-dependent, fine-grained soil behavior. The slope of the relaxation curve, m, only varies from .029 to .140 for the wide range of soil types tested by three independent sources (4,5,23) as can be seen in Table 3. An m value of 0.1 is typical for most time dependent soils and can be used for a conservative estimate if sufficient time dependent data are not available (3). The Allenfarm, Moscow, and Floydada soils shown in Table 4 were used in the study, since a complete range of triaxial and creep data were available. The soil properties for the other two soils used in the factorial study were obtained from data published by Duncan (6). Since no creep data were available for these soils, m was assumed to be 0.1. A complete summary of the soil parameters associated with the five in-situ soils and the backfill material used in the study is shown in Table 4. The values of the soil parameters used represent a typical range of fine grained soils.

It is often difficult to determine the strength properties of the

TABLE 3. Power Law Exponent m for Different Soil and Water Contents

Soil Location	Unified Classification	Liquidity Index, L.I.	Average m	Reference
Louisiana	MH	1.33	.140	(23)
Coast	MH	1.05	.103	(23)
(different	MH	.65	.065	(23)
samples at	MH	.63	.041	(23)
different	MH	.65	.064	(23)
depths)	MH	.75	.044	(23)
	MH	.73	.041	(23)
	MH	.52	.029	(23)
Mississippi	CH	1.31	.104	(4)
delta	CH	1.20	.090	(4)
(same soil	CH	.99	.087	(4)
remolded)	CH	.92	.085	(4)
	CH	.70	.082	(4)
Allenfarm	ML	NA	.106	(5)
Floydada	CL	.13	.079	(5)
Moscow	CH	.055	.101	(5)
(Texas soils at optimum water content)				

$$L.I. = \frac{w_n - w_p}{I_p}$$

where

LI = liquidity index

w_n = nature water content

w_p = plastic limit

I_p = plasticity index

TABLE 4. In-situ Soil Parameter Used in Factorial Study

Parameters	Soil Types					
Unified Soil Classification	Allenform ML	Moscow CH	Floydada CL	Birch Dam Shell ML	Somerville Dam CL	Backfill Material
I_p	0.0	55.0	13.0	1.0	30.0	NA
ϕ	36.5	25.0	32.0	27.0	1.0	33.0
n	0.47	0.50	0.10	0.84	0.18	0.4
R_f	0.93	0.73	0.87	0.77	0.85	0.7
w%	16.5	31.0	18.7	16.6	26.0	NA
m	0.106	0.101	0.079	0.10	0.10	NA
K (10 yr)	239.94	159.06	543.05	22.39	6.05	200.0
γ_{wet}	122.4	121.5	133.4	133.9	123.36	120.0
C psi	0.0	0.0	0.0	7.5	6.25	0.0
μ	0.45	0.45	0.45	0.45	0.45	NA

w = water content (percent)

I_p = plastic limit

C = cohesion

ϕ = angle of internal friction

n K(t) Rf = dimensionless Duncan soil parameters (10 yr. values)

m = slope of creep compliance curve from Ref. (5,3)

γ_{wet} = wet unit weight

μ = Poisson's ratio

coarse-grained backfill used immediately around the pipe. Different construction procedures and compaction efforts can produce large variations in backfill properties. Since this irregularity is hard to predict, a conservative backfill was used in all runs. A conservative set of parameters for a coarse aggregate material, with a relative compaction of 90% of standard AASHTO, is available within CANDE and was used to represent a standard backfill soil. The properties of the coarse-grained materials were assumed not to be time dependent, requiring no reduction of the nonlinear soil parameters with time.

The time dependence of the polyethylene pipe can also be represented by using an appropriately reduced elastic modulus. A master relaxation curve showing the relationship between flexural relaxation modulus and time was constructed from manufacturers' data using a simple time-temperature shift, in which curves produced by short duration tests at different temperatures were shifted to a curve corresponding to a reference temperature. The result is a relaxation curve which predicts the flexural relaxation modulus for a large time span (see Figure 12). Manufacturers data was used to construct the yield strength vs. time curve shown in Figure 13. Figures 12 and 13 were then used to estimate the time dependent elastic modulus and yield strength used in the modified CANDE program.

Although the above methods for determining time-dependent properties are a simplification of the actual viscoelastic properties of the materials, they give a realistic insight into the creep of the pipe and the soil. Extensive soil and pipe creep tests would allow a more accurate representation of the time variable, since the amount of

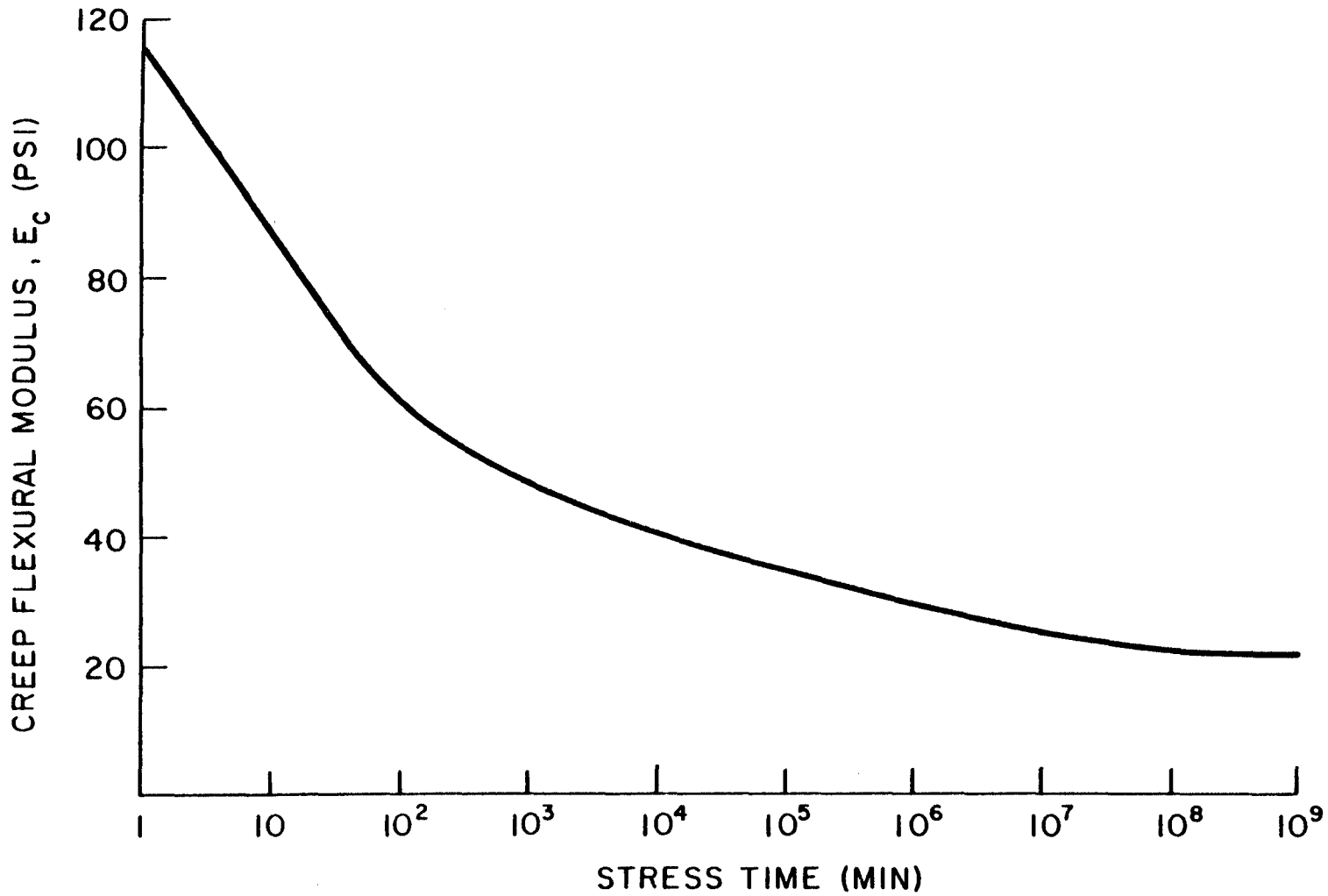

FIGURE 12. Flexural Creep Modulus vs. Time Curve for High Density Polyethylene

(Reference Temperature = 20°C)

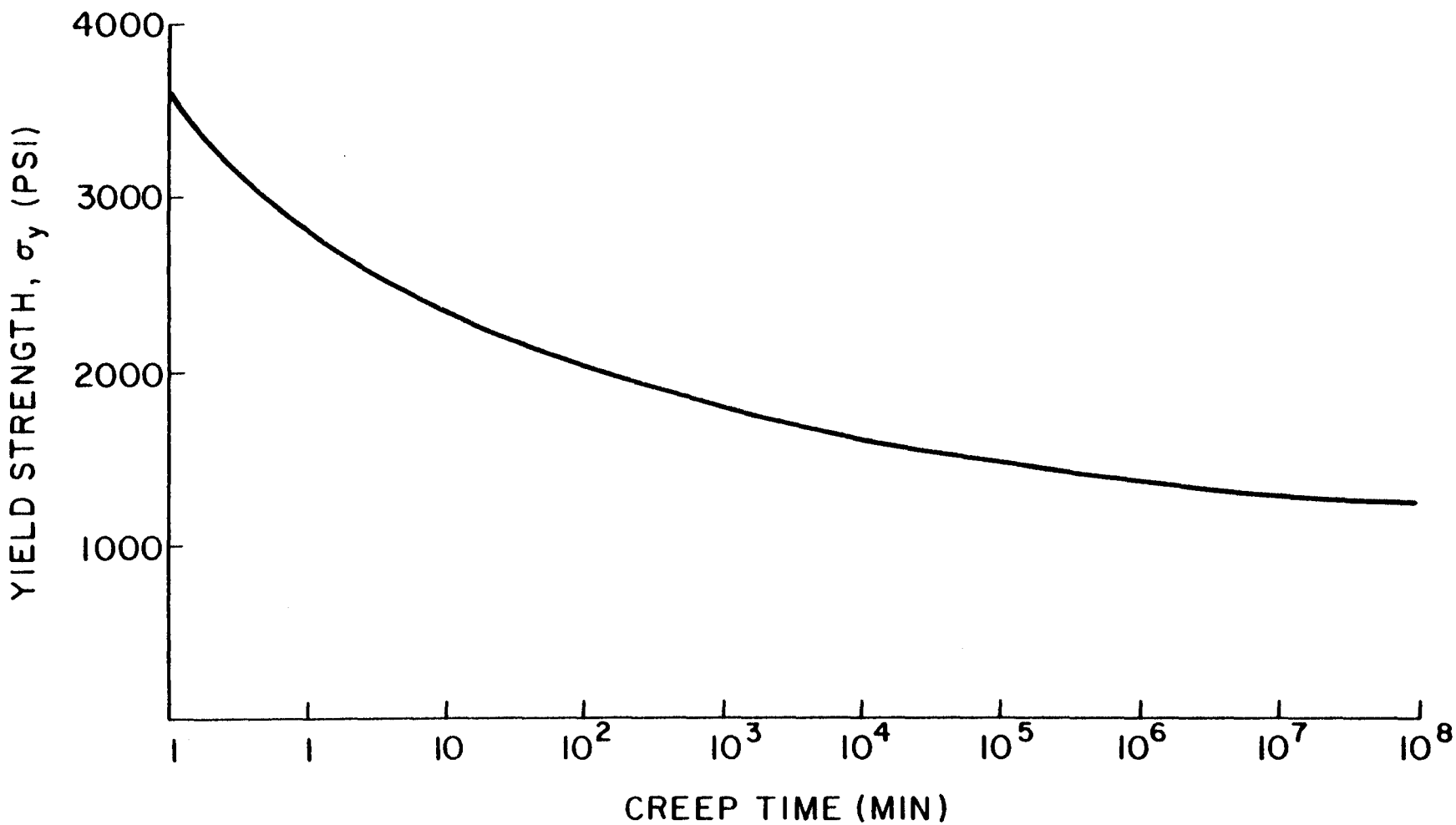

FIGURE 13. Yield Strength vs. Time Curve for High Density Polyethylene

available data was limited during this study.

The time dependent pipe and soil properties corresponding to initial short-term response and the behavior after 30 days, 10 years, 25 years, and 50 years were then input into a standard trench mesh configuration. A plot of maximum pipe strain (Figure 14) for a typical weak silt illustrates the effects of creep. Since the majority of reduction in strength occurs in the first 10 years, this value was used in all the runs for the factorial analysis. A 30 day deflection or strain measurement, which is commonly measured in the field, is, however, a good indication of the expected long-term distress levels. Figure 15 shows that approximately 66% of the maximum long-term vertical deflection occurs in the first month; Figure 14 indicates that approximately 77% of the strain is also realized in the first month for this soil type and trench configuration.

Time dependent pipe and soil properties for a silty clay were also investigated. A two-hour prediction was analyzed in addition to the initial, 30-day, 10-year, 25-year, and 50-year responses. The deflection and strain plots shown in Figure 16 and 17 respectively show that a large percent of the total creep occurs in the first 2 hours of loading. These data reveal the fact that creep occurs very rapidly in fine-grained soils and helps explain some of the observations made by the engineer at actual flexible polyethylene pipe installations. Since it is hard to completely fill a trench in less than 2 hours, a large amount of creep will occur before any initial creep measurements can be made. This fact leads many uninformed

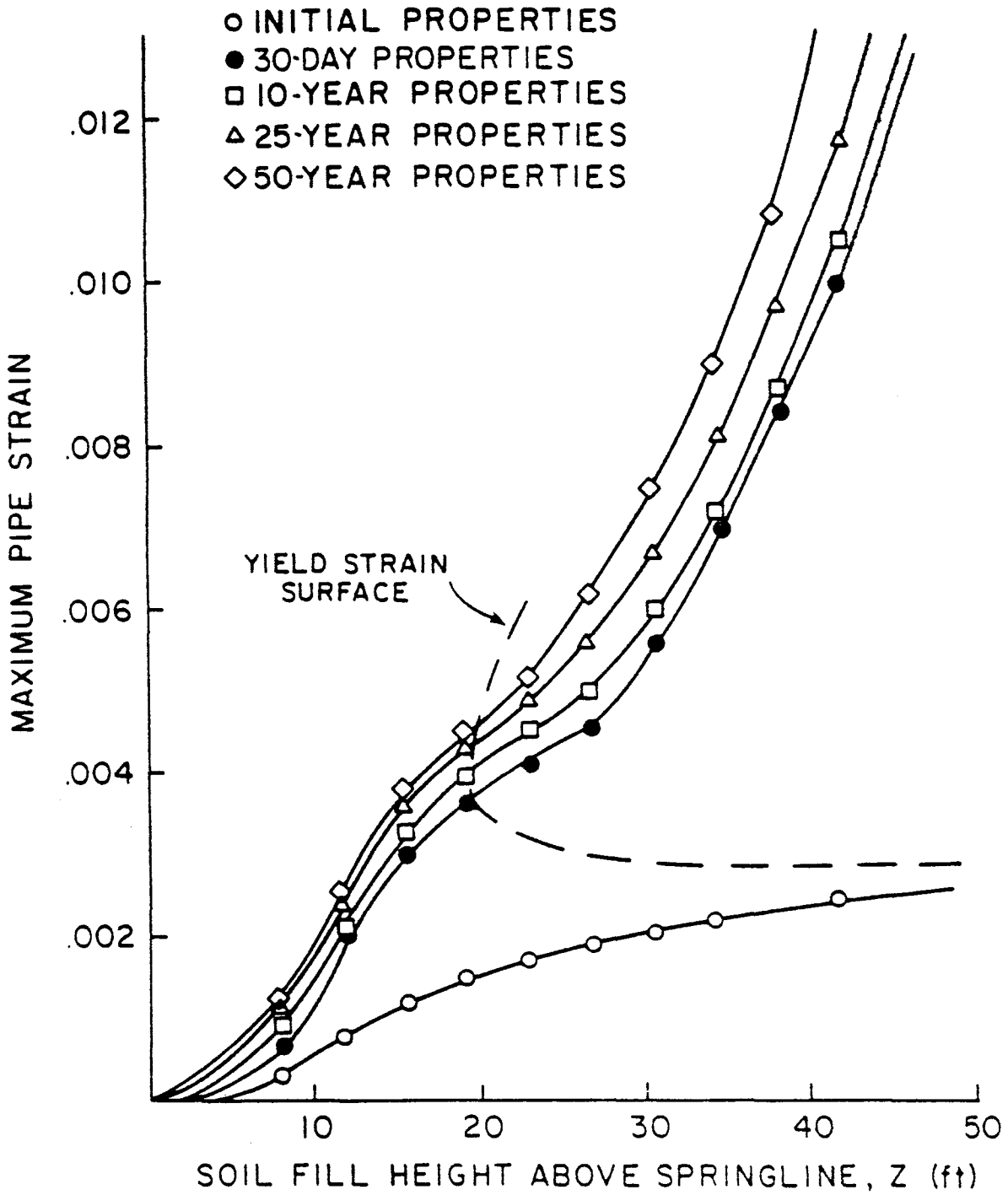

FIGURE 14. Effect of Creep Time on Maximum Pipe Strain for a Weak Silt

(D=48, Profile #9, T=72, P=0)

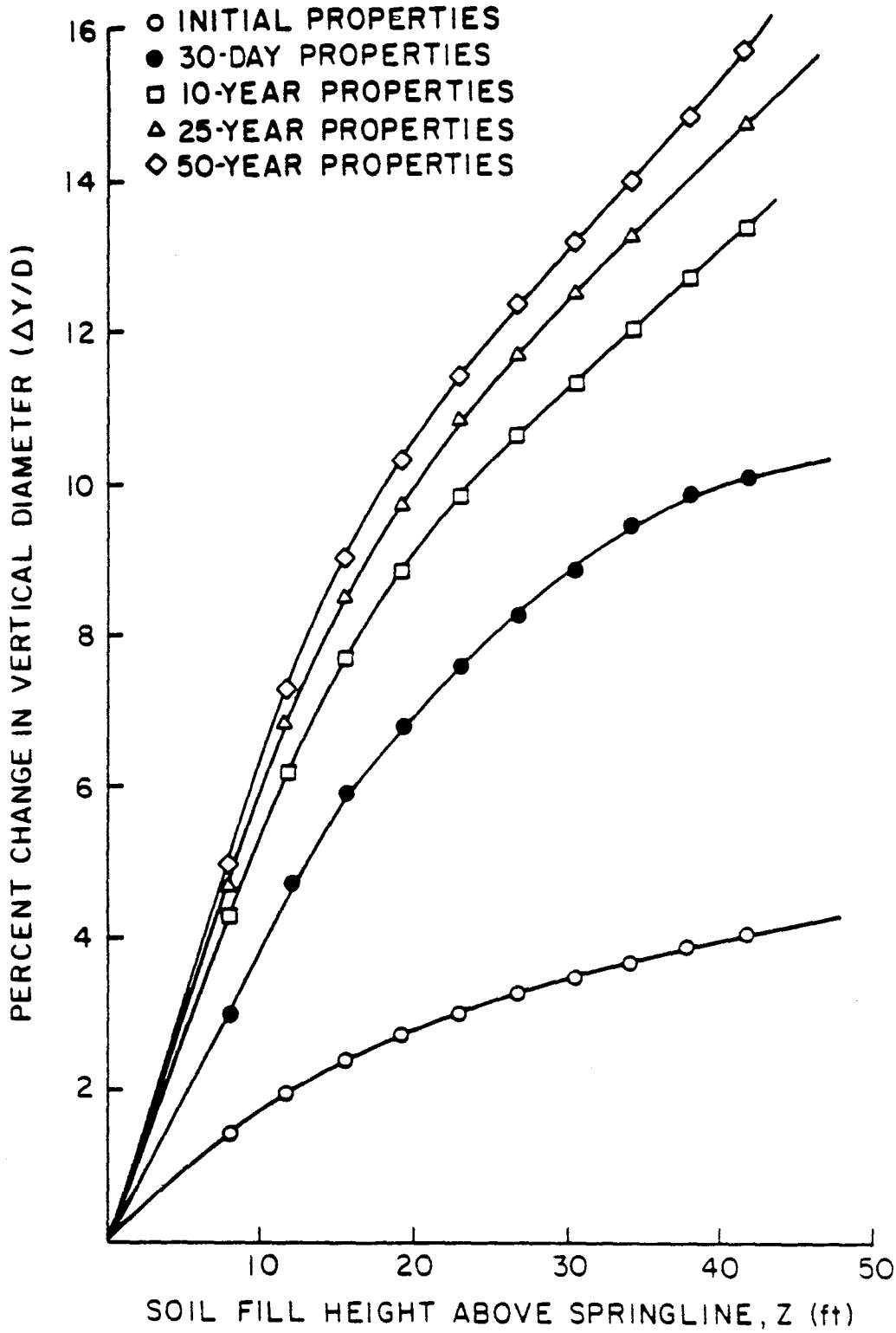

FIGURE 15. Effect of Creep Time on Pipe Deflection for a Weak Silt

(D=48, Profile #9, T=72, P=0, Z=38)

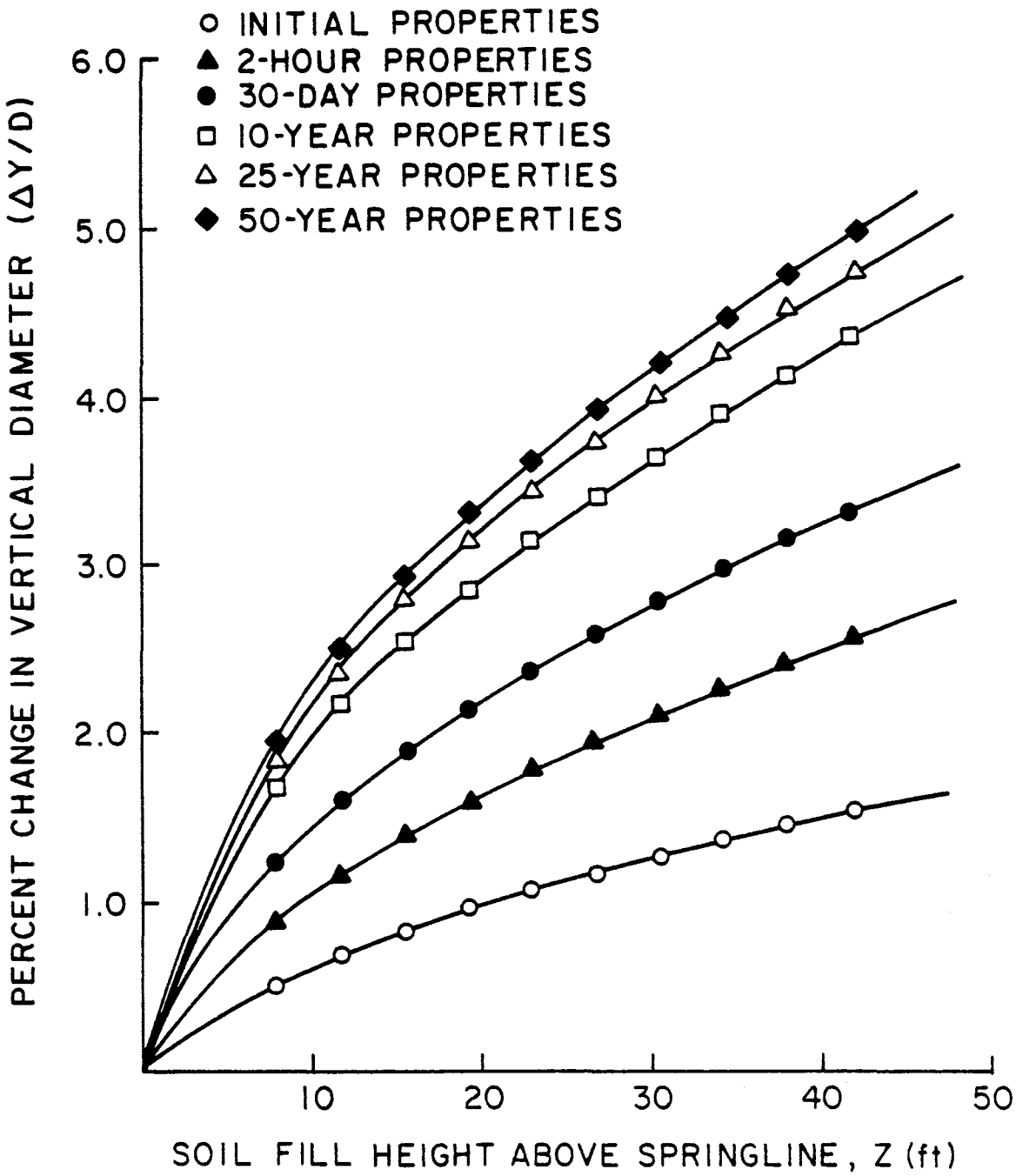

FIGURE 16. Effect of Creep Time on Pipe Deflection for a Silty Clay

(D=48, Profile #9, T=72, P=0)

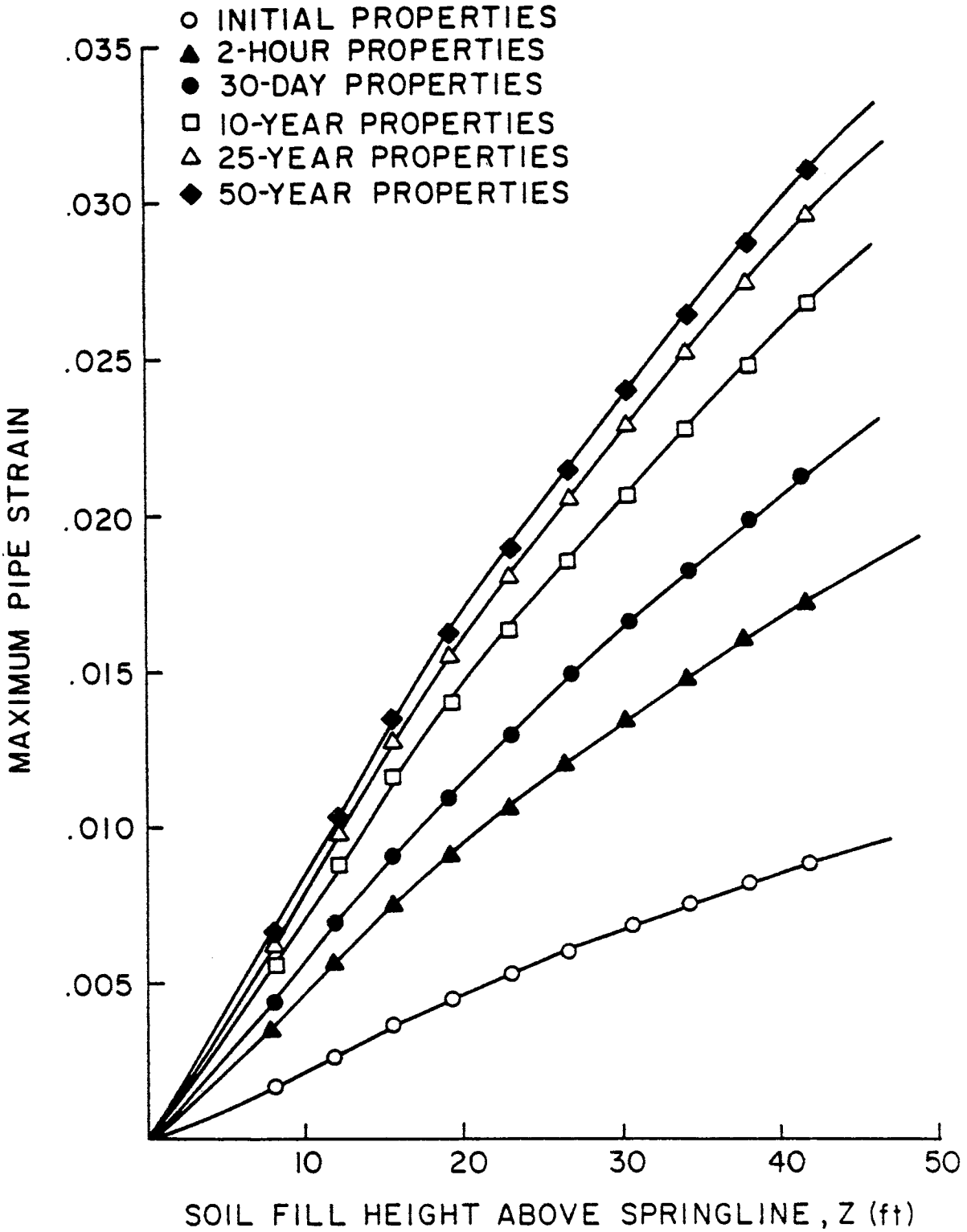

FIGURE 17. Effect of Creep Time on Maximum Pipe Strain for a Silty Clay

(D=48, Profile #9, T=72, P=0)

observers to false conclusions regarding the amount of creep which may occur. It is, however, almost impractical to report initial data corresponding to a zero time since it is virtually impossible to measure. For the remainder of this study, the smallest creep time analyzed will be 2 hours.

The large changes in strain and deflection are produced by the reduction of in-situ soil stiffness with time due to soil creep. The pipe also undergoes a reduction in stiffness with loading time, but this effect causes only limited increases in the deflection or strain levels, since the stiffness of the pipe does not greatly affect the performance of a flexible pipe. Rather, the controlling factor in determining pipe performance is the strength and stiffness of the in-situ and backfill soil. These concepts will be verified with results in the next section.

The idea of creep in soil is something that has been ignored in the design of both flexible and rigid pipe. This study shows that creep can largely affect the response of all buried conduits. Some of the unexplained failures of rigid pipes (1) could, in fact, be due to the creep which occurs in fine grained soils.

Pipe Size and Stiffness

When a flexible pipe is placed in the ground surrounded by a compacted granular material, the stiffness of the surrounding material is higher than that of the pipe. Therefore, when a given load is applied to the soil-pipe system, the stiffer soil will carry the majority of the load. Conversely, when a pipe material with a

stiffness greater than the soil is used, the reverse is true. The pipe, due to its high stiffness, is required to carry the majority of the load. Consequently, the stiffness associated with a rigid pipe has a greater significance in design practice than that associated with flexible pipe.

Soil and pipe properties for a 10-year creep time were used in CANDE to obtain the effects on maximum pipe displacement when changing pipe stiffness. The results of this analysis are shown in Figure 18. The short-term ASTM D2412 pipe stiffness and the pipe-wall unit area (A) for the profiles shown in Figures 18 and 19 are listed below:

Profile 9 $\quad \frac{EI}{.149\ r^3} = 109.8$ (psi) $\qquad A = .472\ in^2$

Profile 7 $\quad \frac{EI}{.149\ r^3} = 73.3$ (psi) $\qquad A = .346\ in^2$

Profile 5 $\quad \frac{EI}{.149\ r^3} = 48.3$ (psi) $\qquad A = .290\ in^2$

Changing the pipe stiffness by a factor of 2.3, when going from the #5 Profile to the #9 Profile, only changes the deflection by a factor of 1.3. The contention that pipe stiffness is the controlling variable for determining flexible pipe deflection is clearly in error. Other variables such as backfill type and compaction, in-situ soil type, and the height of water table have greater effects on pipe deflection, as is shown in the next section.

Figure 19 shows the effect of profile sizes on maximum pipe-wall strain. Changing the pipe-wall unit area by a factor of 1.70, when

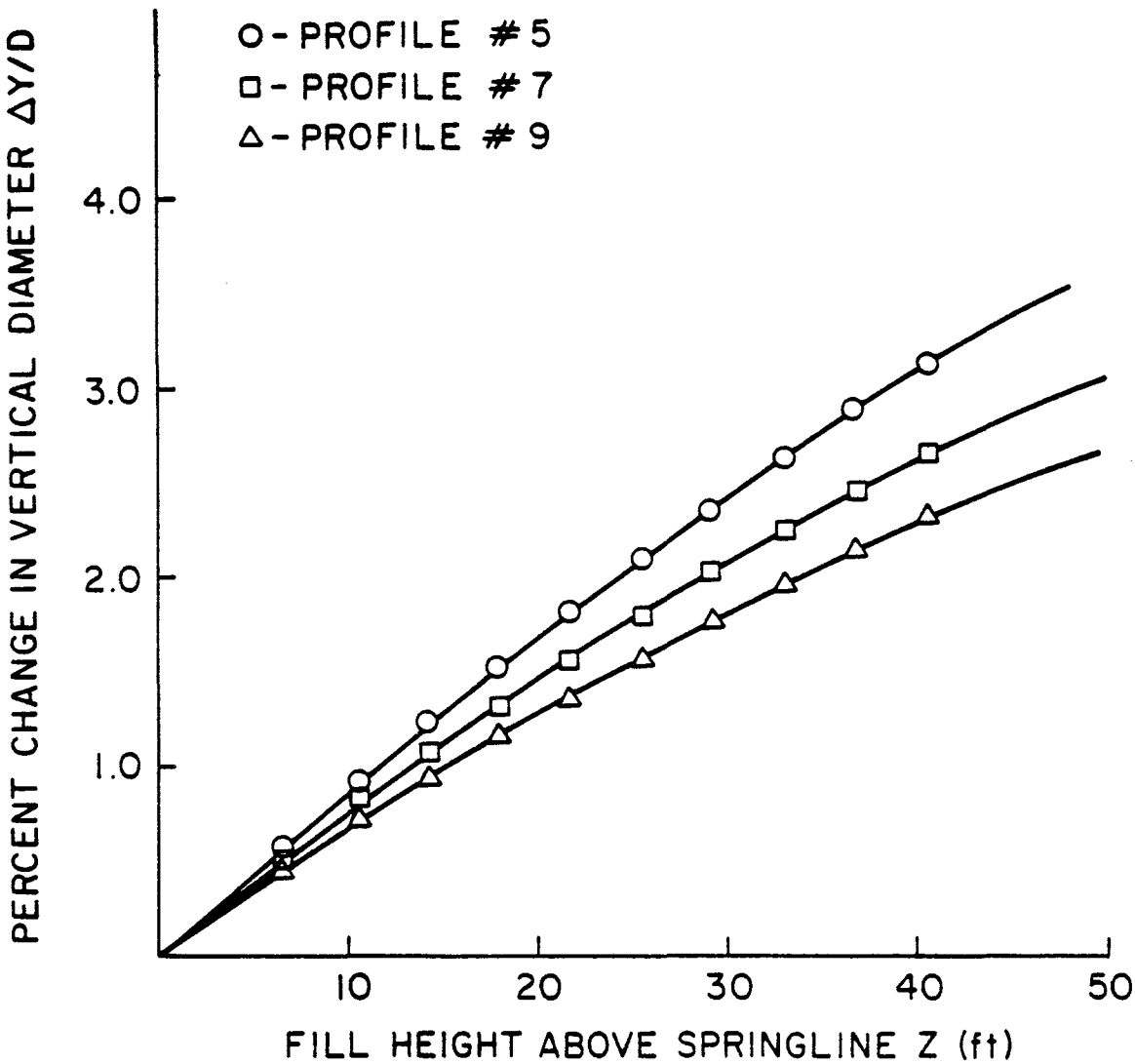

FIGURE 18. Effect of Pipe Profile on Deflections for an 18 in. Pipe

(T=27, P=0, Strong Silt In-situ Soil)

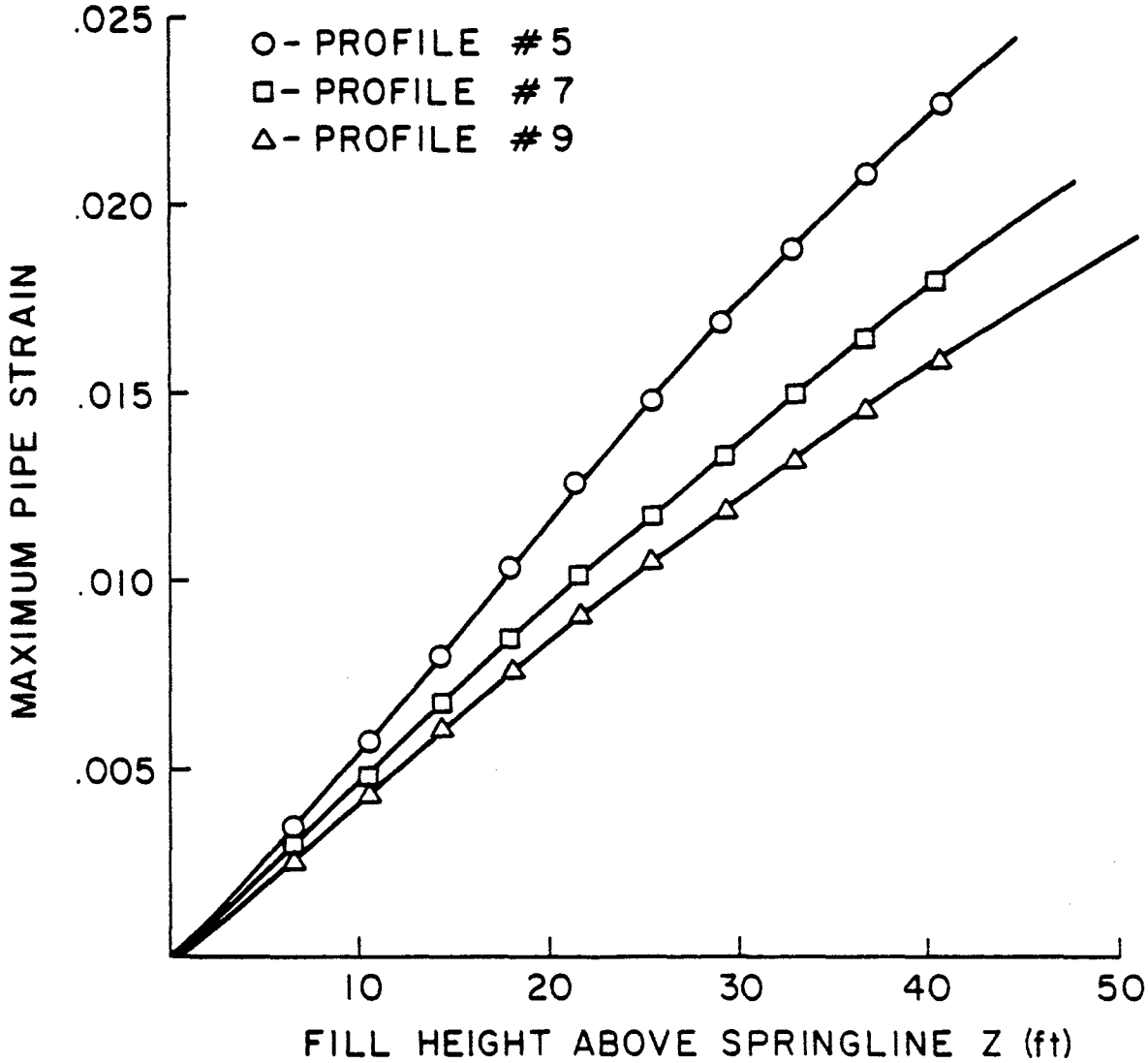

FIGURE 19. Effect of Pipe Profile on Maximum Pipe Strain for an 18 in. Pipe

(T=27, P=0, Strong Silt In-situ Soil)

changing from the #9 Profile to the #7 Profile, is associated with a change in maximum strain of only 1.36. These data do not support the theory that the pipe-wall thrust load is equal to the weight of soil above the pipe. If this were the case, a percentage reduction in pipe area would produce the same percentage increase in strain. Instead of the thrust load being constant for all pipe sizes and stiffnesses, the smaller pipe sizes increase the thrust load carried by the soil arch around the pipe and reduce the amount of load carried by the pipe.

Since the effect of pipe stiffness was shown to be minimal in the preliminary study as well as in full-scale tests (24), only two different pipe diameters, having the same cross section, were used in the factorial study. The effect of pipe diameter and the EI/r^3 ratio could thus be analyzed simultaneously.

Water Table Depths

Large amounts of ground water above a flexible pipe can greatly affect pipe performance; therefore, different water table heights, expressed as a fraction of the soil height, were investigated using effective stress concepts. Effective unit weights of the soil elements were used in conjunction with hydrostatic water pressure boundary conditions around the pipe. The effect of different percentages of water table heights on pipe deflection and maximum pipe-wall strain is shown in Figures 20 and 21, respectively. The variation in maximum strain is much larger than the variation in deflection. The larger strains are produced by the higher thrust load on the pipe. Since the water pressure loads are not reduced by soil

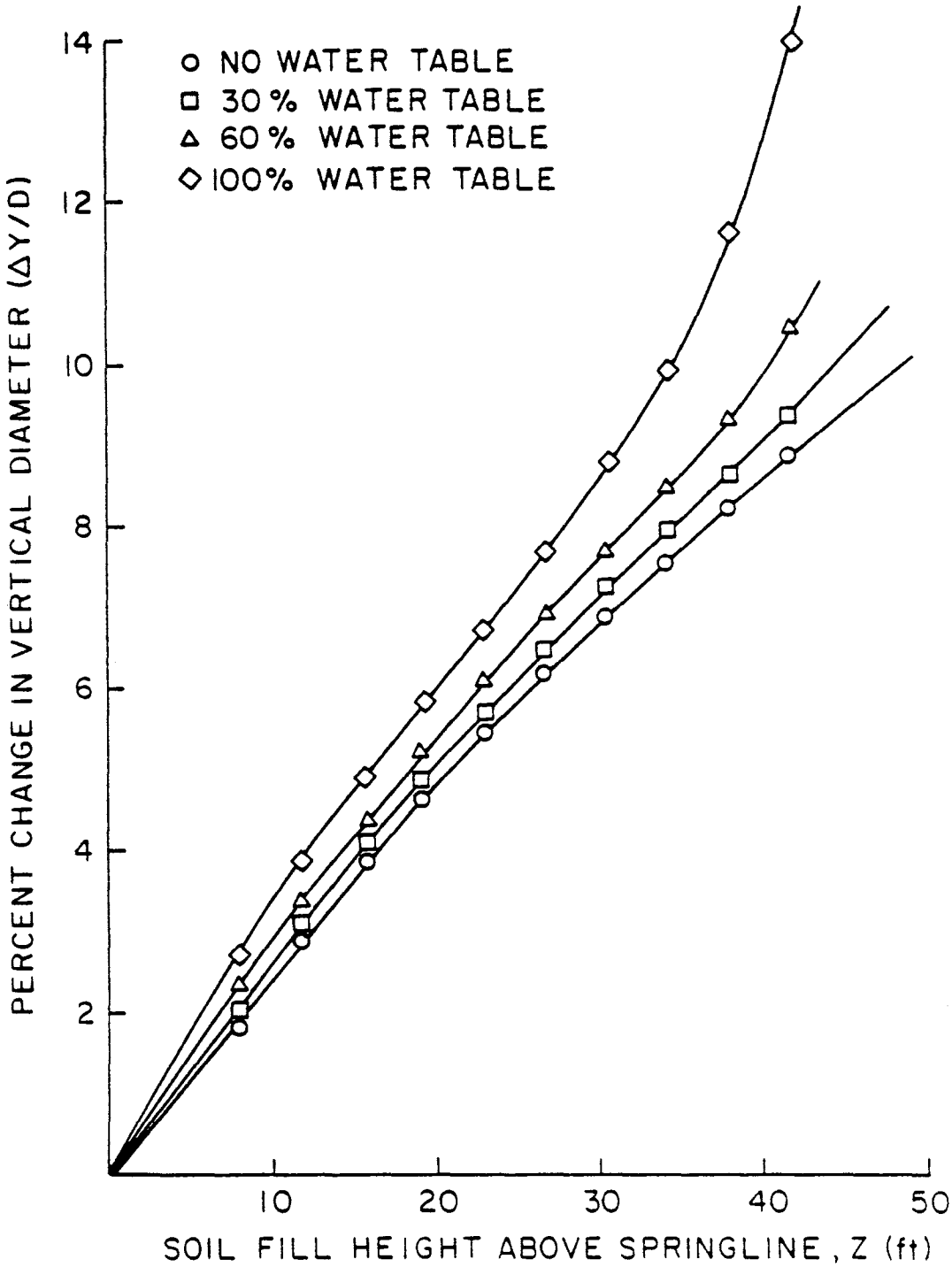

FIGURE 20. Effect of Percent Water Table Height on Pipe Deflection

(D=48, Weak ML, Profile #9, T=96)

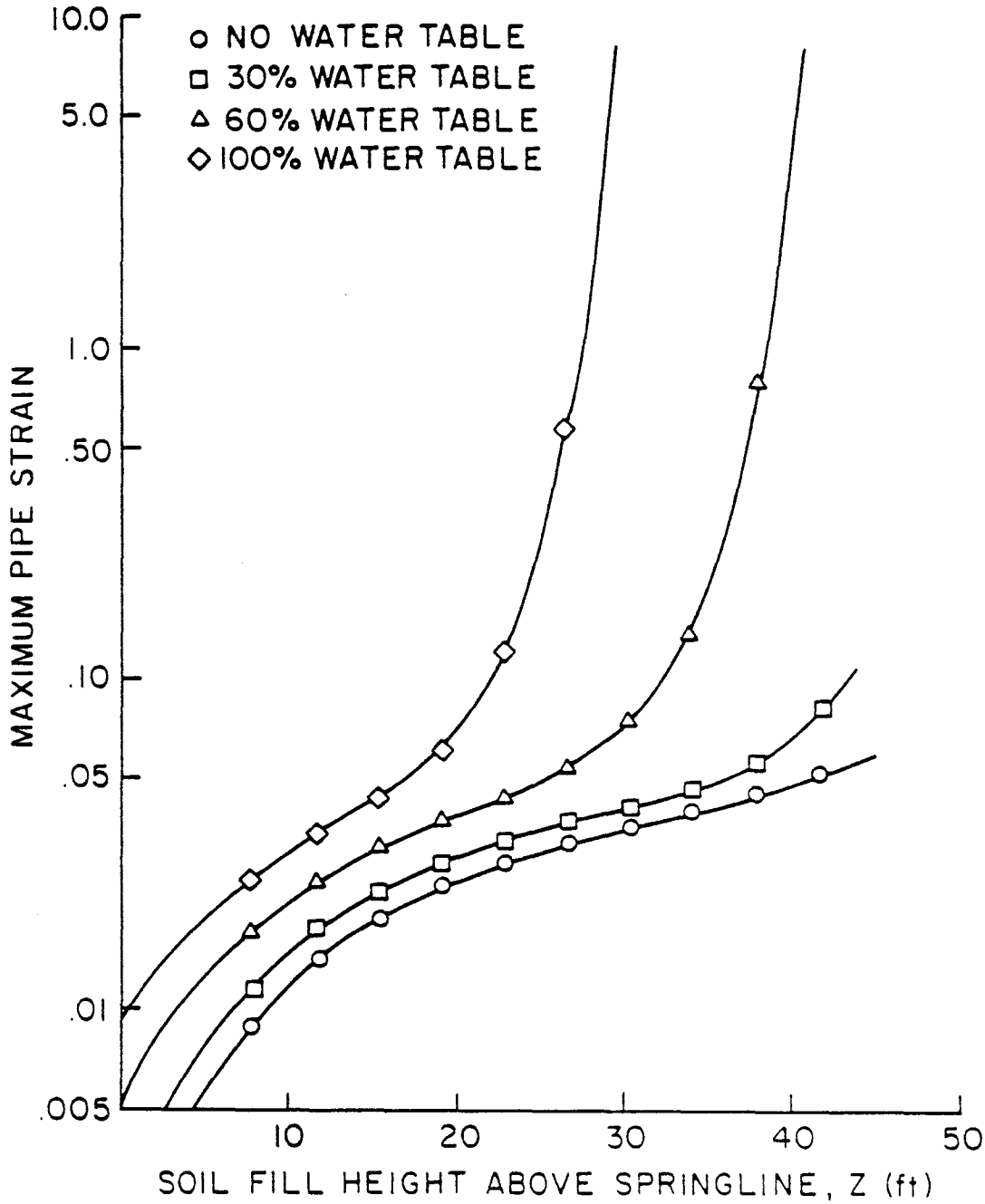

FIGURE 21. Effect of Water Table Heights on Maximum Pipe Strain

(D=48, Weak ML, Profile #9, T=96)

arching, the water table runs produce a higher thrust load than the dry case (see Figure 22).

The hydrostatic pressures due to the ground water also cause a larger, but more even, normal pressure distribution (see Figure 23). This smoother normal distribution produces moments which are smaller than the dry ground case (see Figure 24) and changes the strain distribution (see Figure 25). Figure 26 shows the deformed shape of 48 inch #9 Profile pipe buried to a depth of 30.5 feet. Figures 22 through 26 are for the above mentioned pipe embedded in a weak silt in-situ soil and backfilled with a low density granular material. The properties of this backfill material are typical of conservative values for a low density fill material.

Four water table depths were used in the factorial analysis in order to create a data base which fully represented the interaction of the ground water parameter with the other factorial variables. Water table heights of 0, 30, 60, and 100 percent of the total height were investigated for each combination of pipe size, soil type, height of cover, and trench width.

TRENCH WIDTH

Many engineers in the underground conduit industry regard trench width as an important design parameter. The contention is that a larger zone of granular backfill material beside the pipe will reduce the amount of load transferred to the pipe. This reduction in lateral load due to the larger trench width is assumed to produce smaller

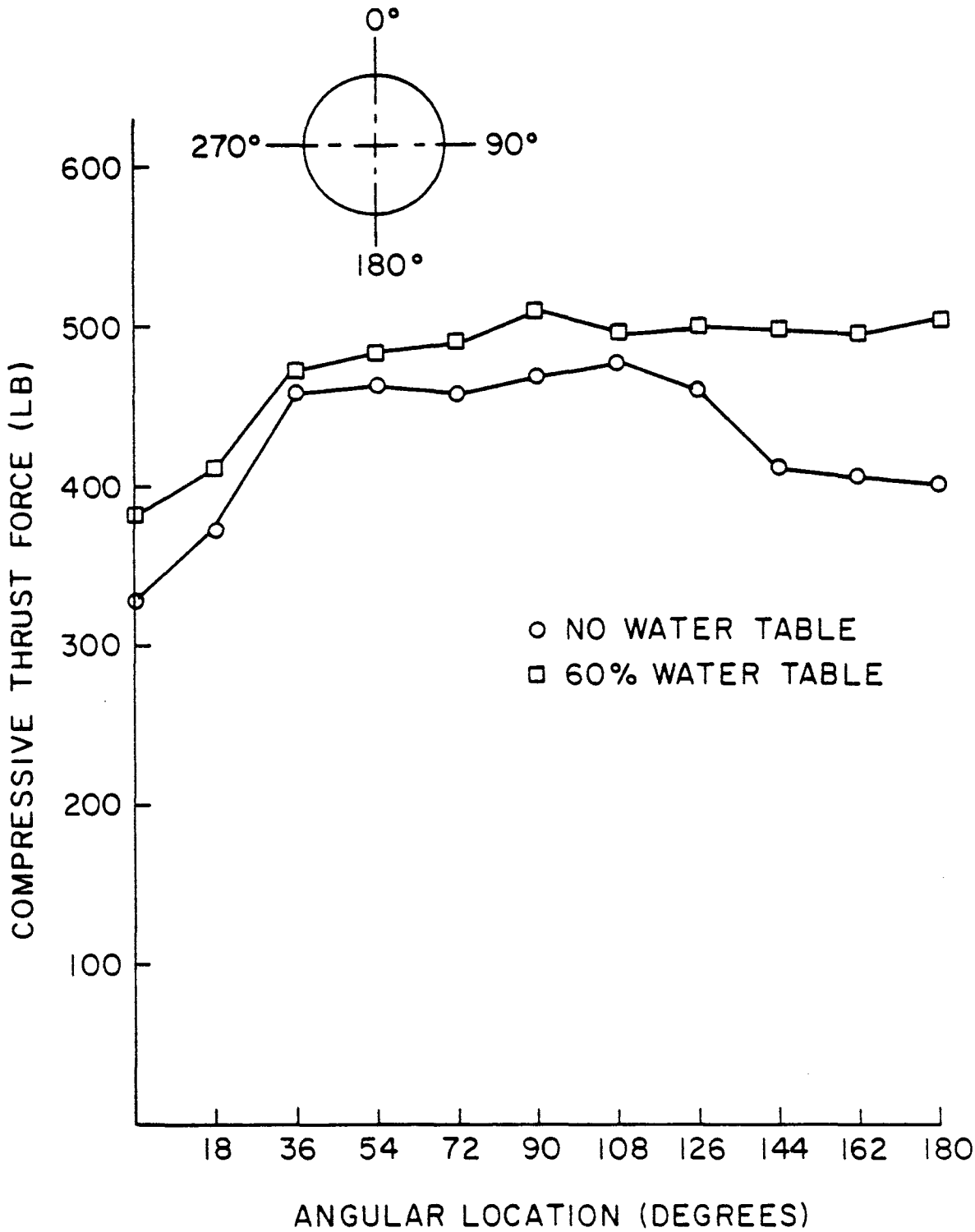

FIGURE 22. Effect of Water Table on Thrust Load

(D=48, Profile #9, T=72, Z=30.5, Weak Silt In-situ)

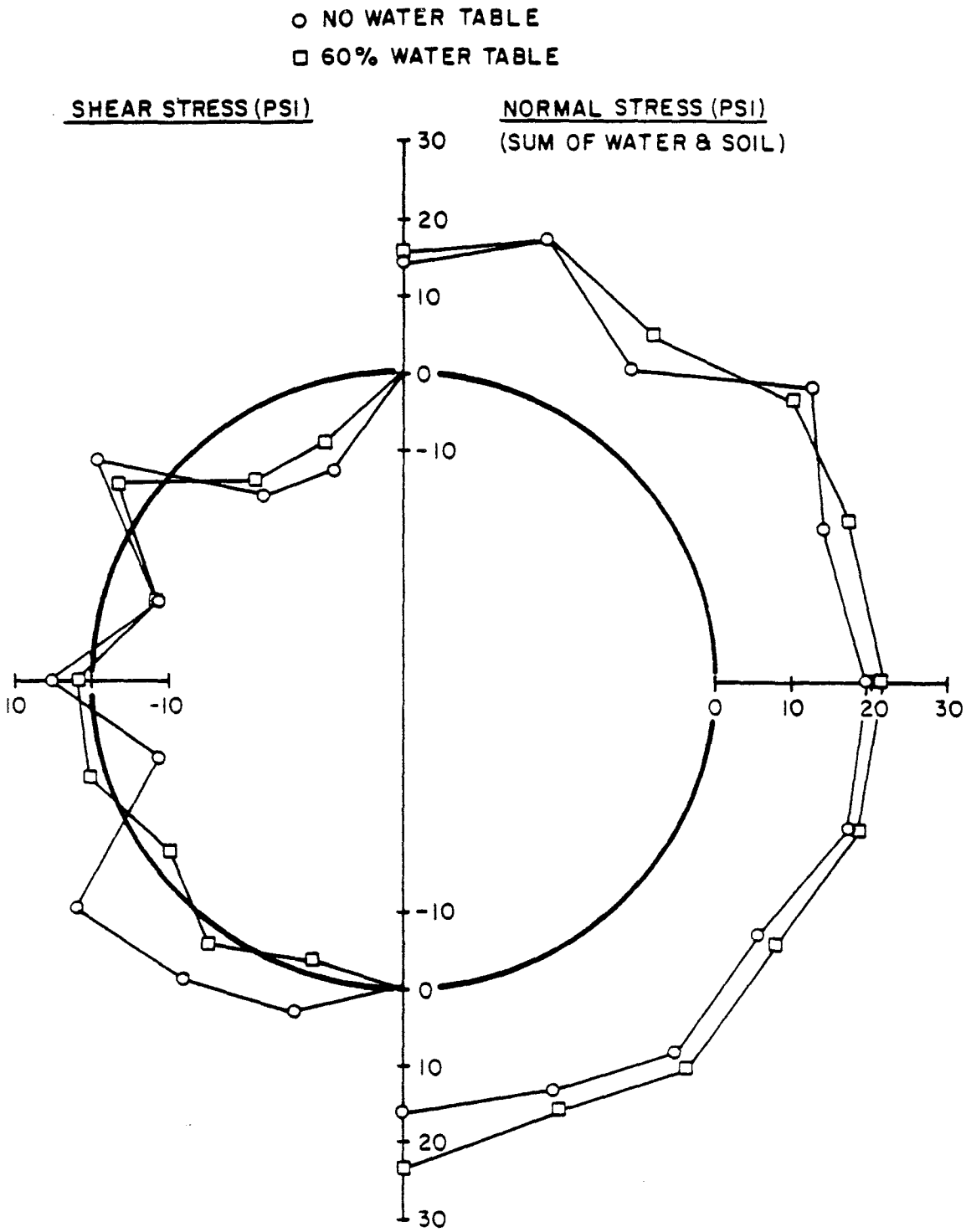

FIGURE 23. Effect of Water Table on Normal and Shear Pressures

(D=48, Weak ML, Profile #9, T=72, Z=30.5)

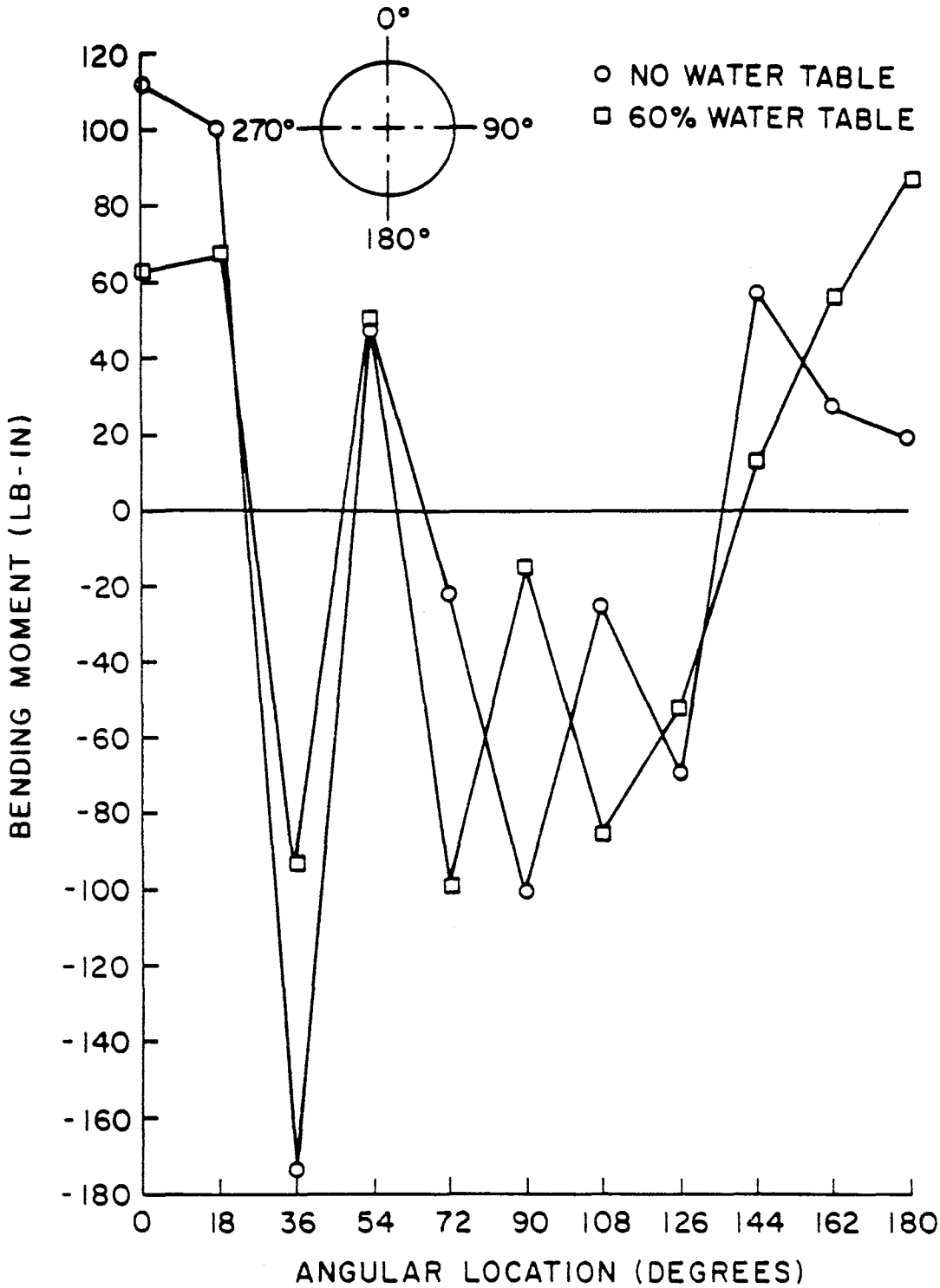

FIGURE 24. Effect of Water Table on Bending Moments

(D=48, Profile #9, T=72, Z=30.5, Weak Silt In-situ Soil)

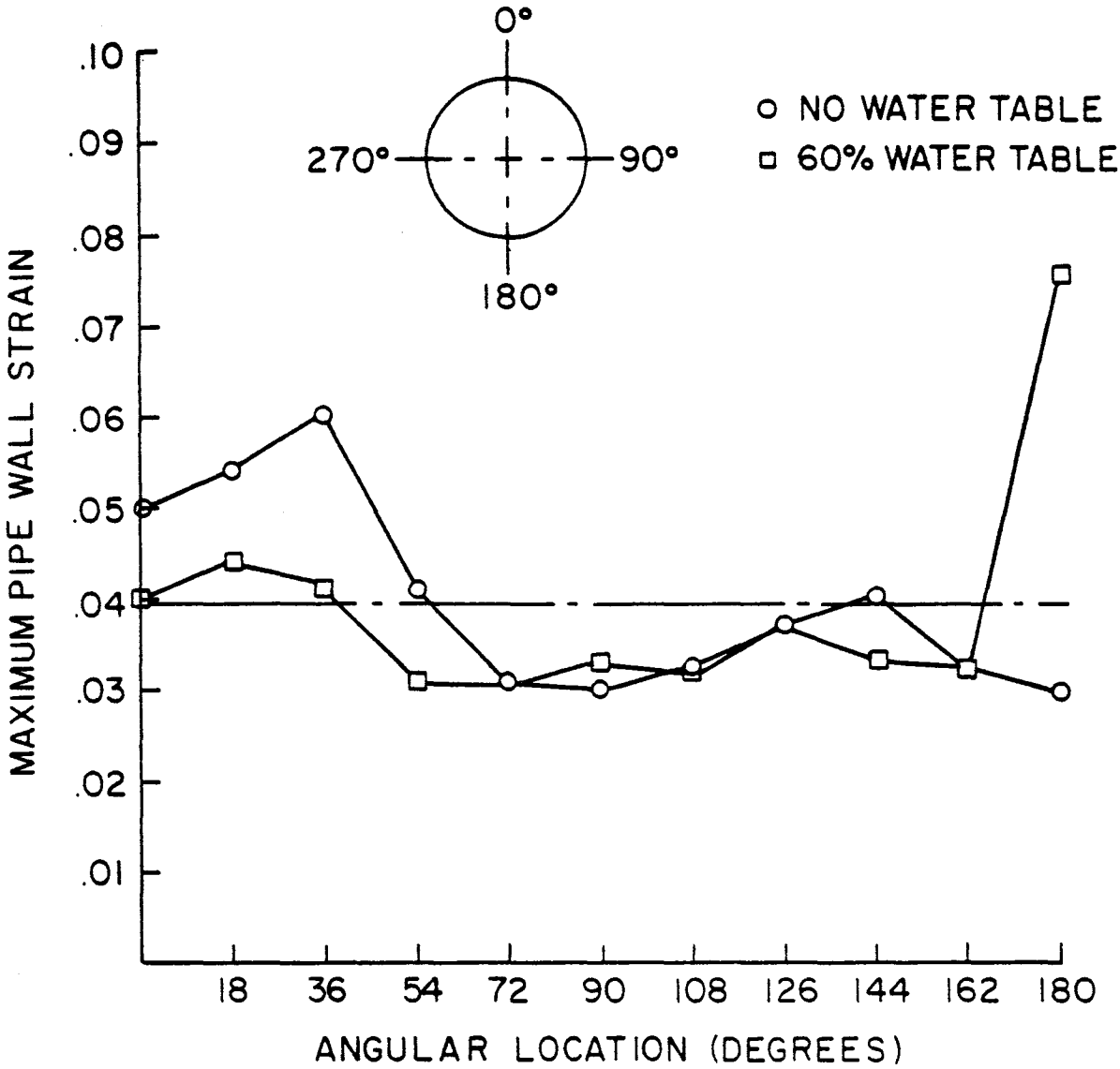

FIGURE 25. Effect of Water Table on Maximum Pipe-Wall Strain

(D=48, Profile #9, T=72, Z=30.5, Weak Silt In-situ Soil)

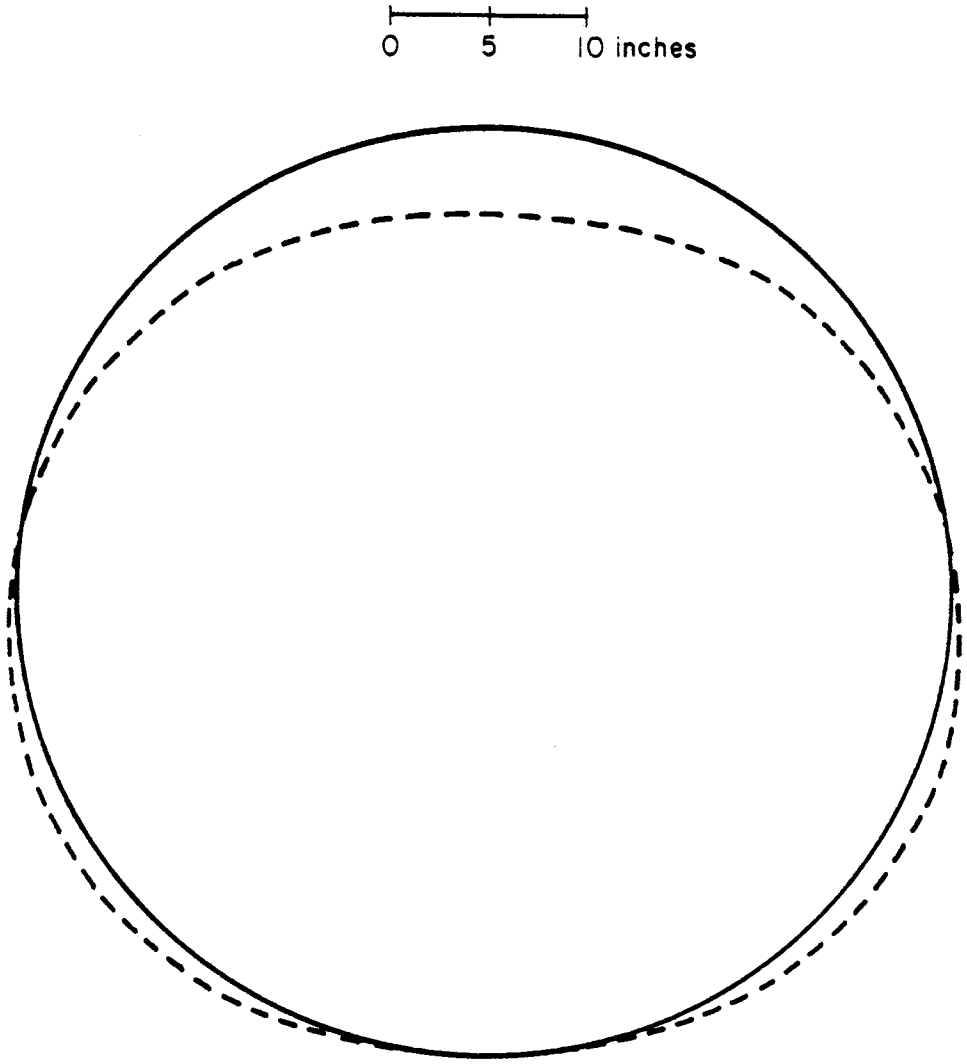

FIGURE 26. Deformed Shape for a 48 in. #9 Profile Pipe With a 60% Water Table

(Weak ML, Z=30.5, T=72)

deflections in the flexible pipe. Because of this strong contention in the industry, the factorial study incorporated three different trench widths: 125, 150, and 200 percent of the pipe diameter.

This study shows that varying trench width has a small effect on pipe performance. Even with a weak in-situ soil, varying the trench width from 125% of the pipe diameter to 150% of the pipe diameter produced only small changes in percent vertical deflection ($\Delta y/D$) and maximum pipe-wall strain (ε_p) (see Table 5). In fact, for this condition the smallest trench width actually produced smaller deflections and strains for depths of cover above the springline, Z, greater than 23 feet. In order to understand this concept, one must investigate the mechanics which dictate the performance of a very flexible pipe:

1. The amount of lateral pressure exerted on the pipe is somewhat reduced by increasing the trench width as can be seen in Figure 27; however, reducing the amount of lateral pressure on the pipe will not reduce the amount of vertical deflection. In fact, increasing the amount of lateral pressure will squeeze the pipe together, reducing the vertical deflection as Table 5 indicates.
2. Soil arching or the reduction in overburden pressure at the pipe crown can be mobilized with small amounts of backfill above and beside the pipe. The fraction of the overburden pressure felt by the pipe crown is relatively the same for the three trench widths studied.
3. The smallest trench width also produces a more uniform pressure distribution than the wider trench widths as can be seen by

TABLE 5. Effect of Varying Trench Width for a 48 in. Pipe in a Weak Soil

Z ft	$\Delta Y/D$ %			ε_p (max)		
	T=1.25D	T=1.5D	T=2.0D	T=1.25D	T=1.5D	T=2.0D
8	4.27	4.02	4.06	.0091	.0087	.0099
11.75	6.05	6.05	6.15	.0233	.0242	.0216
15.5	7.23	7.33	7.44	.0327	.0325	.0288
19.25	8.10	8.35	8.47	.0389	.0379	.0366
23.00	8.88	9.27	9.43	.0450	.0453	.0466
26.75	9.60	10.09	10.27	.0523	.0586	.0601
30.5	10.28	10.85	11.04	.0618	.0734	.0733
34.25	10.94	11.56	11.78	.0742	.0911	.0892
38.0	11.59	12.24	12.48	.0880	.1063	.1013
41.75	12.29	12.90	13.13	.0973	.1216	.1098

carefully examining Figure 27. This smoother pressure distribution produces smaller moments in the pipe wall (see Figure 28) and somewhat larger maximum thrust loads (see Figure 29) as can be expected from structural pipe theory explained in the background material section.

4. The larger moments and uneven pressure distributions found with the larger trench width can be explained by looking at the ratio of fill width at the springline to granular backfill height above the crown. For all three trench widths, granular backfill was only used to a height of 0.25 diameters above the crown; the remainder of the trench was filled with in-situ soil. Keeping the ratio of granular backfill soil above the pipe to granular backfill beside the pipe less than or equal to one prevents stress concentrations which produce the larger moment. These larger moments produce a more square deformed shape as is shown in Figure 30 where the deformed shapes for 125% and 200% diameter trench widths are compared.

5. A large isolated bending moment can produce premature failures or plastic hinging in a small portion of the pipe wall even though the remainder of the pipe is functioning at distress levels well below the elastic limit. Full utilization of the pipe material is only obtained when the complete wall section fails due to a uniform compressive thrust load.

The above claims are further verified with some additional 10-year CANDE runs made with a strong silty clay in-situ soil. Figure 31 shows that smaller deflections can be obtained by increasing the

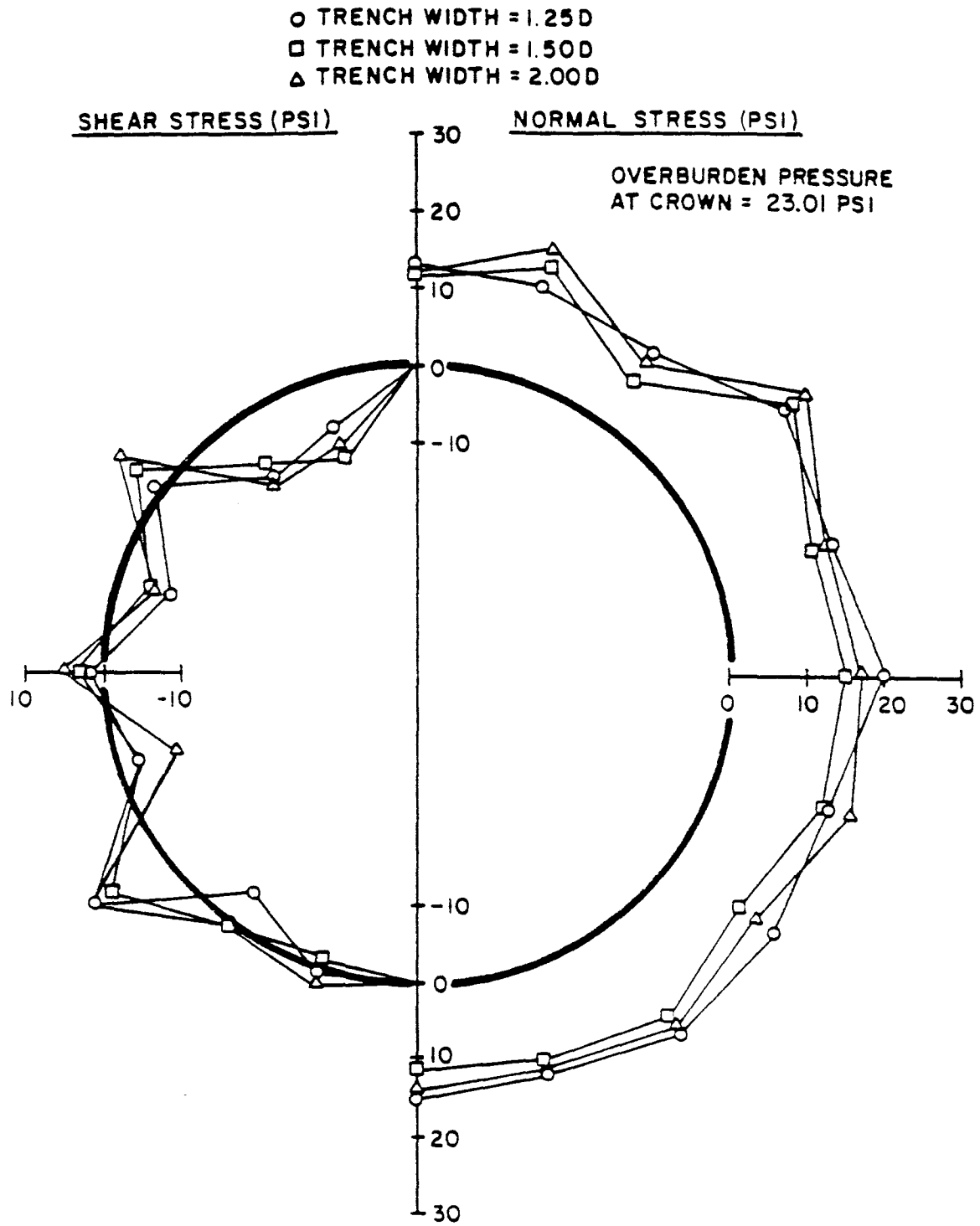

FIGURE 27. Effect of Trench Width on Normal and Shear Stresses

(D=48, Weak ML, Profile #9, P=0, Z=26.75)

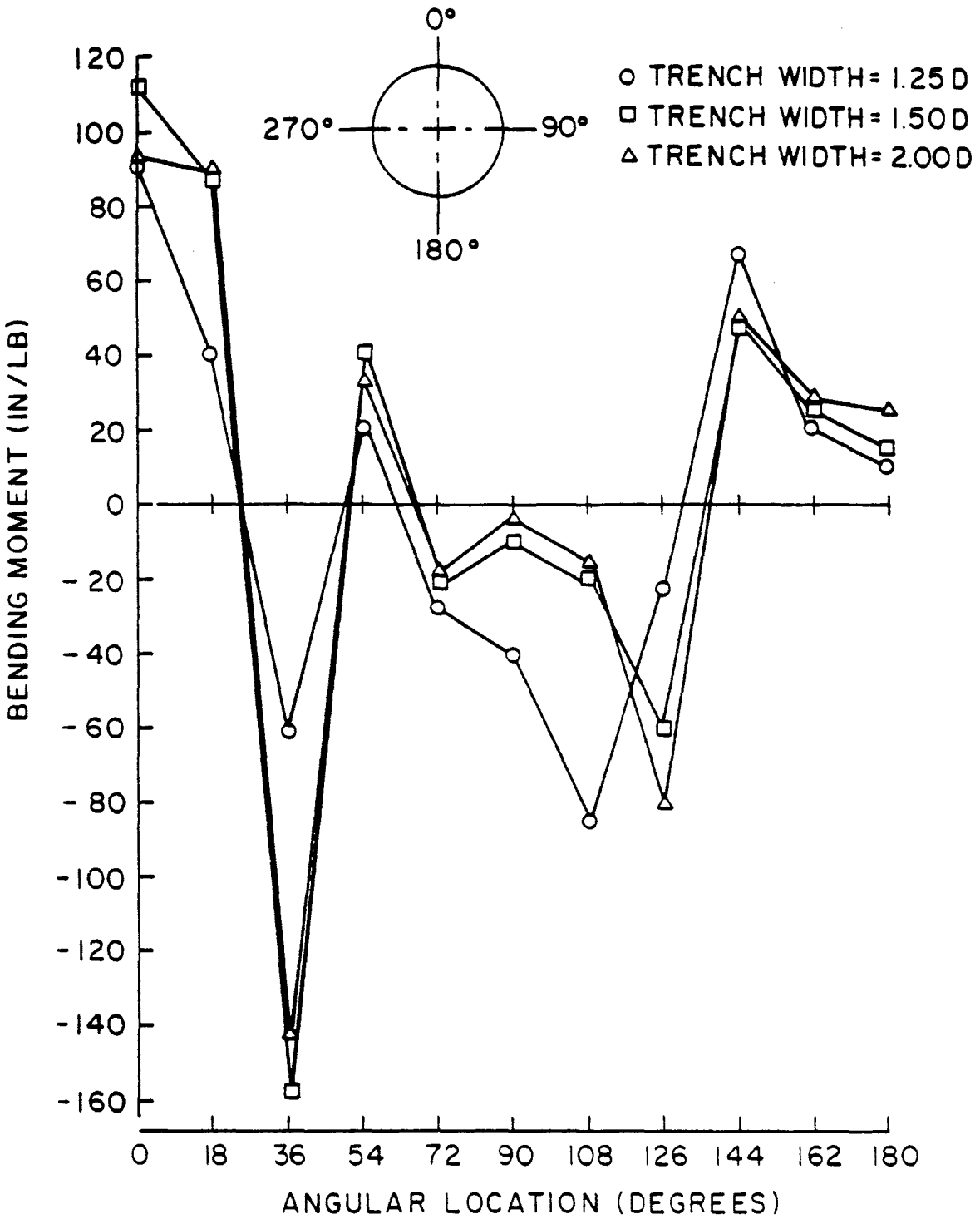

FIGURE 28. Effect of Trench Width on Bending Moment

(D=48, Weak ML, Profile #7, P=0, Z=26.75)

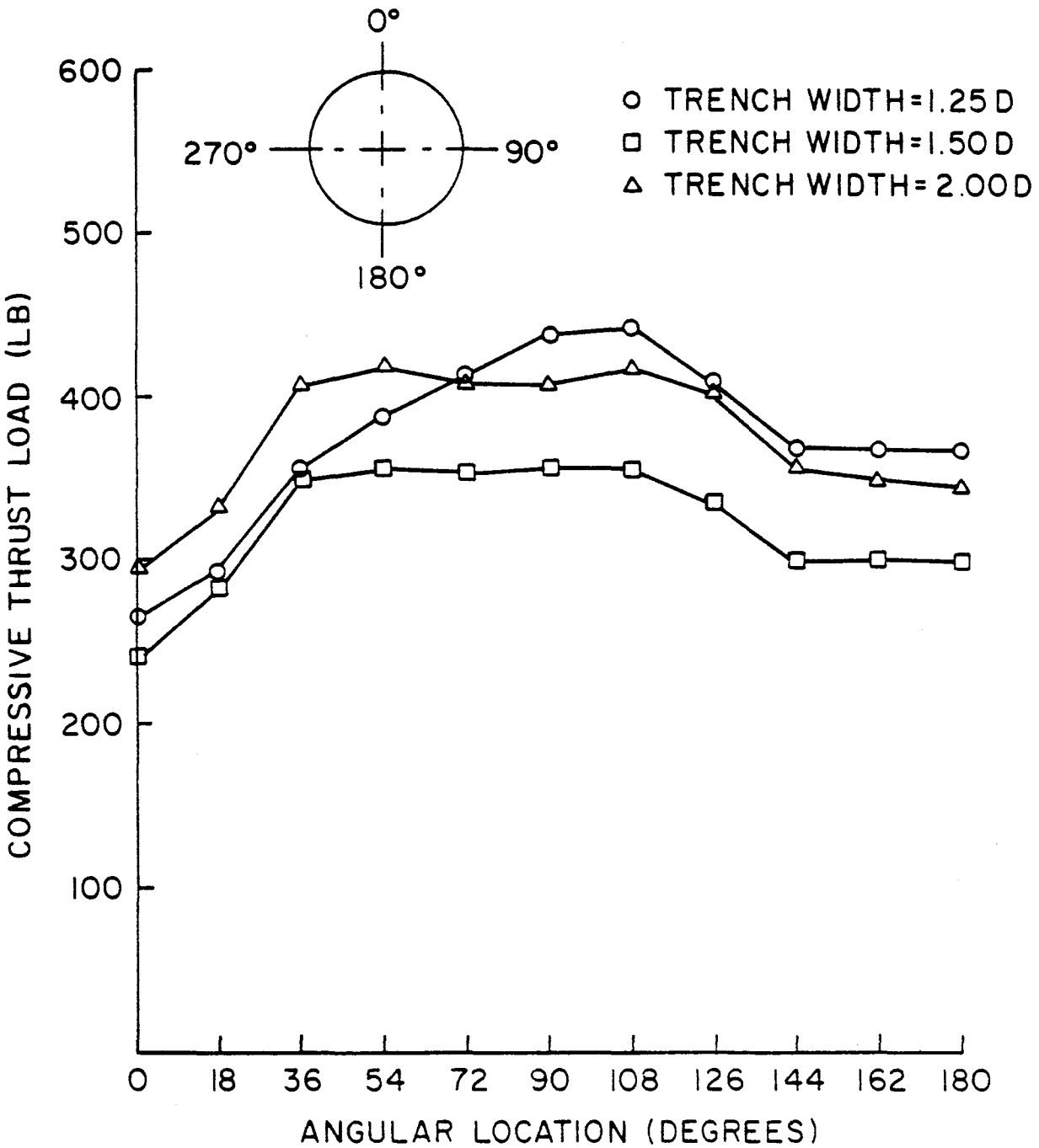

FIGURE 29. Effect of Trench Width on Thrust Load

(D=48, Weak ML, Profile #9, P=0, Z=26.75)

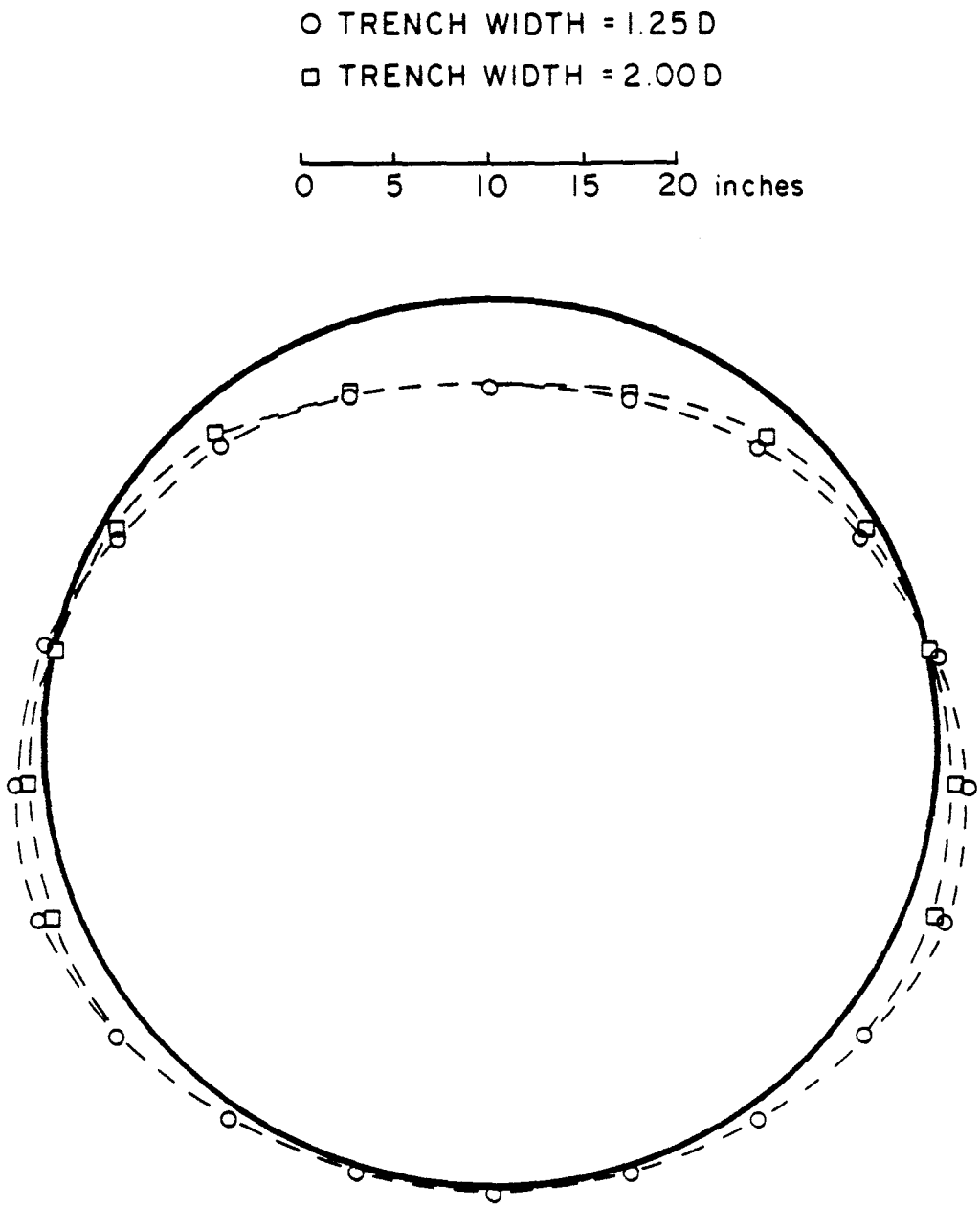

FIGURE 30. Deformed Shape for T=1.25D and T=2.00D
(D=48, Weak ML, Profile #9, P=0, Z=26.75)

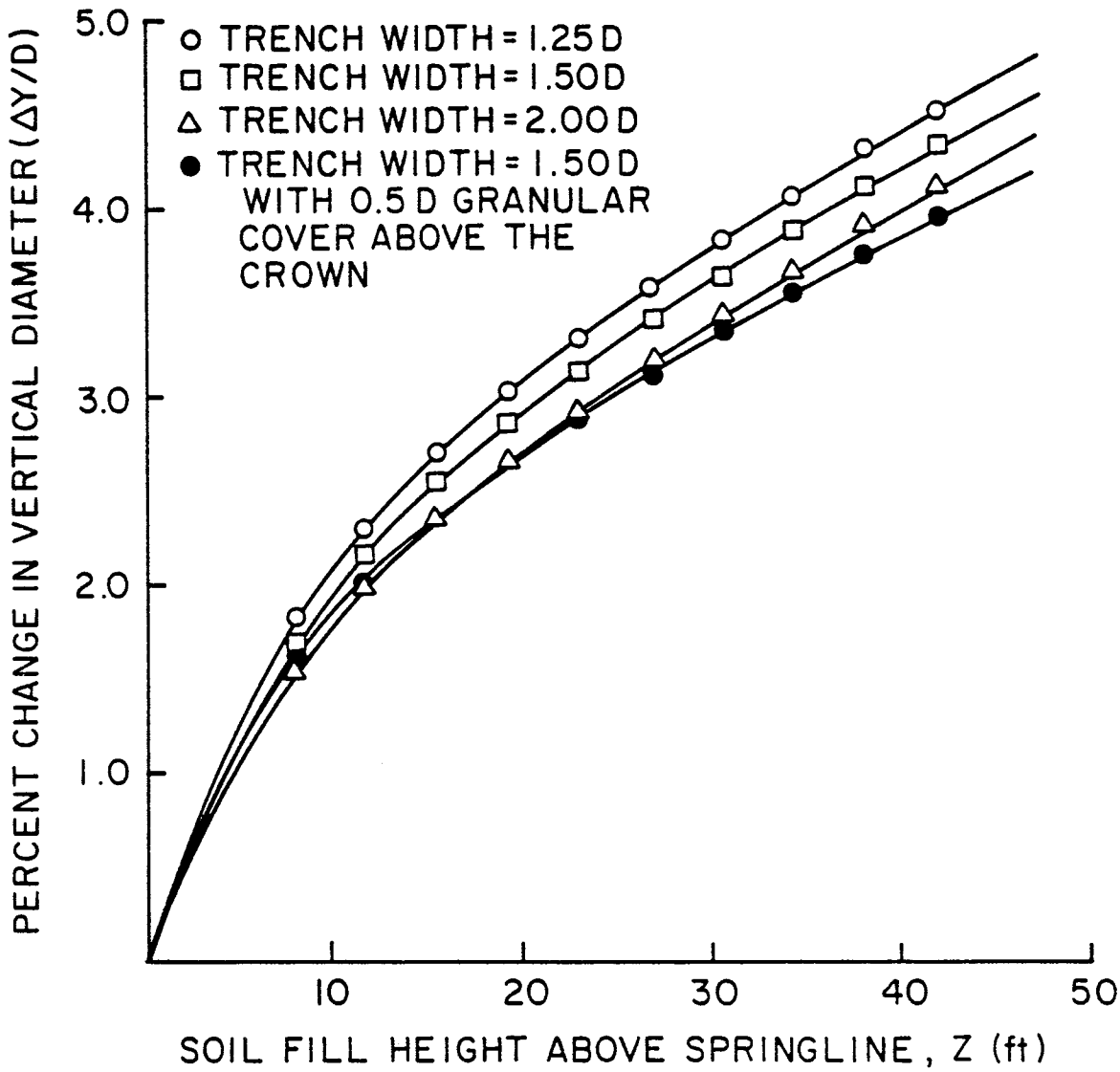

FIGURE 31. Effects of Trench Width and Granular Backfill Height on Pipe Deflection With a Silty Clay In-situ Soil

(D=48, Profile #9, P=0)

thickness of the granular backfill above the crown than can be obtained by increasing the trench width. The additional fill material above the pipe reduces the maximum moment on the pipe which, in turn, reduces the deflection. The additional fill above the pipe, however, does not significantly reduce the maximum pipe-wall strain (see Figure 32). In fact, no reduction in compressive strain should be expected since the thrust load on the pipe is not significantly reduced by simply increasing the amount of granular backfill above the pipe.

It is apparent that solely reducing the amount of lateral load transferred to the pipe will not necessarily promote better pipe performance. The crucial factor is to have a backfill configuration which will produce an even pressure distribution around the pipe. This will reduce the amount of bending moment and allow full utilization of the pipe-wall section.

Summary of Factorial Design Variables

Three trench widths equal to 125, 150, and 200 percent of the pipe diameter were used in the factorial analysis. Four different water table heights, 0, 30, 60, and 100 percent of the total height, were investigated using effective stress concepts. Effective unit weights of the soil elements were used in conjunction with the water pressure boundary condition around the pipe. The five in-situ soil types shown in Table 5 were also incorporated into the full factorial analysis. These basic variables are shown graphically in Figure 29. Each combination of in-situ soil type, trench width, water table height, and pipe type was investigated at ten depths of cover, ranging

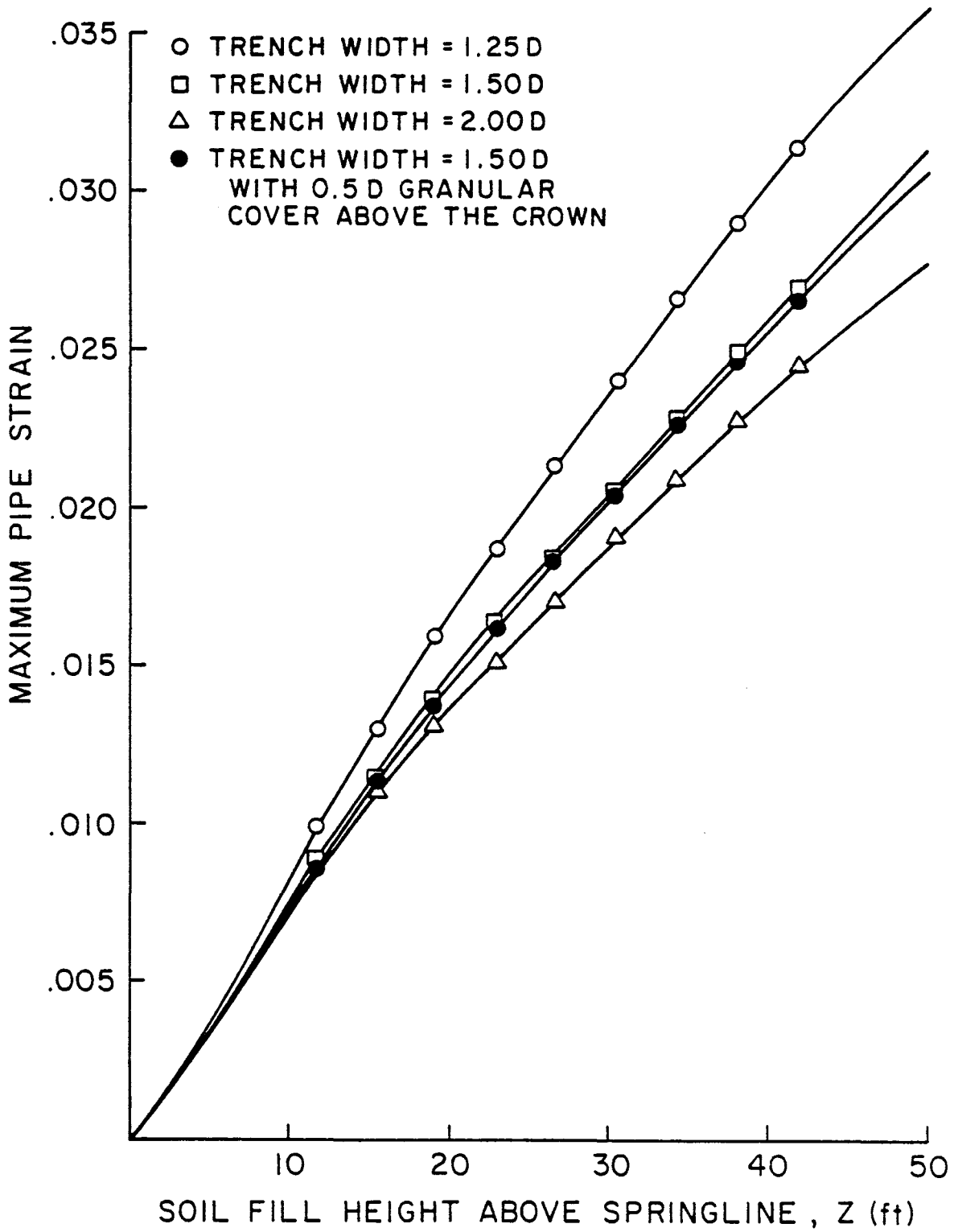

FIGURE 32. Effects of Trench Width and Granular Backfill Height on Maximum Pipe-Wall Strains With a Silty Clay In-situ Soil

(D=48, Profile #9, P=0)

from 8 feet to 42 feet. In total, 1200 observations were recorded from CANDE output in order to establish a complete factorial data base.

BASIC MODEL USED IN THE FACTORIAL STUDY

When establishing a data base from which a design procedure can be reliably established, it is essential to investigate the worst possible combination of design conditions. As previously stated, if the properties of a given variable are somewhat unpredictable, a conservative estimate was made. By fixing some of these variables at a conservative value in the basic model, it was possible to create a data base containing a worst case set of pipe responses. The design equation created from this data base should, therefore, be conservative and reliable.

In addition to using the properties for a rather weak backfill material and bedding the pipe in the in-situ soil (of which both would be considered poor construction techniques for flexible pipe installation), a conservative assumption was made about the soil-pipe interface. No slippage was allowed at the soil-pipe interface. This condition creates larger displacements than a full-slip condition, as is shown in the Parameter Study section. These results are in general agreement with those shown by Leonard (14) and Katona (24). Since it is hard to determine the actual interface properties without extensive testing, the conservative approach is again the best.

The effects of changing the conservative properties used in the

basic model is illustrated in the Parameter Study section. The effect of these assumptions on the design equations which were created from the full factorial data base is also investigated.

The CANDE Level 2 automatic mesh generation option was used to approximate the Basic Geometry shown in Figure 33. The complete standard mesh (see Figure 34), generated from a few input cards, was constructed incrementally before applying any water pressure boundary conditions. This was done in order to simulate actual construction procedures, where pore pressures only build up after the trench is filled.

Pipe responses for depths of cover greater than the mesh height were calculated by applying incremental line loads at the top of the mesh equal to the overburden pressure. Incremental water pressure loads were also applied to the pipe during each additional construction increment to maintain a constant ratio of water table to total height. Recording the data for the regression analysis was started for the first construction increment in which water pressure was applied.

ADDITIONAL FINDINGS

In the past, deflection has been the major design criterion for flexible plastic pipes. This practice stemmed from rigid pipe design, where relatively small deflections produced high enough strains to fail brittle material. However, high density polyethylene has a large strain capacity. This material property, coupled with the general

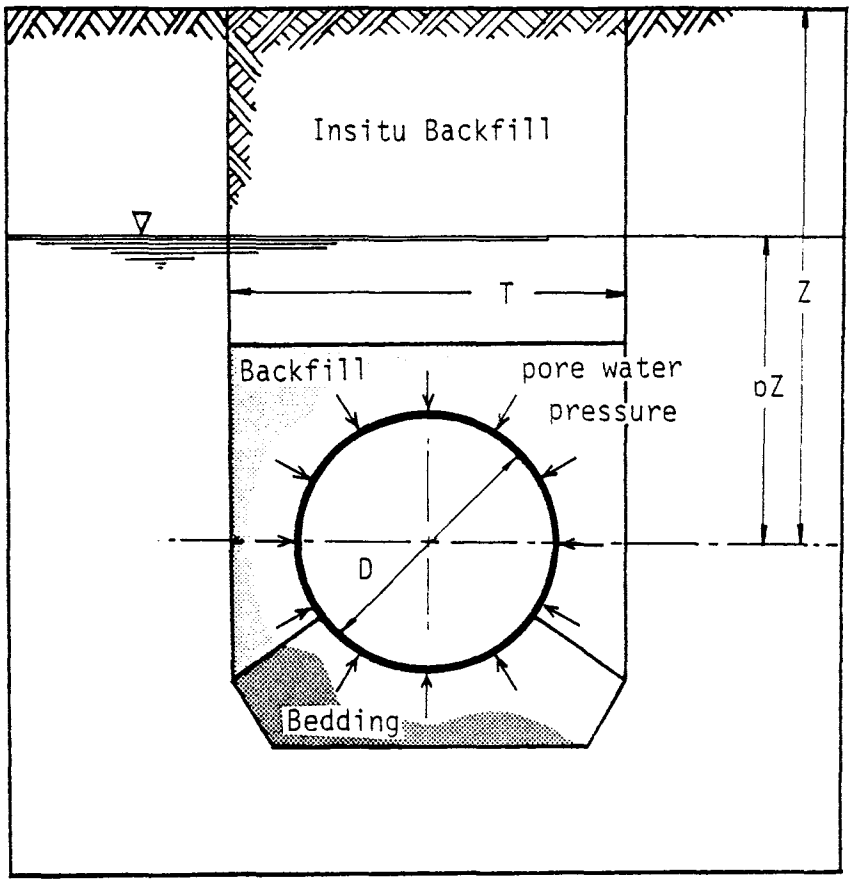

FIGURE 33. Basic Geometric Properties

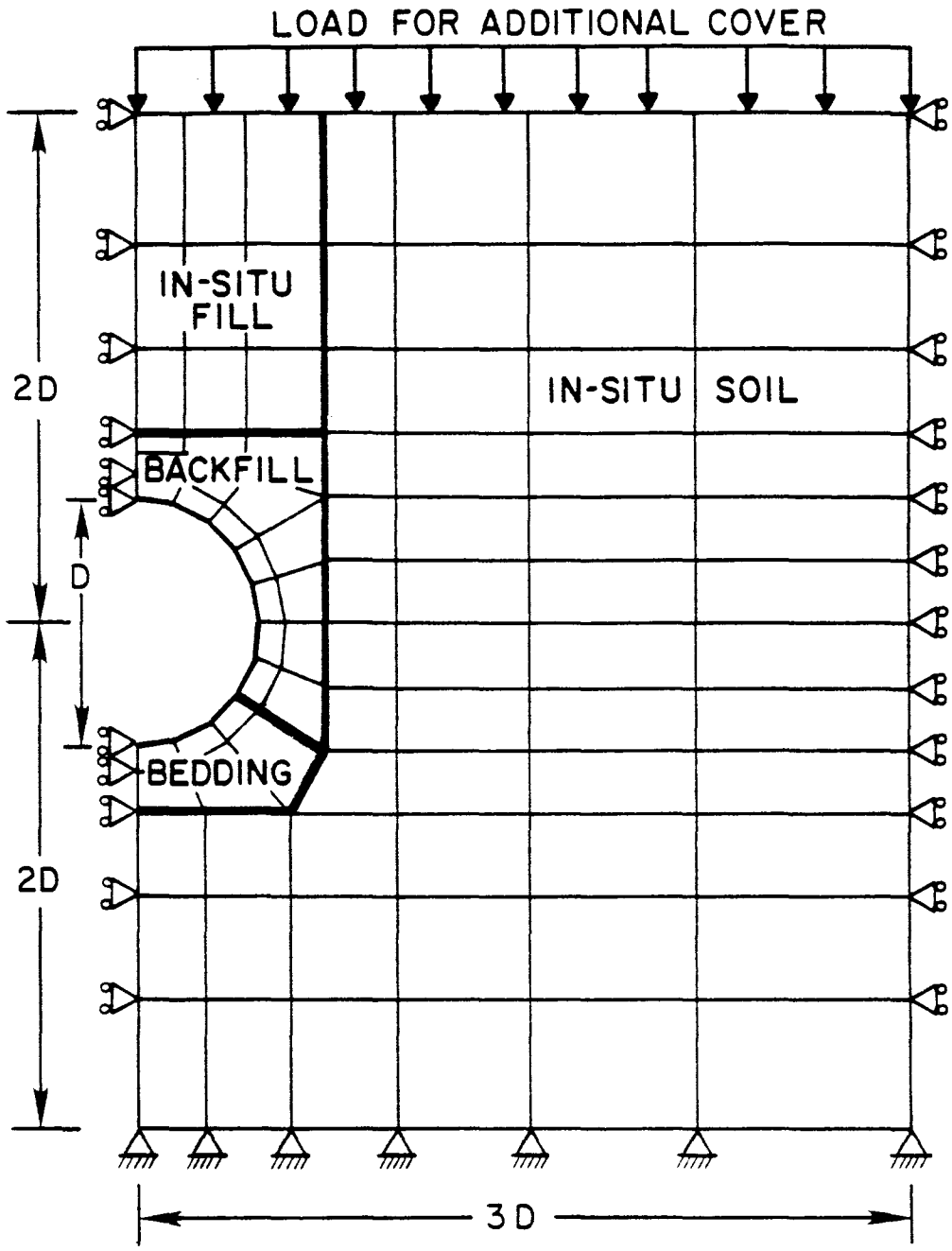

FIGURE 34. Finite Element Mesh

flexibility of the complete pipe, suggests that higher allowable design values for deflection and strain should be used in flexible plastic pipe design. Full scale test studies have suggested that pipe deflections up to 20% are acceptable (25).

Deflections of this magnitude may occur without pipe failure, but they may produce strains above the elastic limit. Table 6 shows the values of maximum fiber strains and percent vertical deflections predicted by the modified CANDE program for a typical run in the factorial analysis. The fact that the ten year yield strain of 0.0393 was exceeded at a deflection of approximately 6.5% is of little consequence when designing a polyethylene pipe which has an ultimate tensile strain of 800%. A typical stress-strain curve for high-density polyethylene and the CANDE bilinear approximation which was used to model it are shown in Figure 35.

Since a ductile pipe can perform equally well at high deflections as long as the strain levels are below the allowable, a more efficient design procedure should be based on strains instead of deflections.

Two additional findings are that dead load due to the weight of the soil mass above the pipe produces compressive yielding of the pipe wall and that in the absence of high live loads the vertical percent deflection is always higher than the horizontal deflection. The yielding in compression is observed because the compressive thrust load produces larger stresses than the typical moments carried by the flexible polyethylene pipe.

TABLE 6. Maximum Pipe Strain and Deflection for Different Depths of Cover

Depth of Cover Z	Maximum Pipe Strain	Deflection $\Delta Y/D$
8	.0046	0.77
11.5	.0081	1.27
15	.0134	2.37
18.5	.0194	3.23
22	.0235	3.88
25.5	.0272	4.49
29	.0308	5.09
32.5	.0344	5.69
36	.0379	6.29
39.5	.0415	6.87

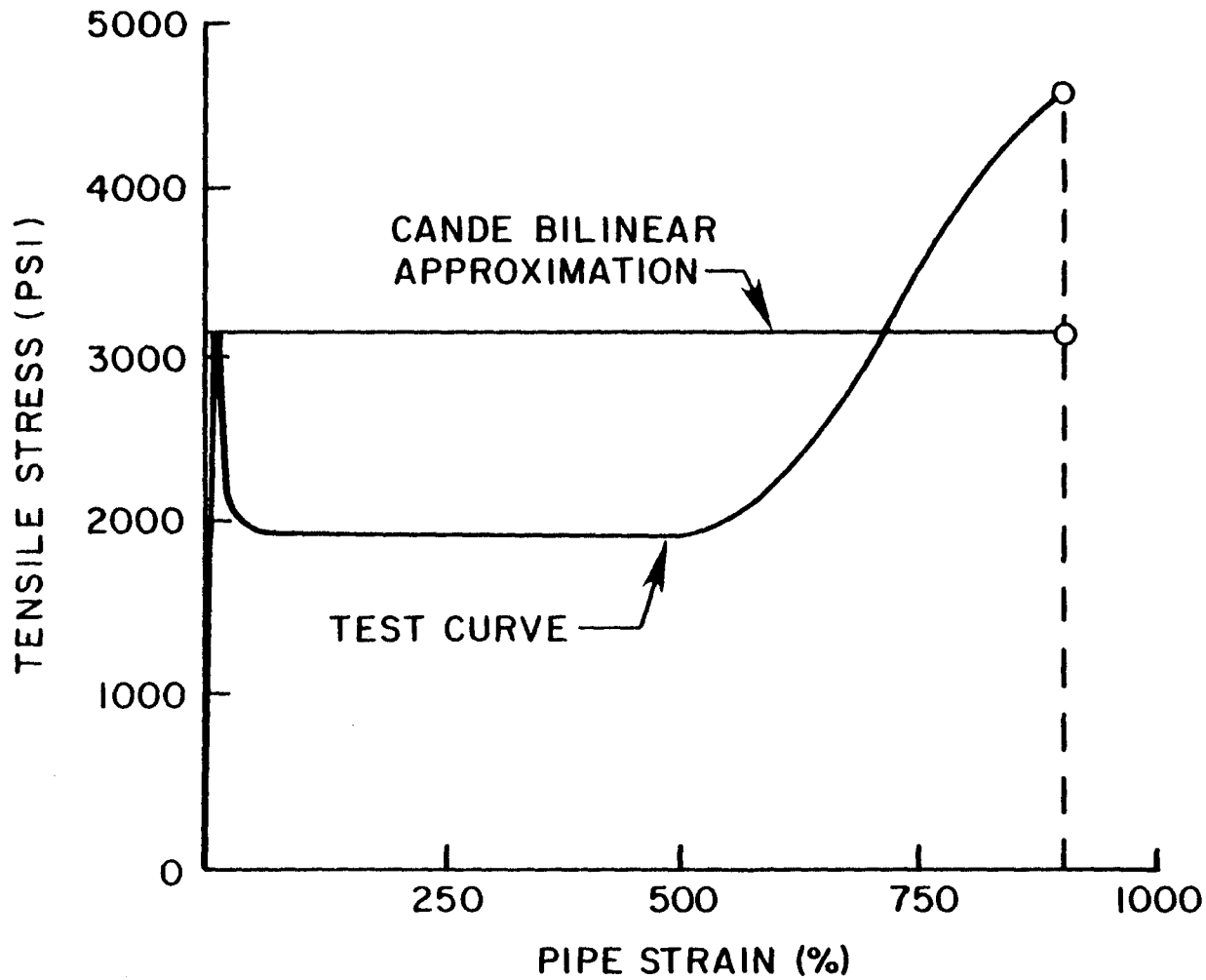

FIGURE 35. Comparison of CANDE Bilinear Stress-Strain Curve With Actual Stress-Strain Data

REGRESSION DESIGN EQUATIONS

The complete factorial analysis produced a data base containing 1200 predictions of pipe performance. Regression analysis was used to find the best fit equations for maximum pipe-wall strain and vertical deflection in terms of known or directly calculable design parameters.

First, a method of predicting a secant elastic modulus, E', of the soil around the pipe was established. A general hyperbolic representation of the backfill material, as explained in the Duncan Soil model section, was adopted:

$$\sigma_b = \frac{\varepsilon_b}{a+b\varepsilon_b} \qquad \text{or } \varepsilon_b = \frac{a\ \sigma_b}{1-b\sigma_b} \tag{45}$$

where

σ_b = the average backfill soil stress,

ε_b = the average backfill soil strain, and

a,b = material constants for the backfill material.

The secant elastic modulus can be defined as the average soil stress divided by the average soil strain.

$$E'_b = \frac{\sigma_b}{\varepsilon_b} = \frac{1}{a+b(\varepsilon_b)} \tag{46}$$

The average stress can be expressed in terms of an empirical number, K_o, and the effective overburden pressure, $\gamma'_t Z$.

$$\sigma_b = K_o \gamma'_t Z \tag{47}$$

where

γ'_t = the average effective unit weight of the in-situ soil,

Z = depth of cover above the springline, and

K_o = dimensionless empirical pressure coefficient.

The empirical number, K_o, can be determined by combining Equations 46 and 47.

$$K_o = \frac{\varepsilon_b}{\gamma'_t Z \varepsilon_b(b) + \gamma'_t Z(a)} \tag{48}$$

The average of the horizontal and vertical strains in the granular backfill at the springline of the pipe were recorded for each observation in the data set. This value was used in Equation 48 to calculate a value for K_o. The standard form for the soil constants a and b (6) was altered slightly in order to produce an expression which can be evaluated without determining confining pressure.

$$1/a = \bar{E}_{ib} = K_b p_a \left(\frac{\gamma'_t Z}{p_a}\right)^{n_b} \tag{49}$$

$$1/b = \frac{2\ C_b \cos \phi_b + 2\gamma'_t Z \sin \phi_b}{R_{fb}(1 - \sin \phi_b)} \tag{50}$$

where

K_b, n_b, R_{fb} = Duncan soil parameters for the backfill material,

ϕ_b = the friction angle for the backfill material, and

C_b = the cohesion of the backfill material.

A set of linear regressions was performed to determine the variables or combination of variables that best predict K_o. The final model, containing seven basic variables, produced an R-squared of 0.88. K_o can be estimated by the following equation:

$$K_o = .082 + .212(T/D) - .00296(Z/D) + .00363\left(\frac{\bar{E}_{ib}}{p_a}\right) - .424(\phi_i) - .000374\left(\frac{\bar{E}_{ii}}{p_a}\right) + .776\left(\frac{C_i}{p_a}\right) \quad (51)$$

where

D = pipe diameter,

T = trench width,

ϕ_i = angle of internal friction for the in-situ soil type,

C_i = cohesion of the in-situ soil,

$\bar{E}_{ii}$ = $K(t)_i p_a \left(\frac{\gamma' t^Z}{p_a}\right)^{n_i}$,

p_a = atmospheric pressure,

$K(t)_i, n_i$ = Duncan soil properties of the in-situ material (10 yr),

γ'_t = the average effective unit weight of the in-situ soil $\gamma_T - \frac{p\gamma}{Z} w$,

p = the water table height above the springline,

γ_w = the unit weight of water, and

γ_T = the total unit weight of the in-situ soil.

Using Equation 51, a value for K_o can be found and used in Equation 47 to evaluate σ_b. Equation 45 can then be used to predict the backfill strain, ε_b. The secant modulus E'_b can then be found by using Equation 46. The net result is that a

realistic approximation for E'_b can be calculated from the site conditions, pipe type, and Duncan soil properties of the in-situ and backfill materials.

The range of the main variables in the factorial study is listed below. Any extrapolation beyond these values should be done with extreme care.

Diameter: 18 in $\leq$ D $\leq$ 48 in

Trench Width: 1.25(D) $\leq$ T $\leq$ 2.00(D)

Water Table Height: 0 $\leq$ P $\leq$ Z

Depth of Cover Above Springline: 3 ft $\leq$ Z $\leq$ 42 ft

Soil Type: Any fine-grained soil

Since Equations 46 and 51 were derived from a finite set of variables, some limiting values should be placed on K_o, $\bar{E}_{ib}$, and E'_b in order to ensure a conservative prediction of maximum pipe strain and deflection. The range of K_o should be between 0.4 and 1.8, and E'_b should not exceed 3200 psi, and $\bar{E}_{ib}$ should not exceed 4400 psi.

With E'_b established, a regression equation to predict vertical pipe deformation was formulated. The general form of the commonly used Spangler equation was adopted. Since the Spangler equation form contains a constant in the denominator, it was necessary to use a nonlinear regression analysis; however, once a value was found for the constant in the denominator, linear regression was used to establish the best variables for the numerator. The best-fit equation for percent change in vertical diameter ($\Delta y/D$) had an R-squared of 0.88.

$$\frac{\Delta y}{D} = \frac{.867(K_o \gamma'_t Z) + 1.241(p\gamma_w Z) - .0011(\frac{T\ \bar{E}_{ib}}{D})}{\frac{E_c\ I}{r^3} + .00123\ E'_b} \tag{52}$$

where

$\Delta y/D$ = percent change in vertical diameter,

r = pipe radius,

E_c = ten-year elastic modulus of the pipe, and

I = moment of inertia of the pipe wall cross-section per unit length.

A similar process was used to find the best-fit equation to predict maximum outer fiber pipe strain. However, in order to match the data accurately, two equations had to be used, one for linear strains and the other for post-yield strains. The linear strain equation, with an R-squared value of 0.85, was regressed from predicted strain values less than 2.5 times the yield strain, ε_y. This limit was used in order to reduce the residual error for strain approaching the yield value.

$$\varepsilon_L = \frac{4.835(K_o \gamma'_t Z) + 8.269(p\gamma_w Z)}{\frac{E_c\ c}{r^3} + 2.0\ E'_b} \tag{53}$$

where

ε_L = linear pipe strain

r = the pipe radius

c = the distance from the bending axis to the extreme outer fiber

ε_y = ten-year yield strain (.0393)

If the simple linear strain equation predicts a strain greater than or approaching the yield value, the second equation for post-yield strains should also be checked.

The equation for post-yield strains, ε_p, was calculated by finding an equation for $\hat{\varepsilon}$, the difference between the calculated post-yield strain and the linear strain:

$$\hat{\varepsilon} = \varepsilon_p - \varepsilon_L \tag{54}$$

Values for $\hat{\varepsilon}$ were determined from calculated plastic strains in the range of 0.1 to 5.0 and tabulated to create an additional data base. The equation for $\hat{\varepsilon}$ shown below, with R-squared equal to 0.54, was the best fit curve found from this data:

$$\hat{\varepsilon} = \varepsilon_p - \varepsilon_L$$

$$= \frac{23.86\left(\frac{\Delta y}{D}\right)\frac{(pZ)^2\gamma_w}{D} + 33.723\left(\frac{\Delta y}{D}\right)\gamma'_t Z - .1795\bar{E}_{ii}\left(\frac{Z}{D}\right) - 1.80\bar{E}_{ib}(T/D)}{\frac{E_c I}{rA} + .003\,\frac{E'_b\, r^2}{A}} \tag{55}$$

where

A = the cross sectional area of the pipe.

The smaller R-squared value for this model indicates the difficulty in accurately predicting post-yield strains without direct use of the finite element program. Equation 55 does, however, allow a simple approximation for maximum post-yield strains in the outer fibers. In plastic design, the number of locations and amount of plastic yielding in the pipe are more important than the actual magnitude of the strain. It is therefore recommended that a complete CANDE analysis be used when Equations 53, 54 and 55 predict a strain greater than 5 times the yield strain.

All of the regression equations were formulated in a dimensionless form so that any system of unit could be used. It is possible to change from one system of units to another simply by changing p_a; however, consistant units must be used throughout. The only exception to this is that ϕ must be in radians. The Duncan soil parameters ϕ and C, which are used in the equations, can be found from drained or undrained triaxial tests.

A NEW DESIGN PROCEDURE

The regression equations formulated from the full factorial analysis provide a reasonable approach to the design of high density polyethylene profile-wall pipe. These equations were formulated from a specific set of design variables. In order to evaluate the use of these equations for parameters outside the bounds of the factorial study, some additional runs were made with the CANDE program. These runs were used to establish some additional factors for the design equations which allow the design engineer to extrapolate beyond the bounds of the original factorial study.

ADDITIONAL IN-SITU SOILS AND BACKFILL TYPES

The results of the original factorial study clearly revealed the importance of in-situ soil strength to flexible pipe performance. Since five basic strength parameters are required in the Duncan soil model to represent the nonlinear stress-dependent behavior of soils, it was not possible to investigate a complete range of these parameters in the factorial study. To determine the effect of a larger range of soil parameters, some additional soil types were analyzed.

In-situ Soils

The properties of four additional in-situ soil types (see Table

7) were obtained from Duncan (6) and used in the CANDE program to predict the ten-year displacements (see Figure 36) and the ten-year strains (see Figure 37). Comparing these results with results from the regression equations revealed that the regression equation predictions were conservative for stiff soils. This trend was corrected by determining a multiplier for the deflection equation, F_{id}, and a multiplier for the strain equation, F_{ie}, which assure an accurate representation of the behavior of stiffer soils.

Values for F_{id} and F_{ie} were determined for nine soil types by calculating the ratios of the regression equation predictions to the CANDE results. These values were plotted against different combinations of in-situ soil parameters in an attempt to find a reliable relationship. The best-fit curves for F_{ie} and F_{id} are shown in Figures 38 and 39, respectively. Simple exponential regression analysis was used to arrive at the following equations for F_{id} (R^2=.96) and F_{ie} (R^2=.95).

$$F_{id} = 1.05\ e^{(-1.21\times10^{-3})\{\frac{C_i\ K_i(10yr)}{(1-\sin\phi_i)^2}\}} \tag{56}$$

$$F_{ie} = 1.06\ e^{(-1.11\times10^{-3})\{\frac{C_i\ K_i(10yr)}{(1-\sin\phi_i)^2}\}} \tag{57}$$

These equations allow the direct calculation of multipliers for the regression equation and extends their use to a wider range of fine-grained soils. The values of F_{id} should be limited to between 0.2 and 1.0 and the value of F_{ie} should be limited between to 0.22

TABLE 7. Additional Soils Analyzed

Parameters	Soil Types			
Unified Soil Classification	CL Canyon Dam (Silty Clay)	CH Monroe Dam (Fat Clay)	ML Chatfield Dam (Sandy Silt)	CL Chatfield Dam (Sandy Clay)
I_p	19.0	45.0	4	24
ϕ	9.0	1.0	19.0	0.0
n	0.37	0.14	0.59	0.0
R_f	0.65	0.77	0.86	0.95
w%	16.2	26.5	15.6	23.4
m	0.10	0.10	0.10	0.10
K(t) (10 yr)	8.28	14.55	44.78	53.76
γ_{wet}	133.7	122.88	135.3	125.96
C psi	13.89	14.55	25.0	16.67
μ	0.45	0.45	0.45	0.45

w = water content
I_p = plastic limit
c = cohesion
ϕ = angle of internal friction
N k(t) Rf = dimensionless Duncan soil parameters
m = slope of creep compliance curve from Ref. (5)
γ_{wet} = wet unit weight
μ = Poisson's ratio

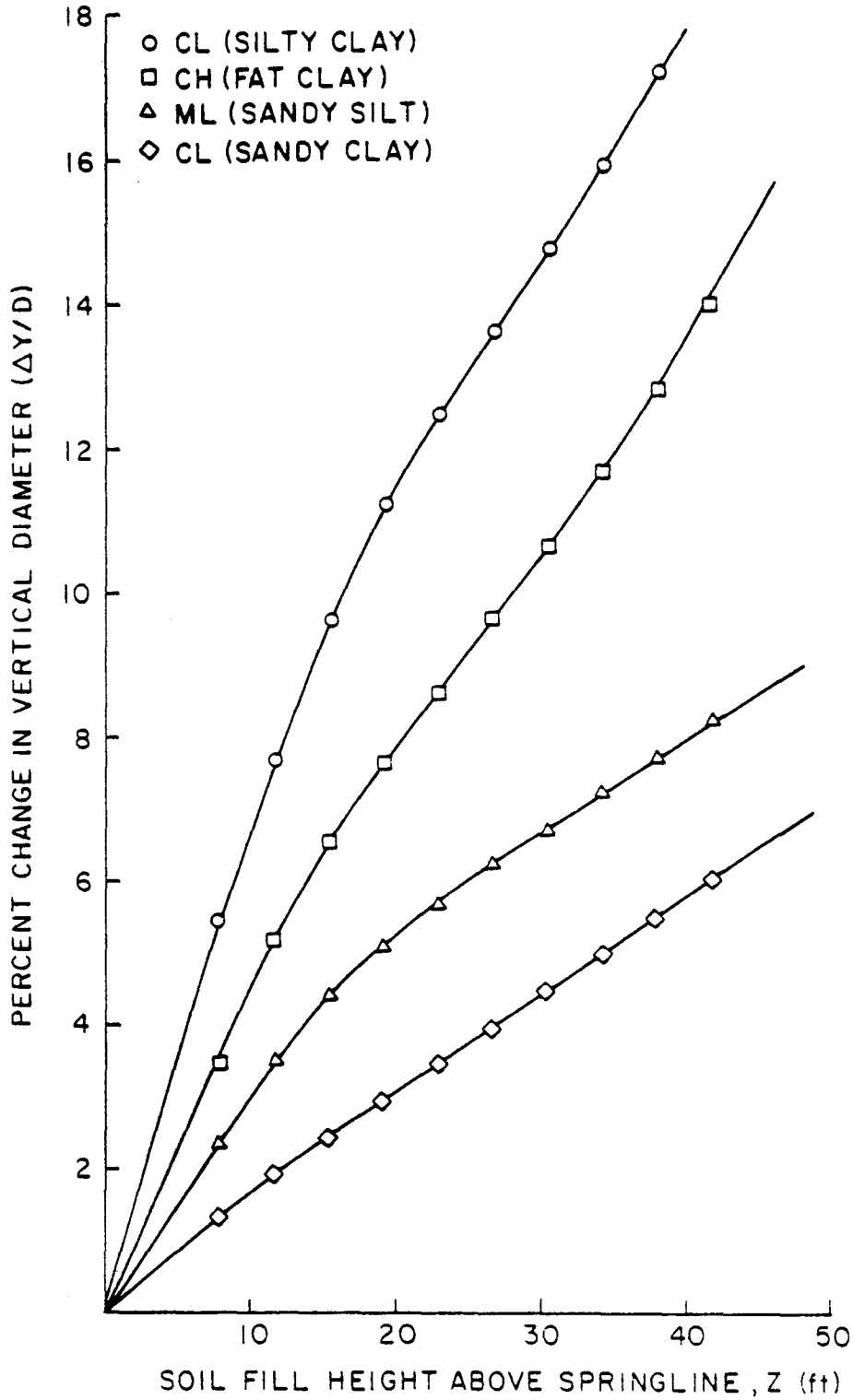

FIGURE 36. Comparison of Pipe Deflection for Different In-situ Soil Types

(D=48, Profile #9, T=72, P=0)

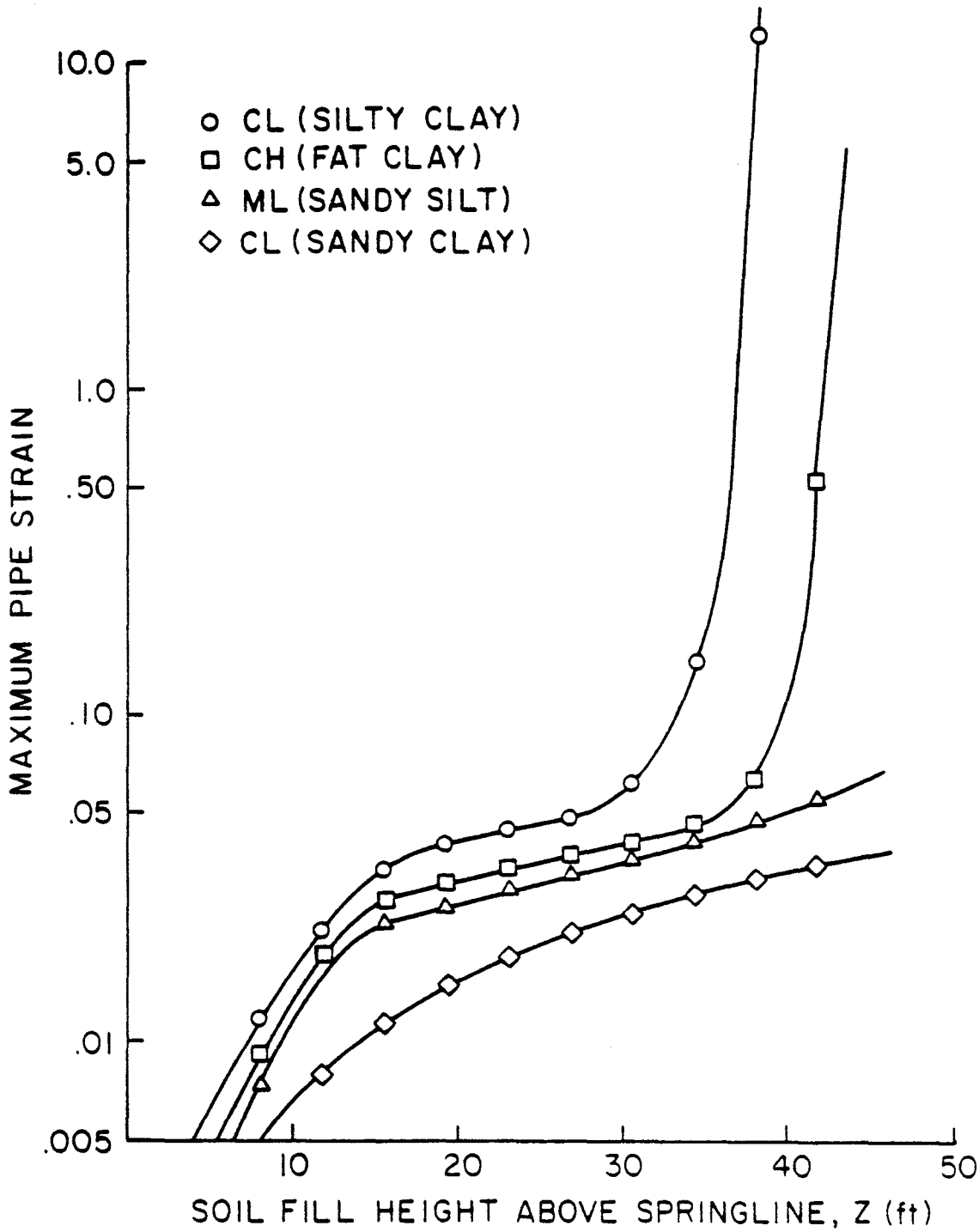

FIGURE 37. Effect of In-situ Soil Type on Maximum Pipe Strain

(D=48, Profile #9, T=72, P=0)

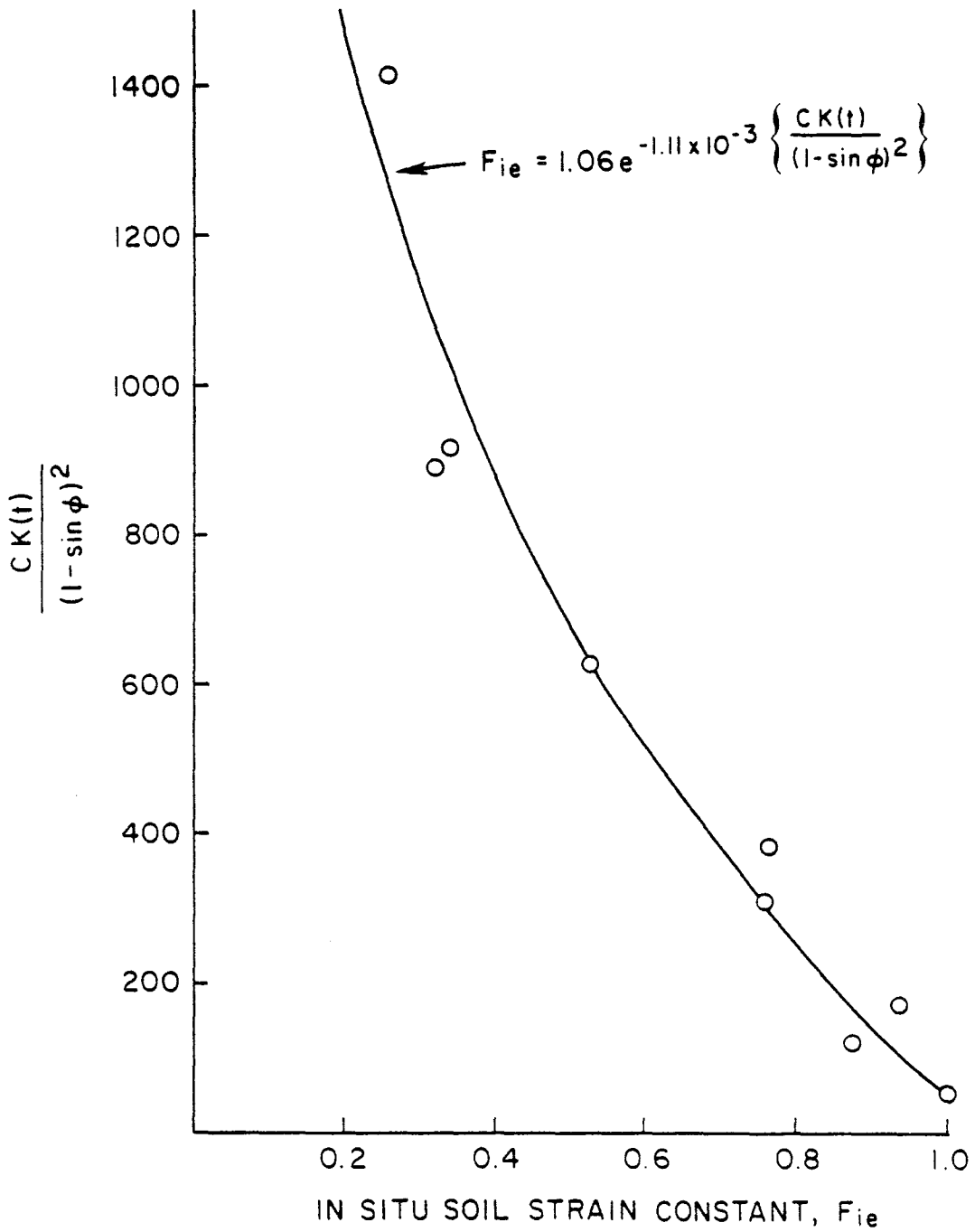

FIGURE 38. Empirical Strain Constant for Different In-situ Soil Types

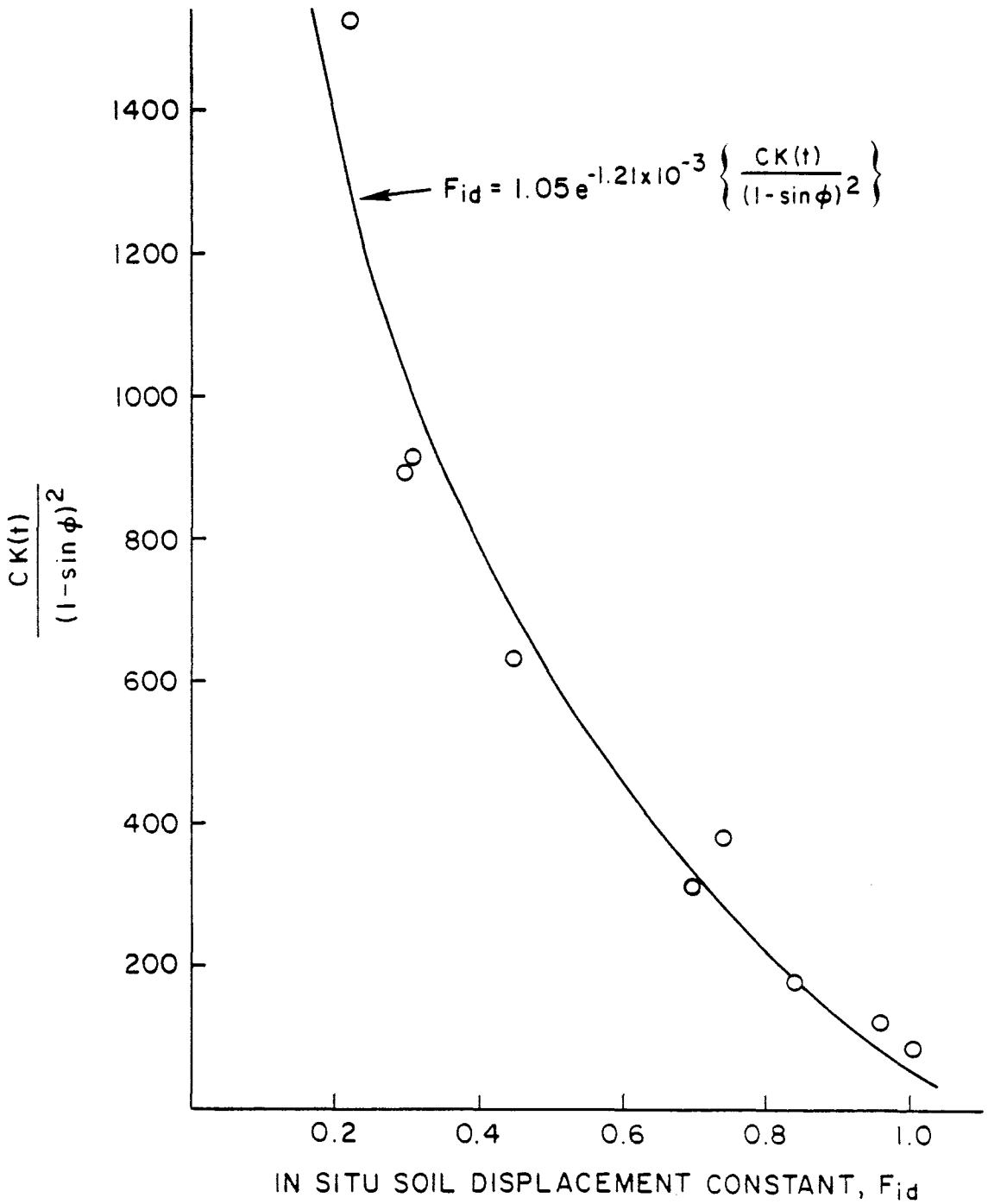

FIGURE 39. Empirical Displacement Constant for Different In-situ Soil Types

and 1.0. If the ten-year value for $K_i(t)$ is less than 23.0, the values of F_{ie} and F_{id} should also be set equal to one to ensure a conservative prediction of strain and displacement.

Backfill Soil Types

Most engineers will specify a granular backfill material immediately around the pipe. However, predetermining an exact value for the strength and degree of compaction of this material is quite difficult. The conservative set of hyperbolic parameters available within CANDE (see Table 8) do, however, offer a good design approximation.

The parameters for the #3 backfill material can be used for slightly-compacted coarse-grained materials. The #2 backfill material parameters can be used for well-compacted sands or gravels or slightly-compacted crushed rock. The strongest parameters, corresponding to the #1 backfill material type, can be used for compacted crushed rock or high density sands and gravels.

TABLE 8. Conservative Soil Parameters for Coarse Aggregate Backfill Material

Backfill Type	Relative Compaction % Standard Proctor	Unit Weight lb/ft	K_b	n_b	ϕ_b	R_{fb}	C_b
#1	105	150	600	0.4	42	0.7	0.0
#2	95	140	300	0.4	36	0.7	0.0
#3	90	135	200	0.4	33	0.7	0.0

The effect of density or stiffness of the backfill material on vertical pipe deflection is shown in Figure 40. Even though only a small zone of coarse aggregate backfill was used, 0.25 diameters above the pipe and 0.25 diameters beside the pipe, changing the density of this material greatly effects pipe performance. Simply changing the relative compaction from 90% to 105% reduces the deflection for a depth of cover of 30 ft. from 10% to 6%, respectively. Approximately the same reduction in maximum pipe-wall strain is observed with equivalent changes in the backfill density (see Figure 41).

Although the regression equations were formulated from a data base containing only one conservative backfill type with 90% of Standard Proctor compaction or a #3 backfill material, they accurately predict maximum pipe strain when other backfill densities are used.

Figure 42 shows the close comparison between the predictions of ten-year strains from the regression equation and actual CANDE results for a 95% Standard Proctor compaction backfill soil. The displacement regression equation predictions, however, have a somewhat lower correlation (see Figure 43). The displacement regression equation predictions are conservative for large depths of cover.

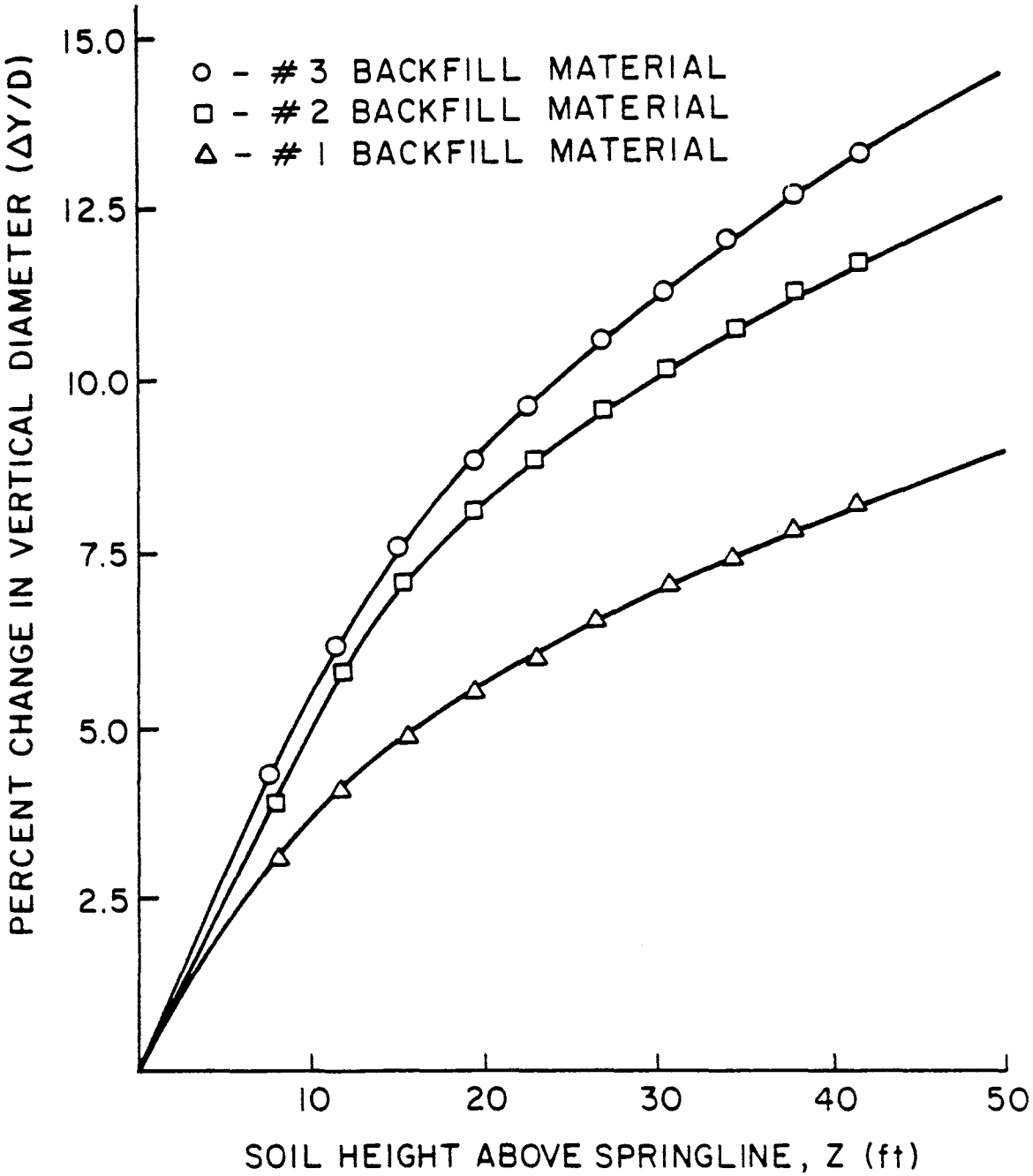

FIGURE 40. Effect of Varying Backfill Density on Pipe Deflection

(D=48, Profile #9, T=72, P=0, Weak Silt In-situ Soil)

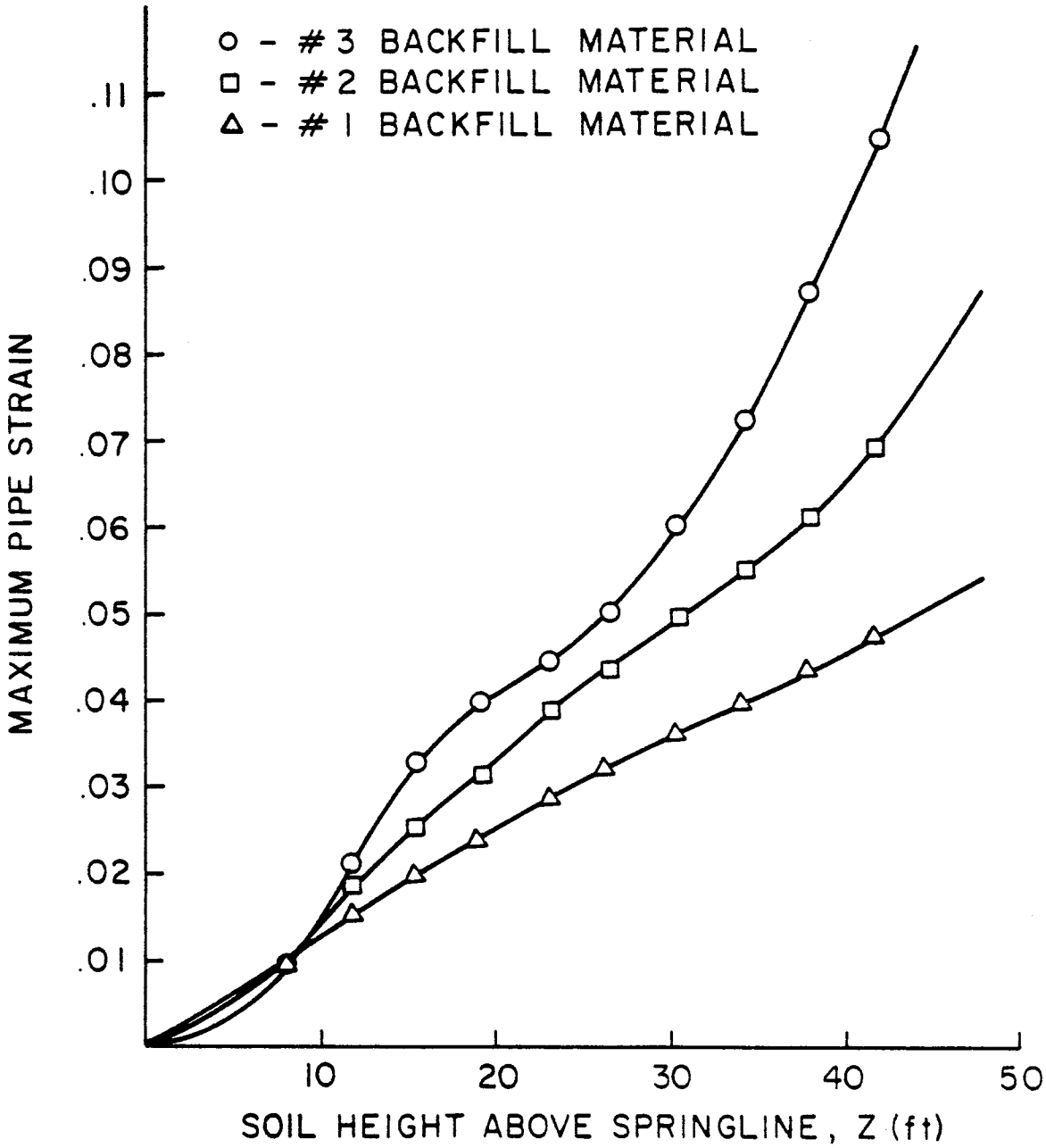

FIGURE 41. Effect of Varying Backfill Density on Maximum Pipe Strain

(D=48, Profile #9, T=72, P=0, Weak Silt In-situ Soil)

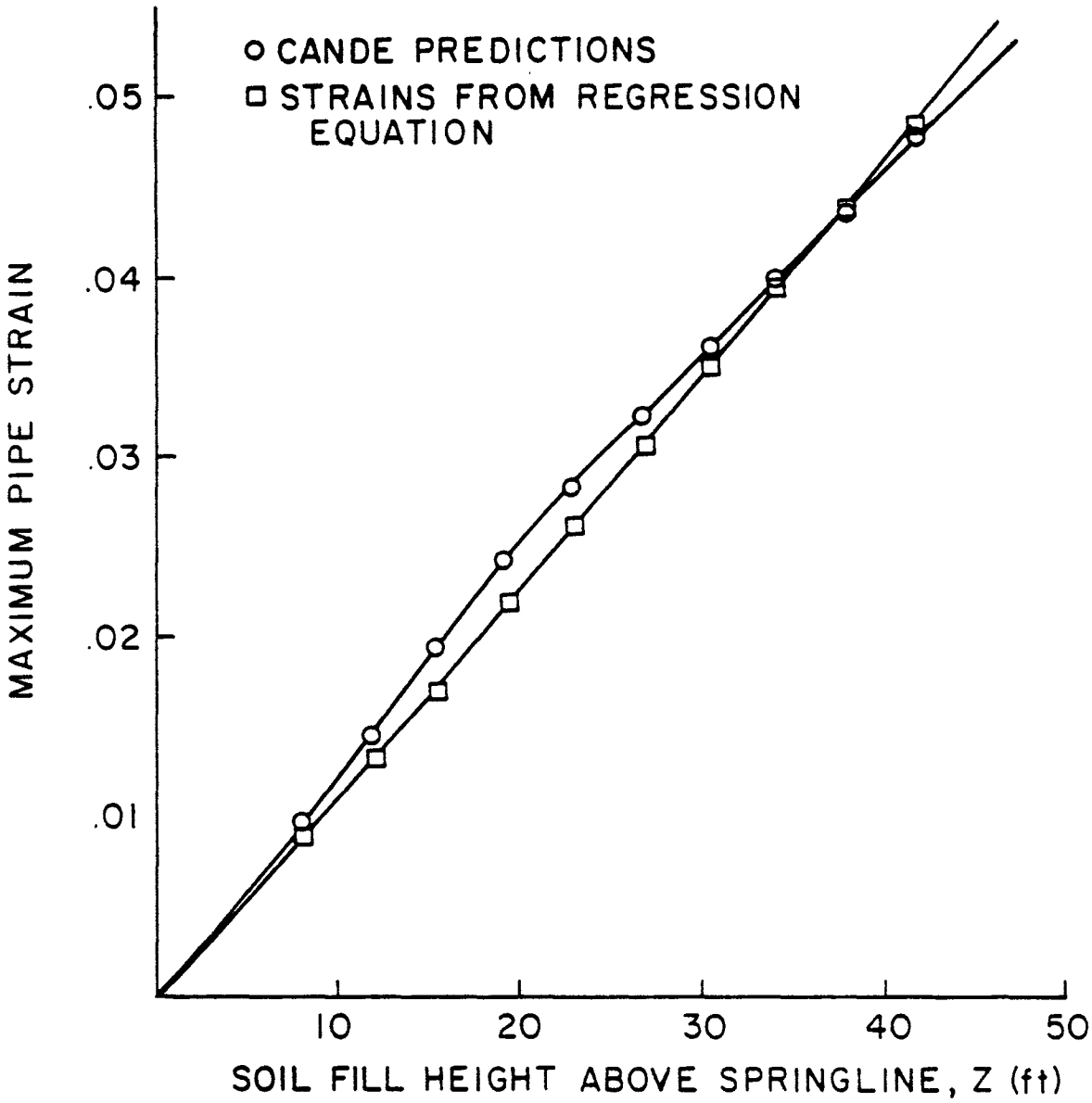

FIGURE 42. Comparison of Regression Pipe Strains Equation With CANDE Results for a Dense Backfill

(D=48, Profile #9, T=72, P=0, Weak Silt In-situ Soil)

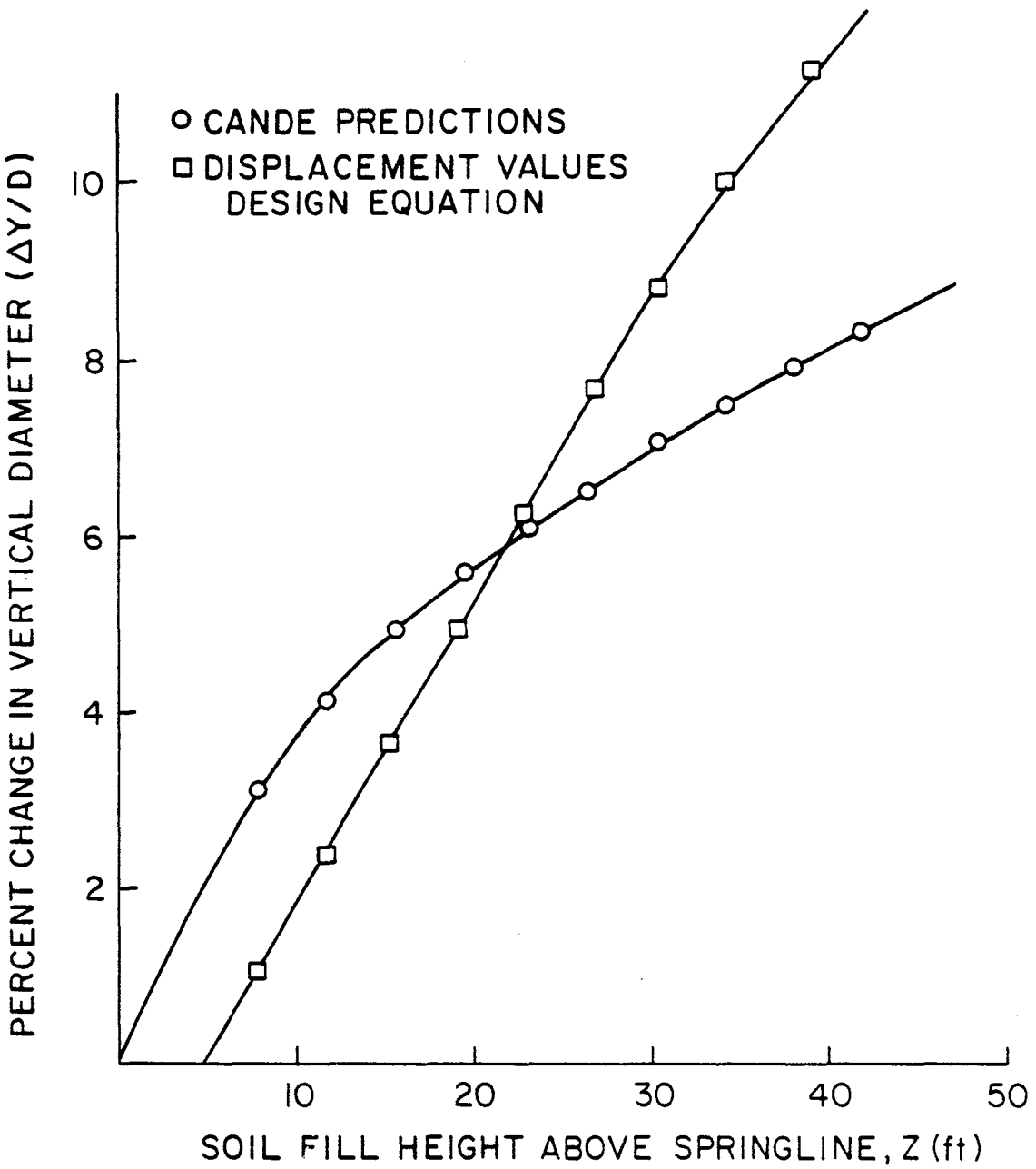

FIGURE 43. Comparison of Regression Deflection Equation With CANDE Results for a Dense Backfill

(D=48, Profile #9, T=72, P=0, Weak Silt In-situ Soil)

COMPARISON OF SPANGLER'S EQUATION WITH CANDE RESULTS

As outlined in the Traditional Methods section, deflection estimates and, in fact, most present day pipe design is based on the well-known Spangler equation (8):

$$\Delta Y/D = \frac{D_1 \; K \; b}{\frac{EI}{r^3} + .061 \; E'} \tag{58}$$

where

ΔY = vertical deflection (in.),

D = pipe diameter (in.),

EI/r^3 = pipe bending stiffness (psi),

D_1 = deflection lag factor,

K = bending constant $\cong$ 0.1,

p = pressure at springline of pipe (psi), and

E' = modulus of soil reaction (psi).

This equation was established for designing rigid pipes or strong flexible pipes, such as corrugated steel or aluminum. However, when highly ductile materials such as polyethylene are used to construct pipes with smaller stiffnesses, a more complex equation must be used to calculate expected deflections.

When an equivalent backfill is used, Spangler's equation will predict the same deflection regardless of the in-situ soil types. The large amount of error associated with this assumption is illustrated in Figure 44, where CANDE predictions for ten-year pipe deflections in several different in-situ soil types are compared with values from

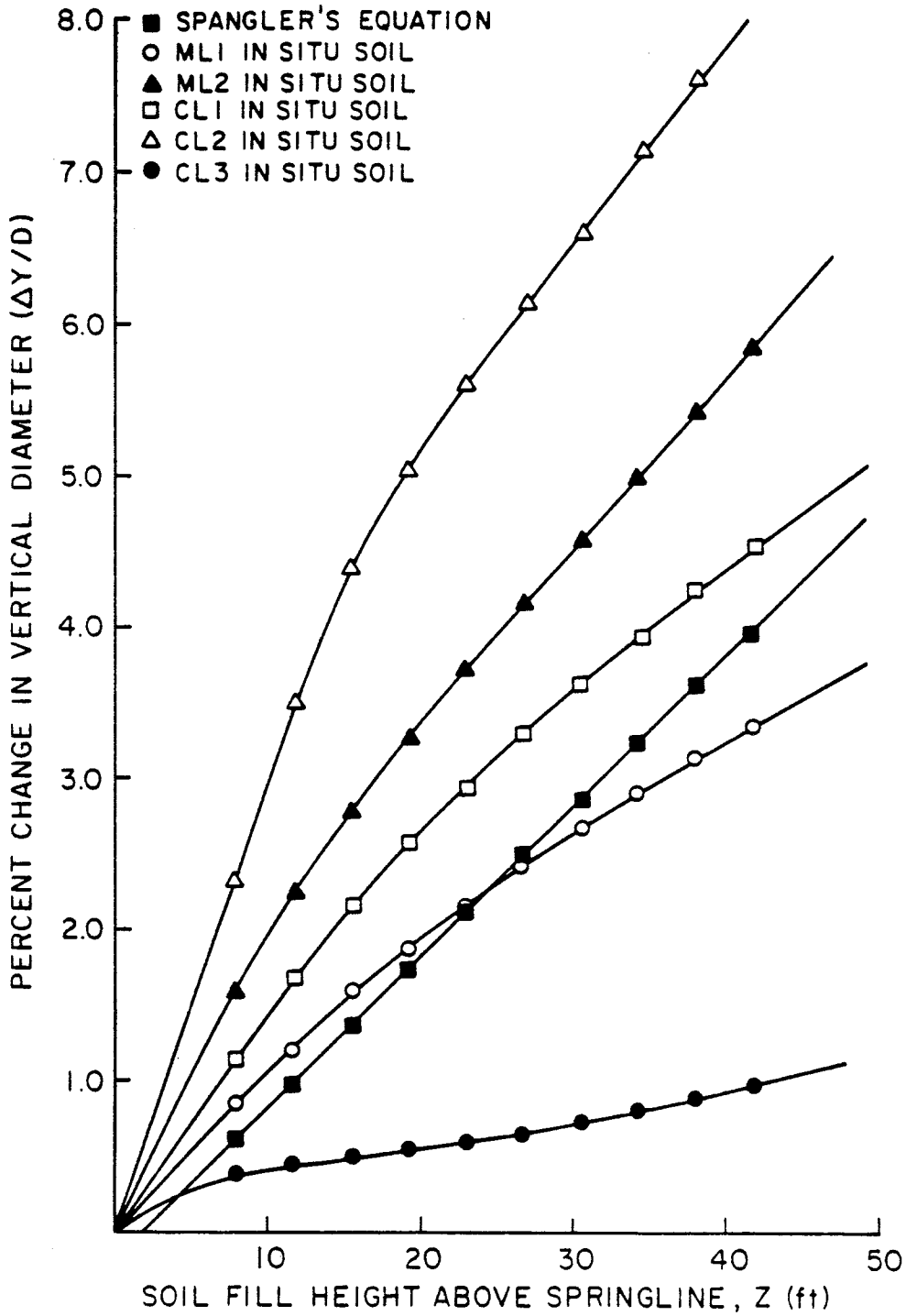

FIGURE 44. Comparison of Spangler's Equation With CANDE Results for Different Fine-Grained In-situ Soils

Spangler's equation. The deflections calculated with Spangler's equation, using a deflection lag factor of 1.5 and a bedding constant of 0.1, vary from 50% underprediction to 300% overprediction of actual displacements for the 48 in., #9 profile pipes. The 10-year pipe stiffness ($1.49\ EI/r^3$) for this pipe is 1.65 psi. Spangler's equation does not have sufficient variables to account for the complex interaction between the pipe, the granular backfill material, and the in-situ soil and therefore can only be used as a crude approximation of pipe performance in fine-grained soils.

TIME AS A DESIGN VARIABLE

Since both polyethylene pipe material and fine-grained soils are time dependent, design time is a necessary consideration. As discussed in the Properties of the Pipe Material and Soils Used section, a simple power law formulation was adopted to model the reduction in stiffness of the pipe and soil material when loaded at a constant stress. This assumption allows the prediction of pipe response at different times, as was shown in Figures 14 through 17. The analysis of several soil types and backfill configurations showed that a linear relationship exists between 10-year predictions for displacements and strains and predictions at other design times.

The ratios between 10-year CANDE predictions and other time periods are tabulated in Appendix B for two different combinations of in-situ soils and backfill types. These results, combined with some additional runs, indicate that the ratios shown in Table 9 may be

multiplied by the standard 10-year regression equation prediction in order to predict expected strain and deflection for different time periods.

TABLE 9. Time Factors for Regression Equations

	Time					
	2 hour	30 day	1 year	10 year	25 year	50 year
Deflection Factor	.57	.76	.92	1.0	1.09	1.15
Strain Factor	.64	.80	.94	1.0	1.11	1.16

EXAMPLE PROBLEM AND PRESUMPTIVE SOIL CHARTS

The design equations formulated in this study are based on soil properties which can be determined directly from several triaxial tests. This procedure is clearly outlined by Duncan (6). However, in many cases when a strong in-situ soil is available and the job is too small to justify large amounts of soil testing, the presumptive soil charts presented in this section can provide a convenient way to estimate in-situ soil properties. The presumptive soil charts were constructed by tabulating and plotting all of the hyperbolic stress-strain soil parameters reported by Duncan (6) and determining a representative curve for each of the in-situ soil types. Large variations from these curves may be found in some cases; however, they

do offer a good estimate of the hyperbolic stress-strain parameters in the absence of rigorous soil testing.

The in-situ soil types have been divided into three classifications according to the Unified Soil Classification system; CL, ML, and CH; and the low plastic clays have been further divided. A CL soil with less than 10% silt or coarse grained materials is classified as a CL on the presumptive soil charts. If the CL material has over 10% silt or over 10% coarse grained particles, it is classified as a CL*ML or a CL*SM, respectively.

In order to fully explain the use of the design equation and the presumptive soil chart, an example problem is presented:

Step #1 - Determine trench geometry and assume pipe size and stiffness.

Diameter = 48 in.

#9 Profile Wall

No Water Table

Trench Width = 1.5D

Lean Clay In-situ Soil

Granular Backfill with 90% Standard Proctor Compaction

Depth of Cover Above Springline = 21-38 ft.

Step #2 - Classify soil from simple soil test data (Figures 45 and 46) and go to presumptive soil charts to obtain soil parameters (Figures 47, 48, 49, and 50).

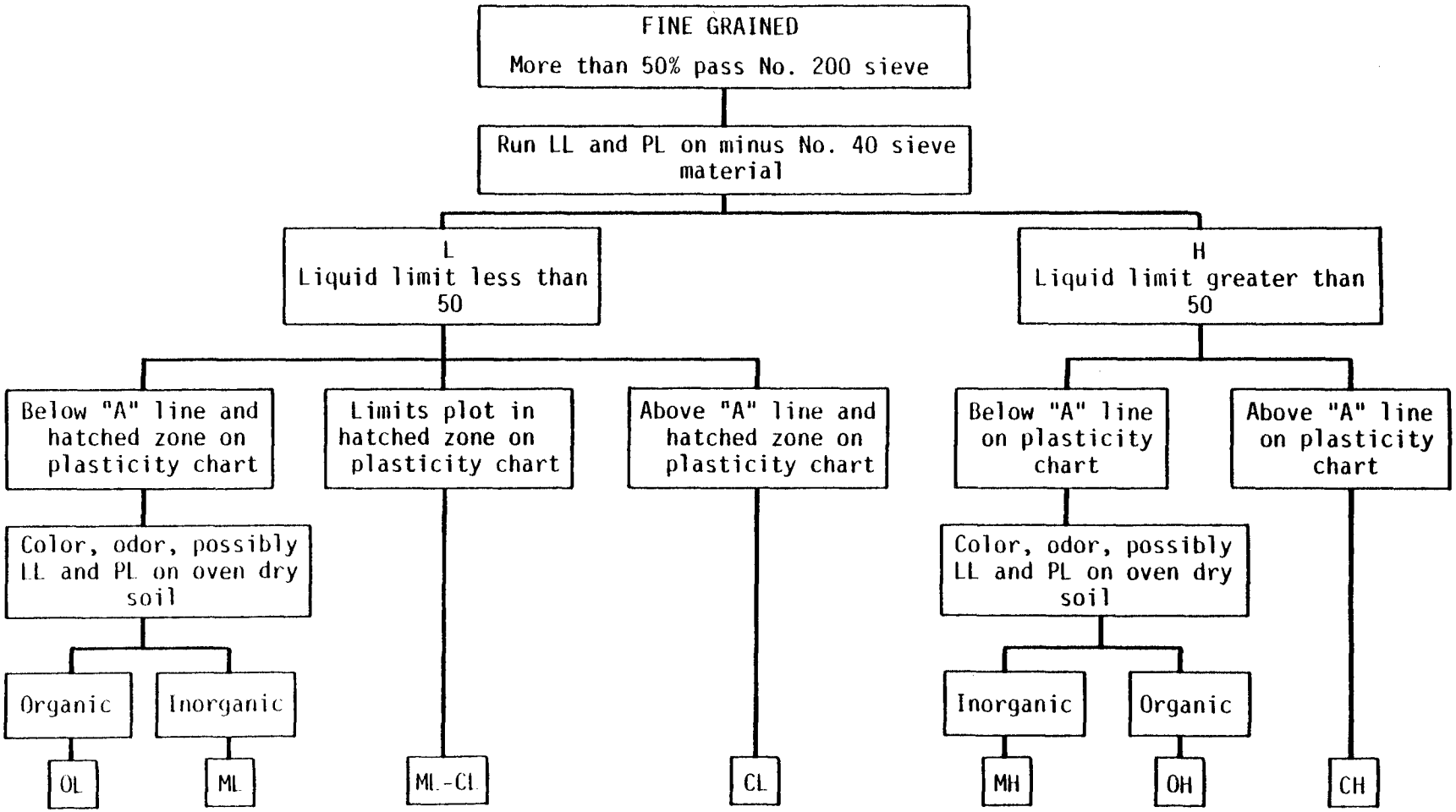

FIGURE 45. Unified Soil Classification Flow Chart for Fine-Grained Soils (After Soils Manual, 35)

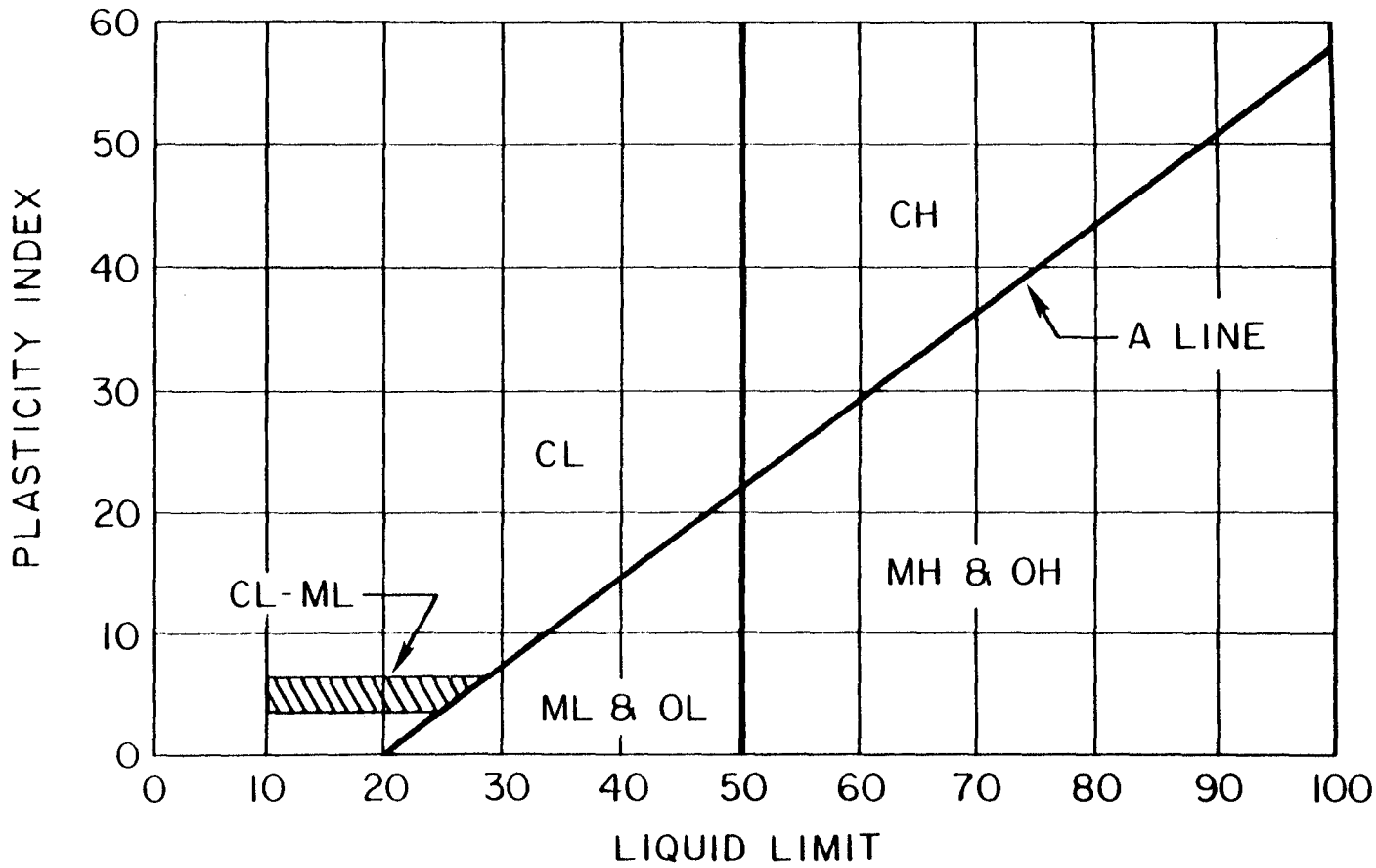

FIGURE 46. Plasticity Chart
(After Soils Manual, 35)

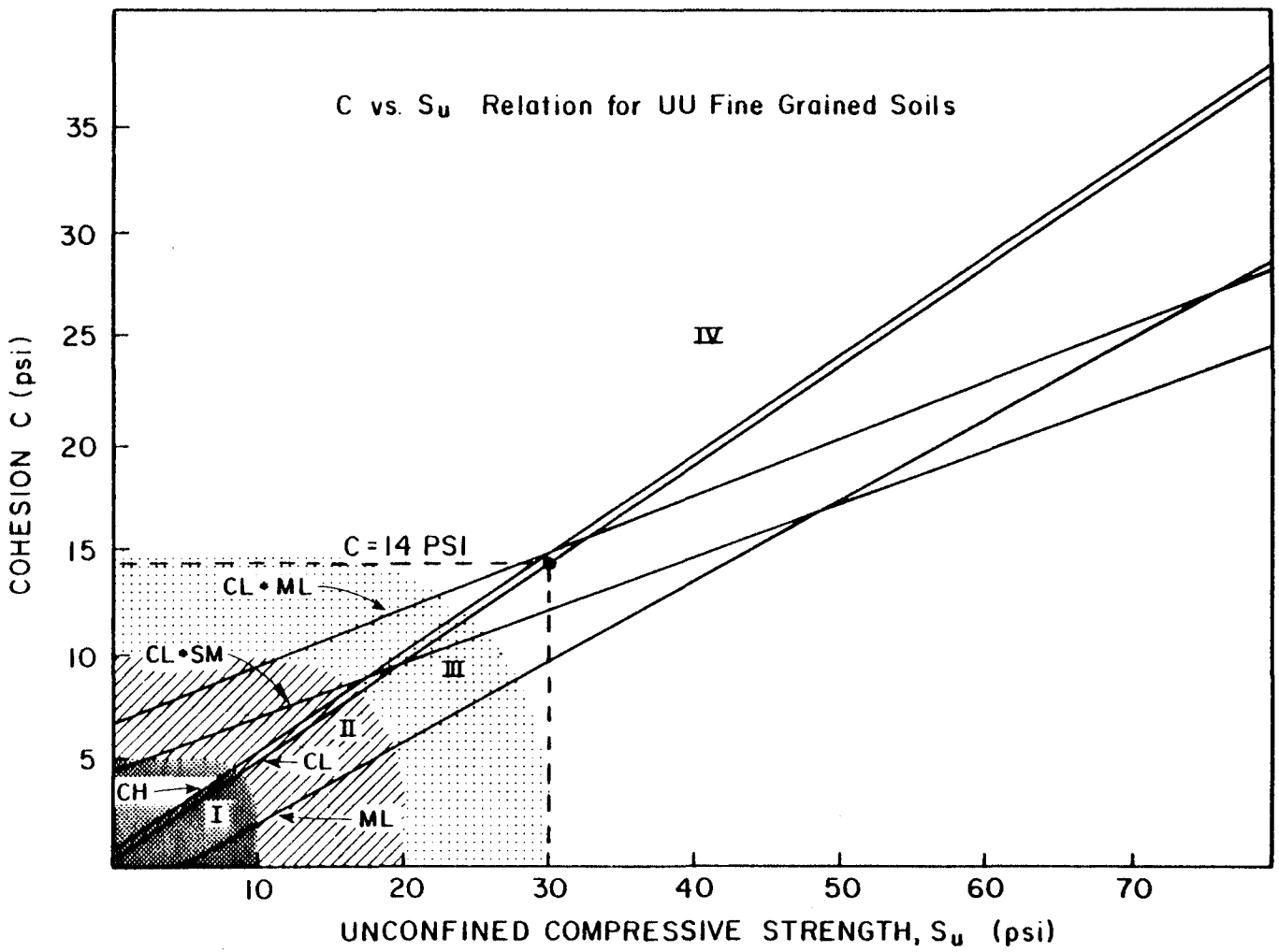

FIGURE 47. Presumptive C vs. S_u Relationship for Unconsolidated Undrained Fine-Grained Soils

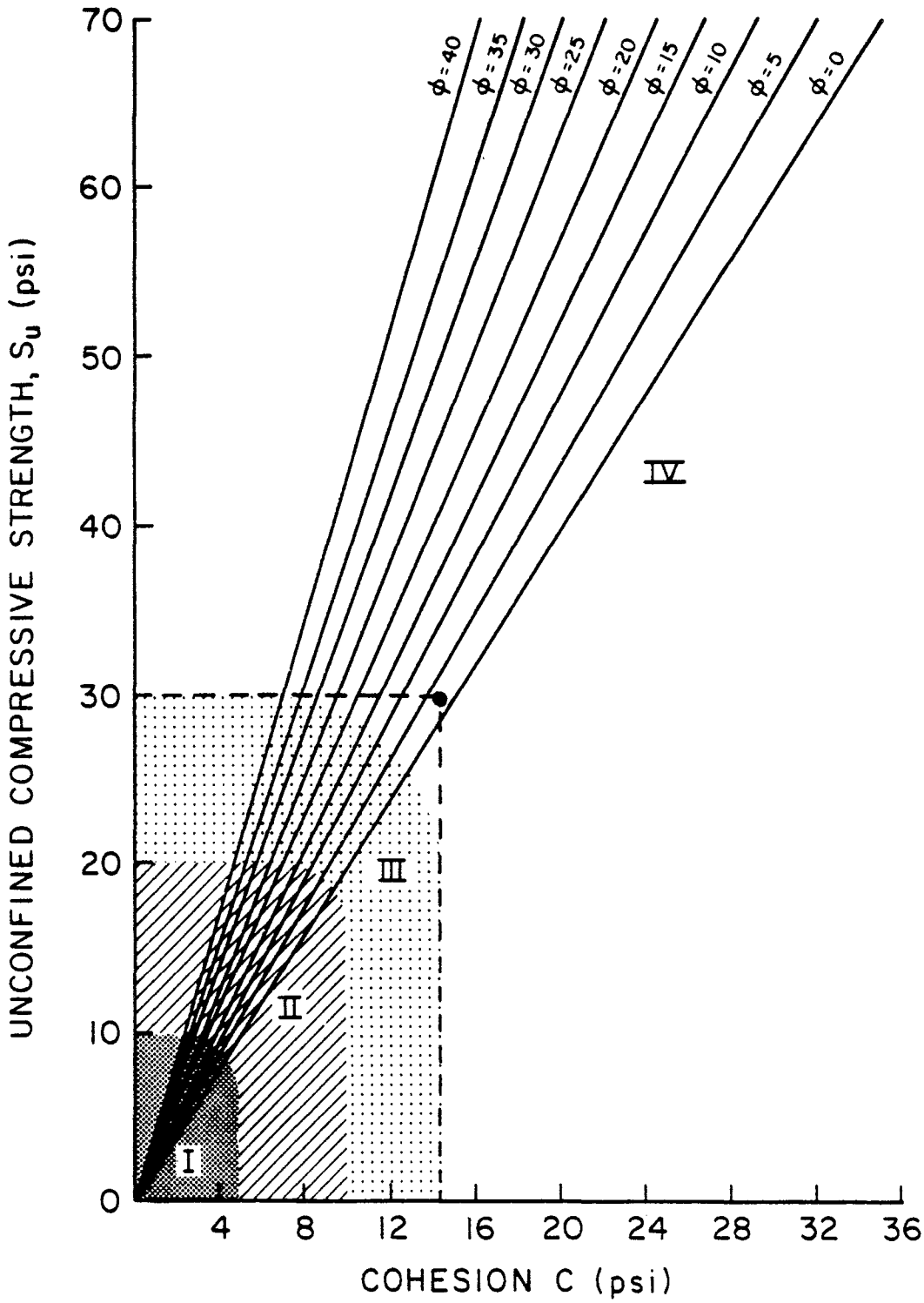

FIGURE 48. Presumptive C, ϕ, and S_u Relationships for Unconsolidated Undrained Fine-Grained Soils

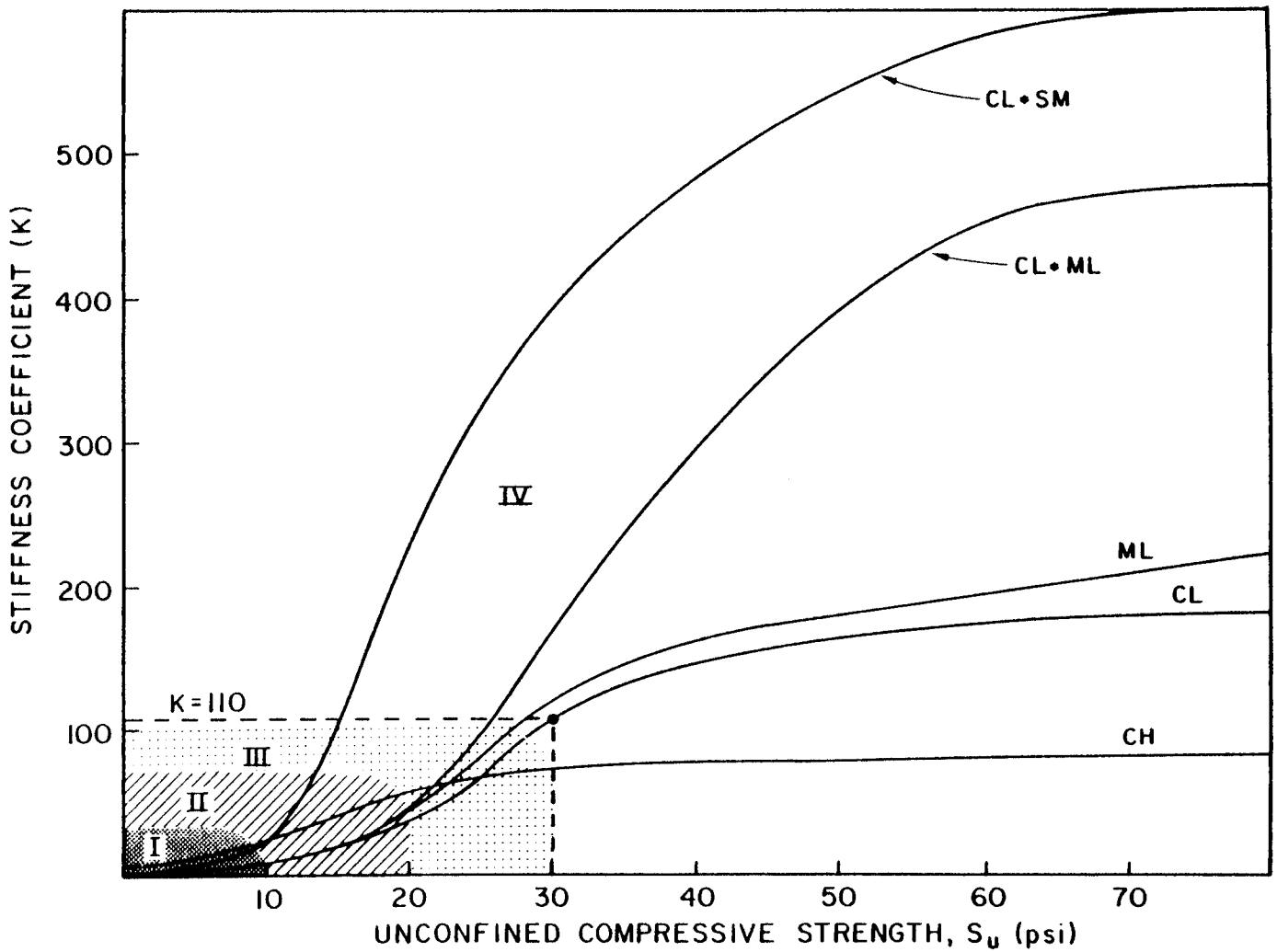

FIGURE 49. Presumptive K vs. S_u Relationship for Unconsolidated Undrained Fine-Grained Soils

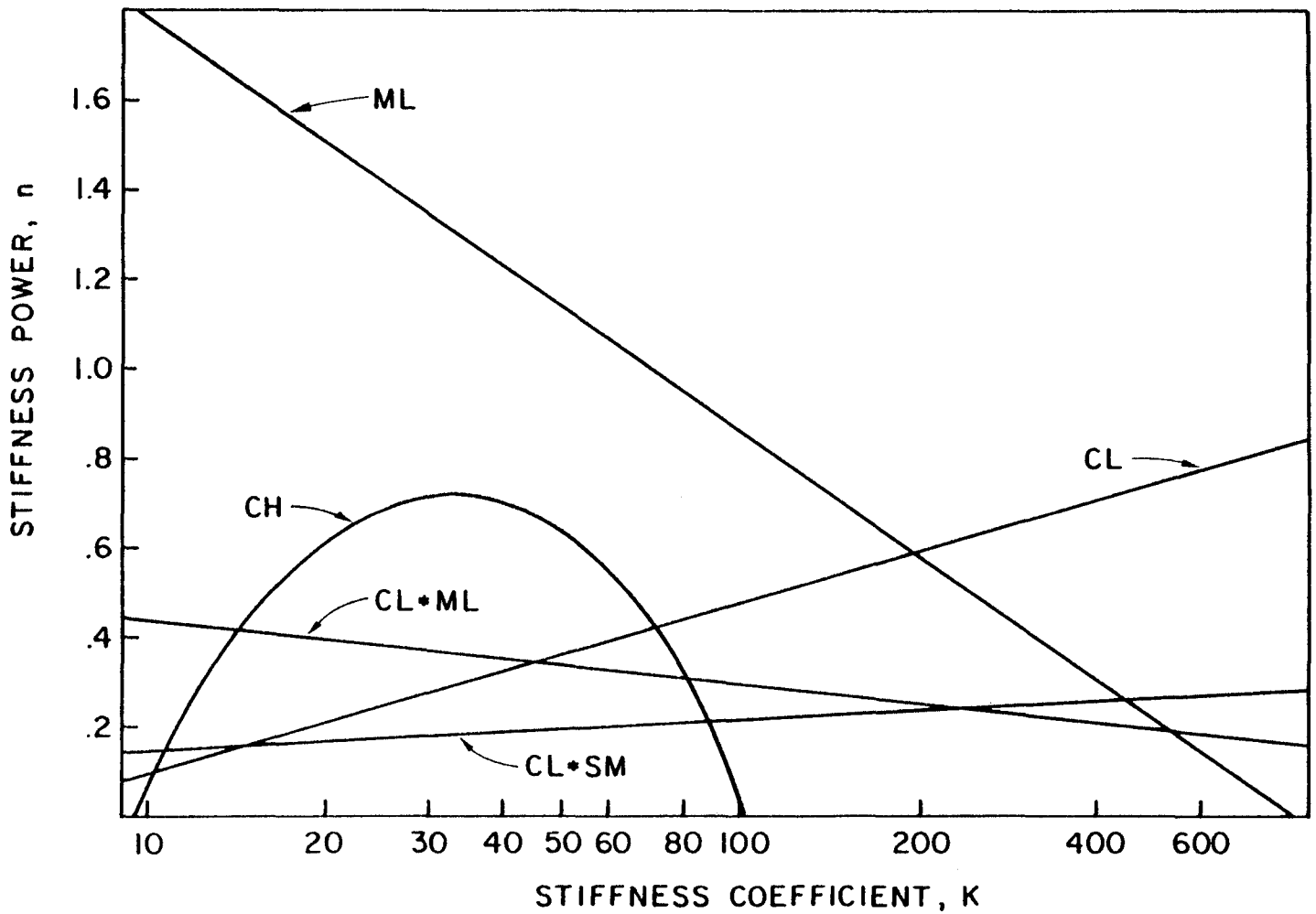

FIGURE 50. Presumptive K vs. n Relationship for Unconsolidated Undrained Fine-Grained Soils

Unit Weight (γ_T) = 130

Liquid Limit (w_L) = 45%

Plasticity Index (PI) = 30%

Unconfined Compressive Strength (S_u) = 30

Description: Lean Clay

The zones on the presumptive soil charts can be defined as follows:

Zone I - These soils require <u>detailed soils investigations</u> (including triaxial soils tests) and <u>computer analysis</u>.

Zone II - These soils require detailed soils investigations (including triaxial soils tests) and computer analysis. However, design equations can be used in place of computer analysis when high quality crushed stone backfill is used.

Zone III - Normal soils investigation and testing and use of design equations is required. Triaxial tests may lower factors of safety for safe design.

Zone IV - Normal soils investigation and testing and use of design equations is required.

Step #3 - Assume a backfill soil type and go to Table 8 to determine backfill soil parameters. (For this example a #3 backfill was assumed.)

Step #4 - Input the following input variables into the design equation

and check to determine if the strains or deflections are above the allowable. The Hewlett Packard 41CV Calculator program shown in Appendix C was used for this step.

Design Time = 10 yrs.

Diameter (D) = 48 in.

Pipe Moment of Inertia (I) = .125 in /in

Average Pipe Cross-sectional Area (A) = .492 in /in

Distances to the Centroid (Z) = .52 in.

(A table of pipe properties can be found in Appendix F.)

Trench Width (T) = 72 in.

Water Table Fraction of Height (P) = 0.0

Depth of Cover above Springline (Z) = 21

In-situ Soil Parameters

$n_i = 0.5$

$K_i = 110$

$C_i = 14$

$\phi_i = 3$

Backfill Soil Parameters

$n_b = 0.4$

$K_b = 200$

$\phi_b = 33$

$C_b = 0.0$

$R_{fb} = 0.7$

Step #5 - Multiply the 10-year strains and displacements determined in

Step #4 by the factors in Table 9 to obtain pipe responses at different times.

The results in Table 10 can be used by the design engineer to determine if the 48 inch diameter pipe will satisfy the given installation specifications.

TABLE 10. Results From Sample Problem

Time	$\Delta Y/D\%$	ε_p	E'_b
2 hours	4.53	.021	1598.0
30 days	6.04	.0264	1598.0
10 years	7.95	.033	1598.0
25 years	8.66	.0366	1598.0
50 years	9.14	.0383	1598.0

COMPARISON OF DESIGN EQUATION WITH FIELD DATA

A test line of high density polyethylene pipe was installed by the manufacturers in Beaumont, Texas on June 17, 1981. The deflections of the pipe were recorded initially, at one month, and at one year. General soils reports from an area consultant revealed that the in-situ soil was a sandy clay with a plasticity index of 18, a liquid limit of 36, and an average unconfined compressive strength of 22.2 psi. These values were used with the presumptive soil charts to

obtain the following in-situ soil parameters: C_i = 10 psi, ϕ_i = 5°, K_i = 230, and n_i = .24. K_i was reduced to account for soil creep, K_i(10 yr) = 51.5. The values for a #3 backfill material were also assumed from Table 8. These soil properties along with a 1.25D trench width and a 60% water table were input into the design equations. The 10-year deflection output from the HP 41CV calculator was multiplied by the creep factors shown in Table 9 to arrive at the deflection for different times. The close correlation of the design equation predictions with the measured data is shown in Table 11.

TABLE 11. Comparison of Regression Equation Predictions With Full-Scale Test Data

	Deflections			
	Initial	1 month	1 year	10 year
Measured	1.35	1.94	2.00	NA
Predicted	1.39	1.85	2.24	2.44

Comparison of CANDE results with the regression equation predictions were also made. Figures 51 and 52 show the close comparison between CANDE results and regression equation predictions for the standard soil and trench configuration used in the factorial analysis when ground water is present. Appendix D shows the accuracy of the regression equations for a typical dry ground factorial run and for cases that were not directly analyzed in the factorial study such as: different profile walls, different pipe diameters, and different in-situ soil types.

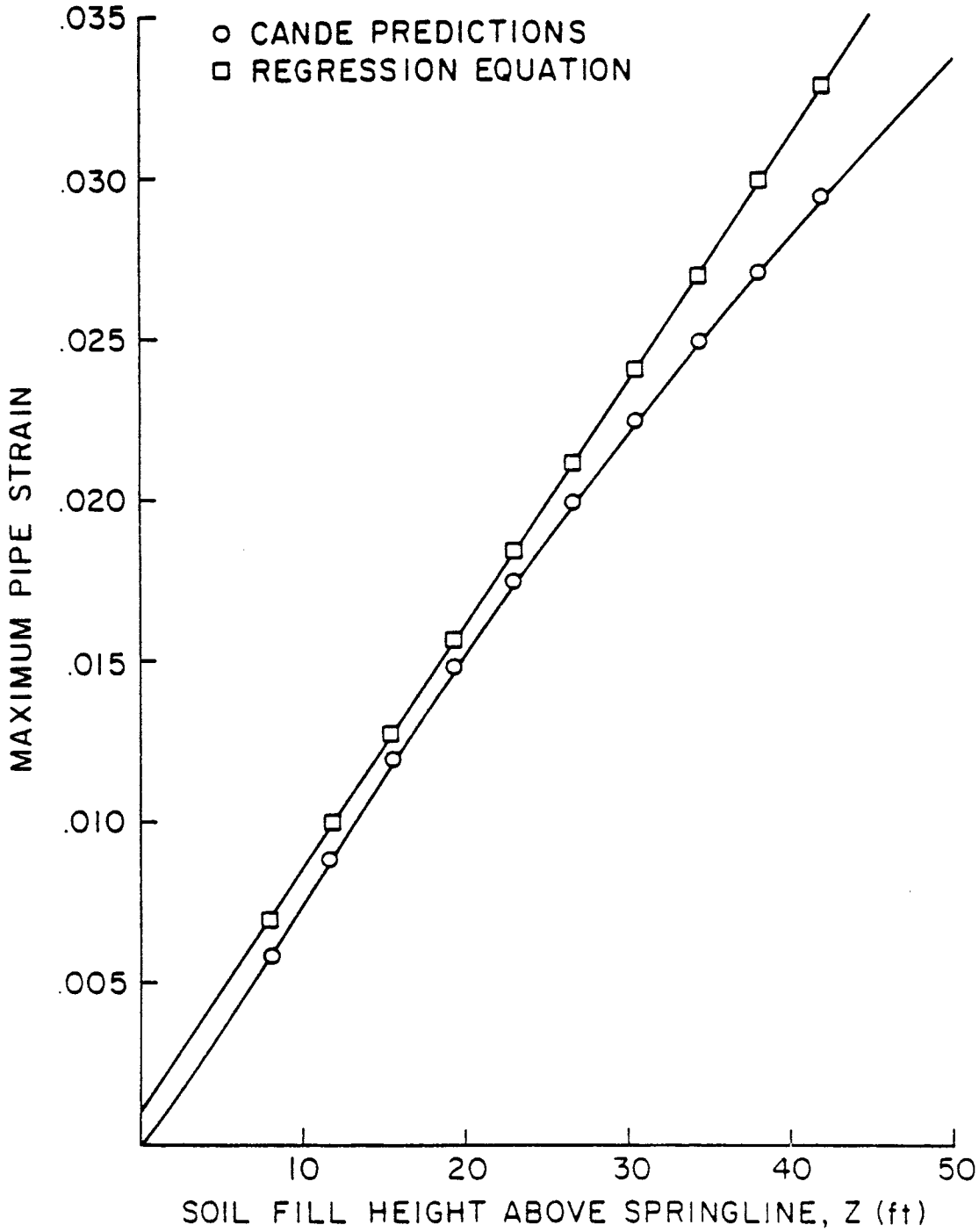

FIGURE 51. Comparison of Regression Strain Equation
With CANDE Results
for a Standard 30% Water Table Factorial Run

(D=48, CH, Profile #9, T=72)

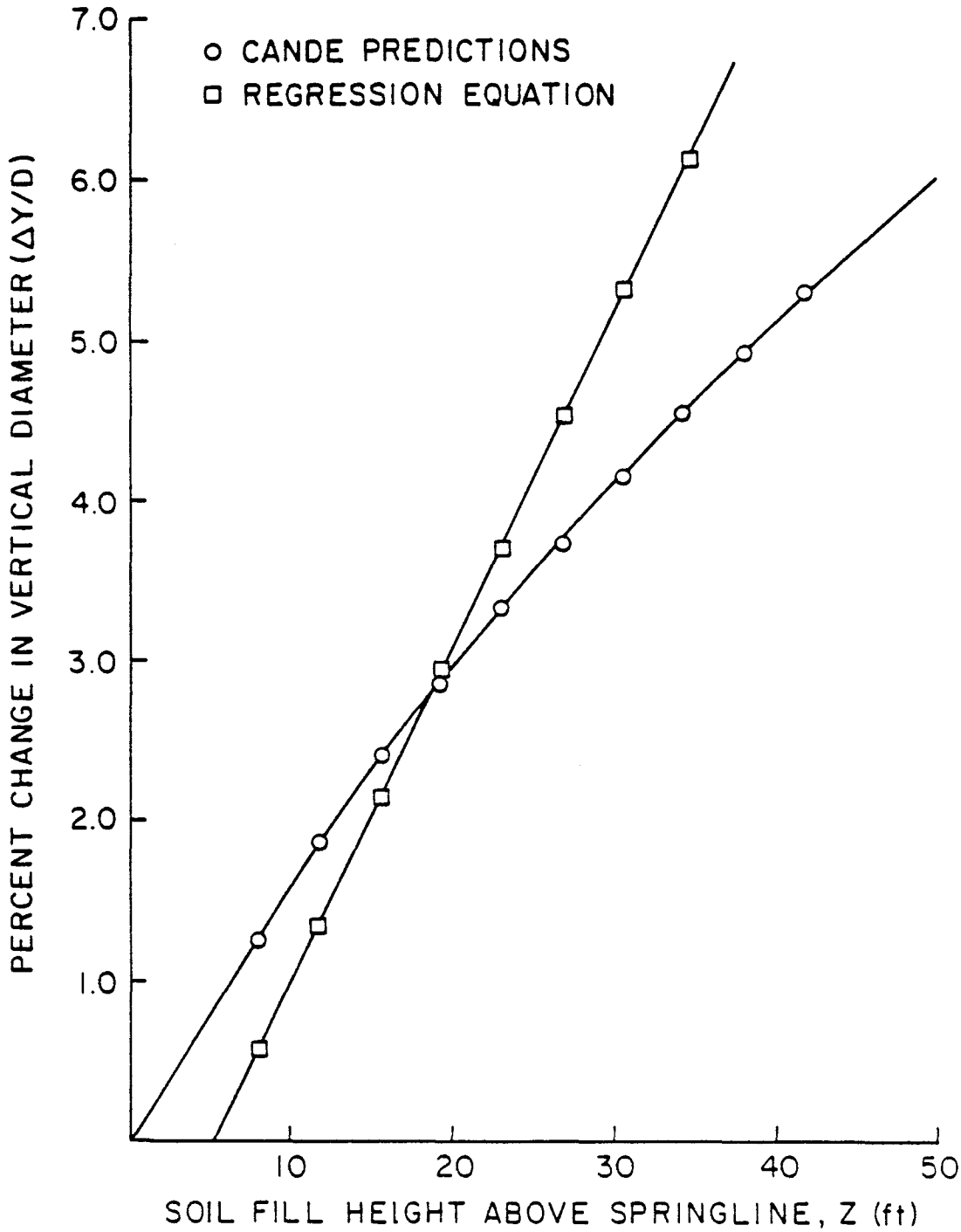

FIGURE 52. Comparison of Regression Deflection Equation With CANDE Results for a Standard 30% Water Table Factorial Run

(D=48, CH, Profile #9, T=72)

PARAMETER STUDY

The full factorial analysis, coupled with the additional studies made to incorporate time and a wider range of in-situ soil types, established a firm base from which high-density polyethylene profile-wall pipe can be designed. There are, however, a few additional design variables which need to be investigated in order to develop a sufficient description of buried flexible pipe performance under a complete range of applications.

SLIP ELEMENT AND BUCKLING

The design equations formulated in this project allow the engineer to calculate two of the important aspects of pipe performance: maximum pipe deflection and maximum pipe-wall strain. This provides an accurate means for the design engineer to investigate all forms of pipe distress except buckling.

When establishing the basic model for the full factorial study, a bonded interface condition was used. This assumption, which requires the soil and pipe to deform as a continuous body with no slippage at the soil-pipe interface, produces larger pipe deflections (see Figure 53) than the full-slip condition. Larger pipe wall strains were also observed for depths of cover below 30 ft. (see Figure 54) with the bonded interface model. Although this assumption produces conservative predictions for the deflection and strain values used in

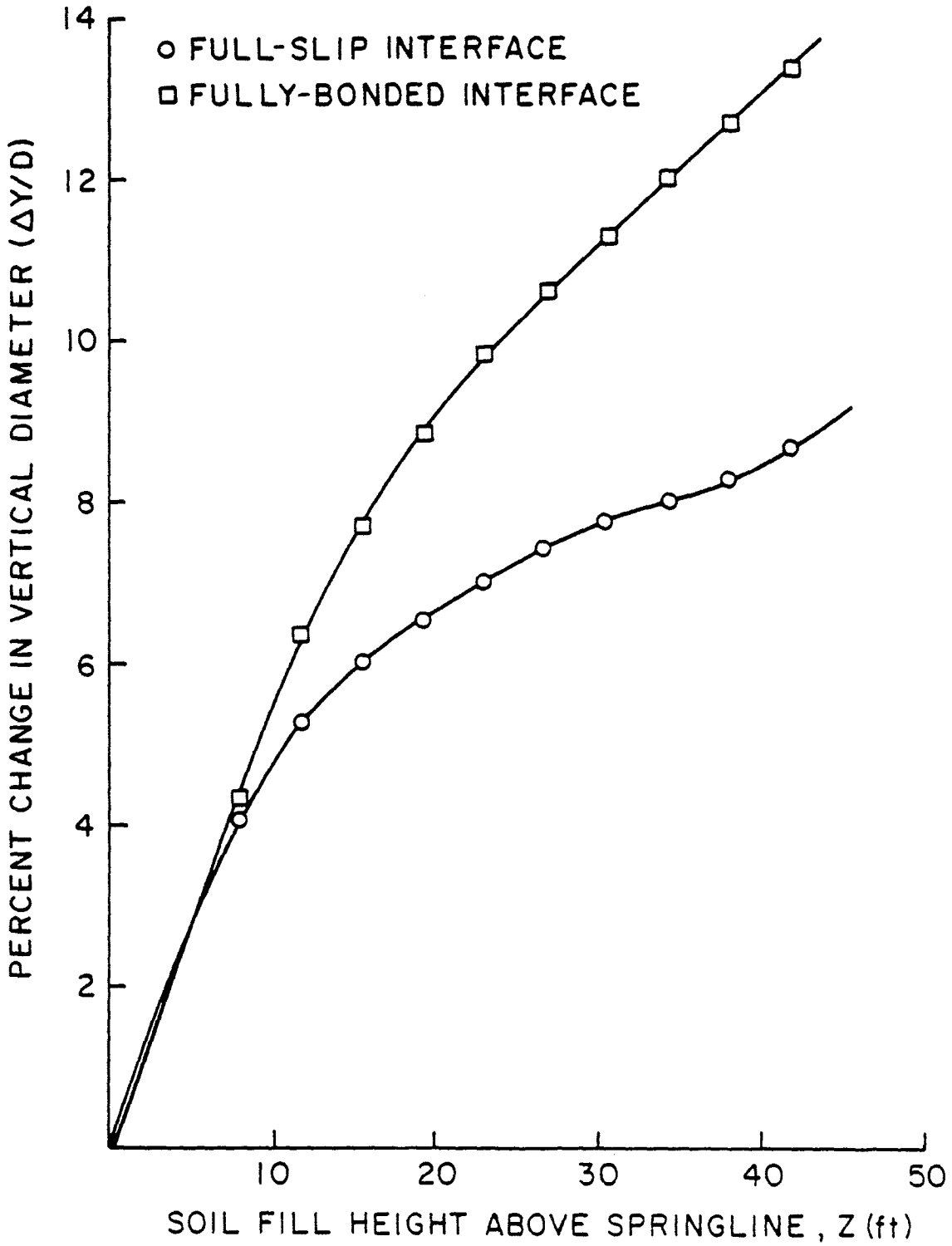

FIGURE 53. Effect of Soil-Pipe Interface Conditions on Pipe Deflection

(D=48, Weak ML, Profile #9, T=72, P=0)

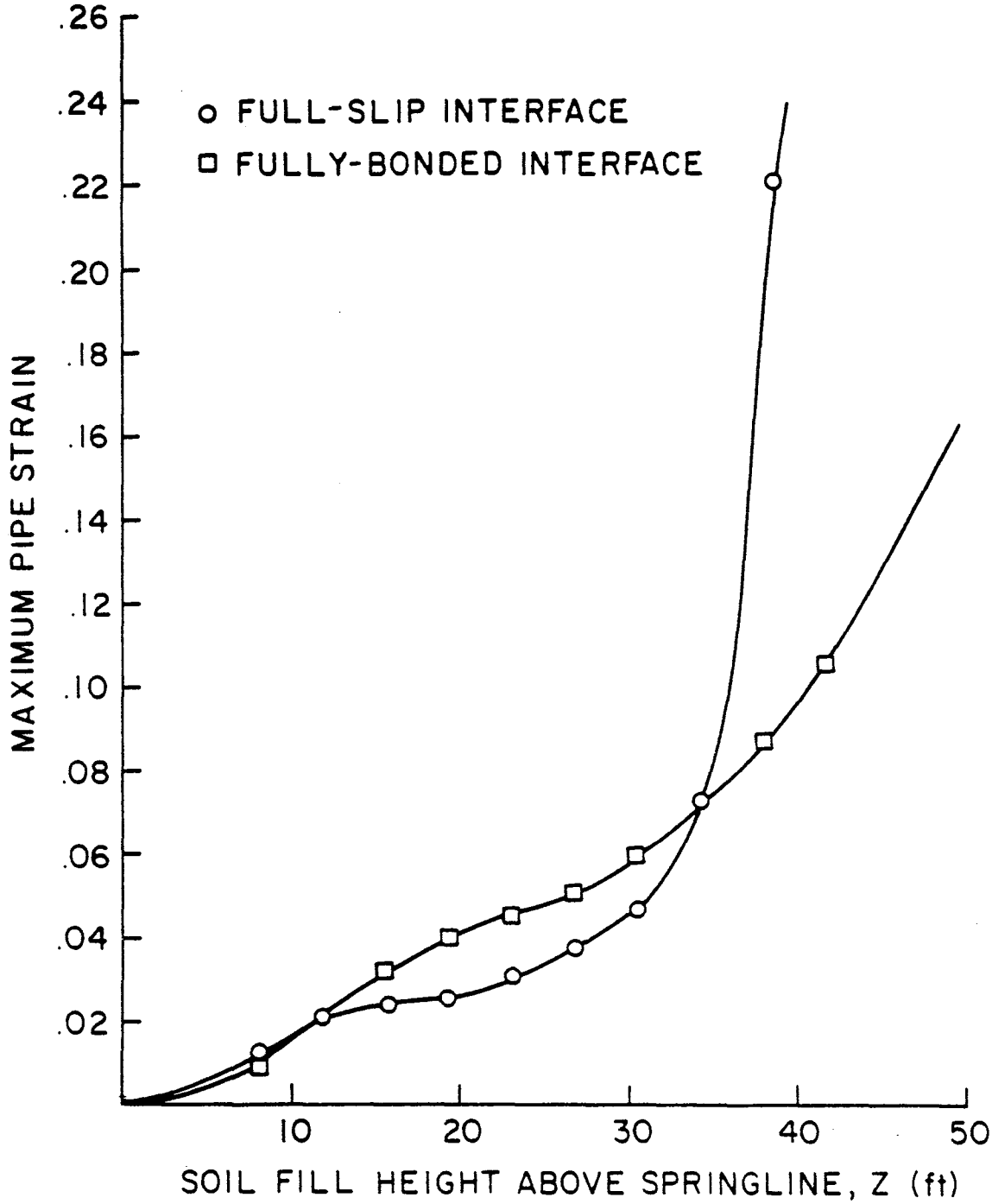

FIGURE 54. Effect of Soil-Pipe Interface Condition on Maximum Pipe Strain

(D=48, Weak ML, Profile #9, T=72, P=0)

formulating the regression equations, it does not allow the soil and pipe to undergo normal separation. The bonded interface assumption will, therefore, not allow the pipe to buckle unless the soil surrounding it also buckles.

In order to determine if buckling is a controlling design criterion, some additional runs were made using the full-slip interface. Since the pipe and the soil are permitted to separate when this interface model is used, it is possible for a buckling failure to occur. However, in a dry, weak silt, no buckling was observed for depths of cover up to 42 ft.

Deformed shapes for the bonded and full-slip interface condition are compared in Figure 55 for a 48 in. profile #9 pipe with 38 ft. of cover above the springline. The magnitude of deflection is smaller for the full-slip condition; however, the maximum wall strain in the pipe is somewhat larger at this depth of cover (see Table 12). This effect is caused by a large reverse moment at the pipe crown (see Figure 56).

The rapid change in the direction of the moment from negative (tension in the outer fibers) to positive (tension in the inner fibers) causes large strains or plastic hinging of the pipe section. This large change in moment is produced by an uneven normal presure distribution at the pipe crown. The value of the normal pressure at a point 18° from the crown is almost twice as large as the pressure at the crown, as is shown in Figure 57. These facts seem to indicate that a pipe buried in the absence of ground water will undergo a strain or wall crush failure before it will buckle.

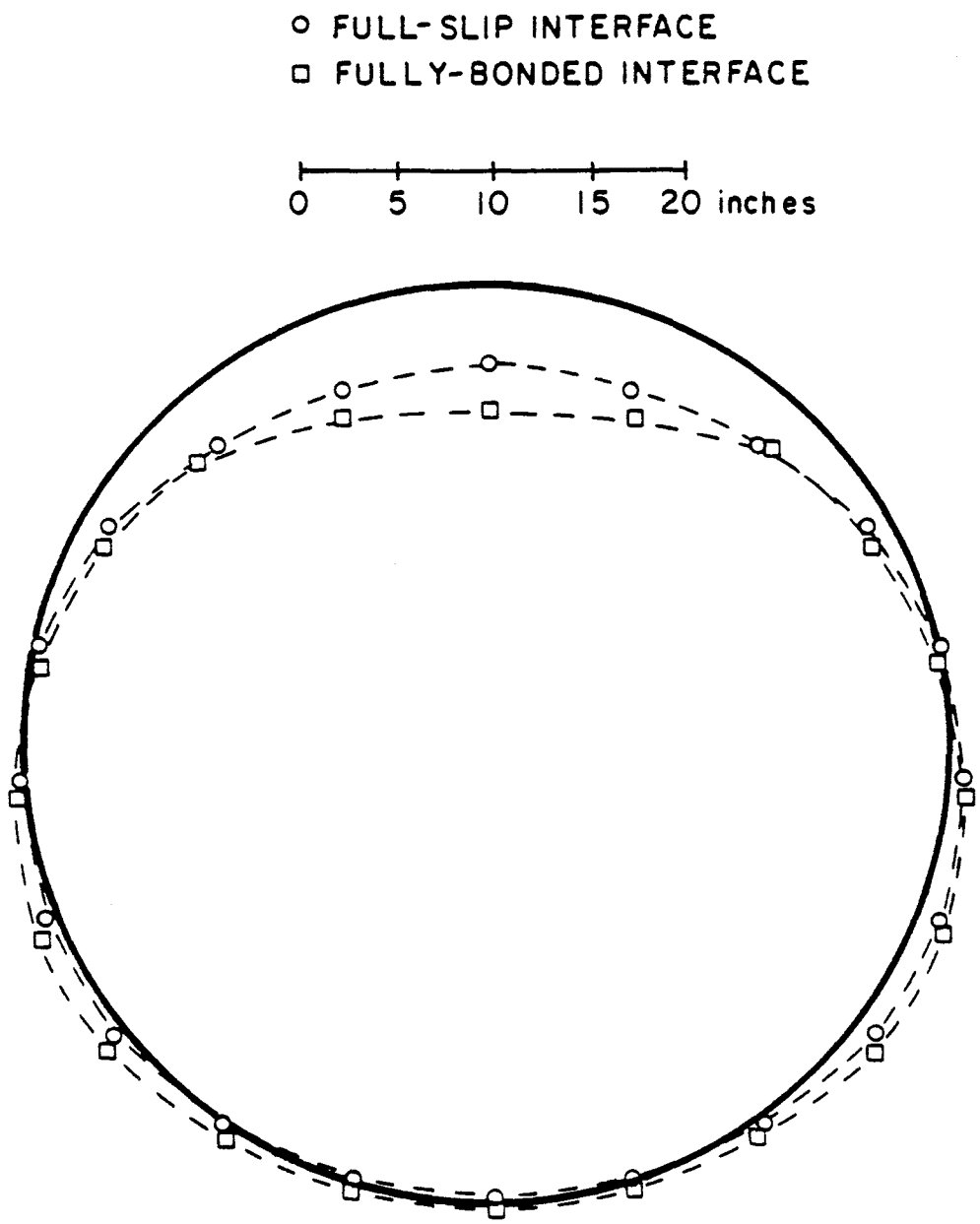

FIGURE 55. Effect of Soil-Pipe Interface on Deformed Shape for Z=38

(D=48, Weak ML, Profile #9, T=72, P=0)

TABLE 12. Effect of Soil-Pipe Interface on Strain Distributions for Z=38

(D=48, Profile #9, T=72, P=0, Weak Silt In-situ Soil)
(Negative Equals Compressive Strain)

Angular Location	Inner-Fiber Strain		Outer-Fiber Strain		Fraction of Wall Yield	
	Bonded	Full Slip	Bonded	Full Slip	Bonded	Full Slip
0	-0.0122	-0.0402	-0.0549	-0.0083	0.365	0.028
18	-0.0148	-0.0031	-0.0660	-0.2279	0.521	0.840
36	-0.0872	-0.0306	0.0008	-0.0282	0.544	0.000
54	-0.0290	-0.0334	-0.0496	-0.0228	0.500	0.000
72	-0.0366	-0.0322	-0.0281	-0.0252	0.000	0.000
90	-0.0361	-0.0340	-0.0324	-0.0215	0.000	0.000
108	-0.0397	-0.0318	-0.0293	-0.0261	0.036	0.000
126	-0.0495	-0.0347	-0.0192	-0.0201	0.336	0.000
144	-0.0245	-0.0263	-0.0527	-0.0375	0.453	0.000
162	-0.0276	-0.0266	-0.0384	-0.0367	0.000	0.000
180	-0.0280	-0.0266	-0.0368	-0.0367	0.000	0.000

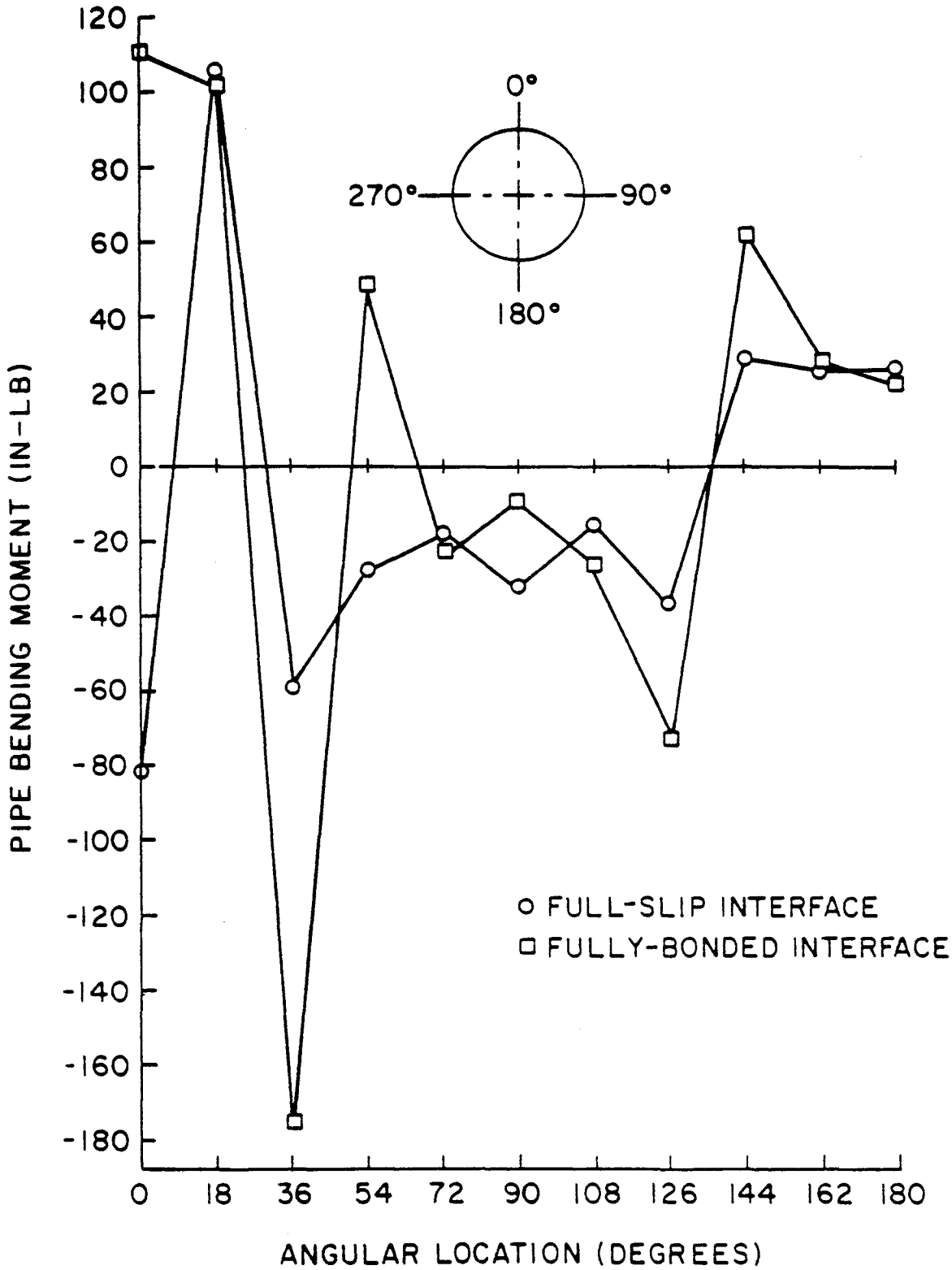

FIGURE 56. Effect of Soil-Pipe Interface Conditions on Pipe Bending Moment for Z=38

(D=48, Weak ML, Profile #9, T=72, P=0)

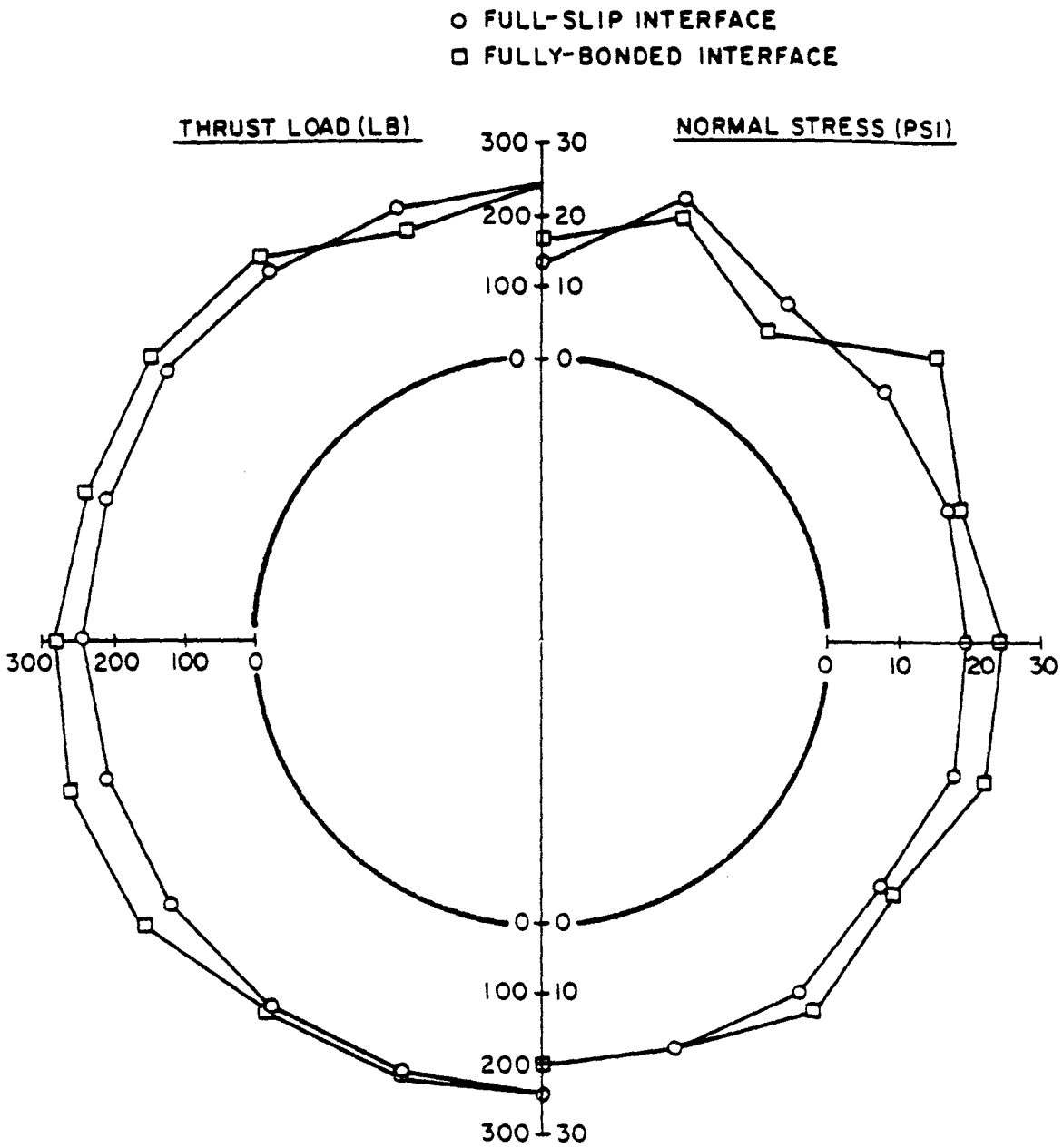

FIGURE 57. Effect of Soil-Pipe Interface on Thrust Loads and Normal Stress Distributions for Z=38

(D=48, Weak ML, Profile #9, T=72, P=0)

When a full-slip interface condition was used in conjunction with high ground water pressures, it was impossible to obtain numerical convergence. It is very hard to determine if this instability is due to the inadequacies of the CANDE interface model to handle pore pressure boundary condition or if, in fact, high ground water pressures produce a definite physical instability. Since no full-scale test data are available to answer this question, a full explanation of this problem will have to be postponed until the appropriate tests have been conducted.

This dilemma does not help the design engineer confront the problem of buckling in high ground water conditions; however, several empirical equations that provide a way to compute the expected buckling load of a buried flexible pipe are available in the literature (11,26,27). One of these equations, developed by Chelapati and Allgood (26) is programmed into CANDE. A factor of safety against buckling is calculated by comparing the average normal pressure on the pipe with the expected buckling load from Chelapati and Allgood's elastic buckling equation given below.

$$P_{cr} = 6\sqrt{M_s(1-K_s)EI/D^3} \tag{59}$$

where

P_{cr} = the critical buckling pressure,

M_s = confined modulus of the soil,

K_s = lateral coefficient of the soil

= $\sqrt{s}/(1-\sqrt{s})$,

ν_s = Poisson's ratio of the soil,

EI = in-plane bending stiffness of the pipe, and

D = pipe diameter.

The soil and pipe properties used in the equation are found by calculating the average pipe stiffness and the average confining modulus and Poisson's ratio of the complete soil mass. For the cases studied in this project, the factor of safety against buckling was always greater than 1.0 when the pipe strains were below the elastic limit.

This fact indicates that the buckling of flexible plastic pipes is, in fact, due to plastic behavior of the pipe wall. It is, therefore, reasonable to assume that buckling will not be a problem if the strains calculated with the regression equation are below the yield value of the pipe material. However, if calculated strain values are greater than the yield value, buckling should be checked with one of the available empirical equations for cases where high ground water tables are expected.

When checking buckling, one compares the empirical buckling pressure calculated with one of the buckling equations with the expected average normal pressure on the conduit. Since calculating this average pressure can be a problem unless a finite element analysis is used, the overburden pressure at the crown is often used for the expected normal pressure around the pipe. This simplifying assumption ignores the soil arching around the pipe and is, in fact, quite conservative.

Figure 58, which was constructed from CANDE outputs, allows the

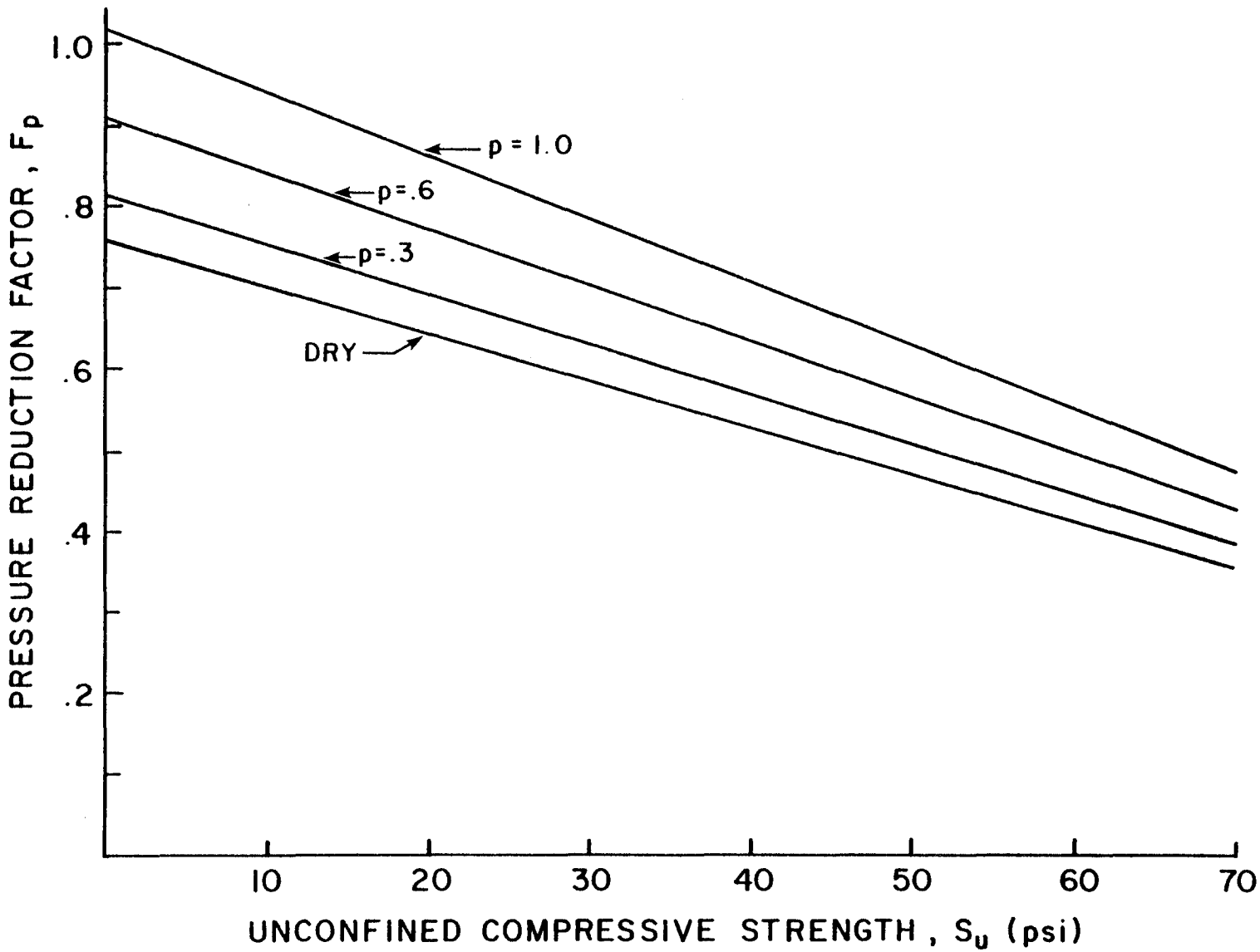

FIGURE 58. Overburden Reduction Factor to Account for Soil Arching

determination of a reduction factor to be multiplied by the overburden pressure at the crown of the pipe in order to account for soil arching. The values calculated from Figure 58 are dependent on water table height and on the unconfined compressive strength of the in-situ soil. These values were determined with the #3 backfill type. If a #2 or #1 backfill type is used, the values found in Figure 58 can be reduced by a factor of 0.91 and 0.77, respectively.

LIVE LOAD STUDY

Extensive full-scale testing of buried corrugated polyethylene pipes under high live or traffic loads has been conducted at Utah State University by Watkins (24). The basic conclusion of his study is that buried flexible polyethylene pipe will function successfully with a minimum depth of cover of one foot even when 54 kips per axle super-loads are applied. Successful pipe performance was even reported with zero depth of cover above the pipe when a compacted backfill material was used.

Watkins' data seem to indicate that depth of cover is of no great concern if the pipe is properly installed. At low depths of cover, the soil pipe system is very dependent on the stiffness and degree of compaction of the backfill material. Adequate compaction and placement of the fill soil around the pipe is, therefore, required for successful pipe performance. Watkins' data also indicated that larger diameter pipes actually perform better than smaller diameter pipes; the majority of the larger pipe is at a great enough depth to not be

affected by the stress concentration at the surface due to the wheel loads.

In order to verify Watkins' results and to see if his data could be extrapolated beyond the largest pipe size tested (24 in. diameter pipe), a CANDE live load analysis was performed. The basic trench geometry for the 48 in. profile #9 pipe loaded with only 6 inches of cover above the crown is shown in Figure 59. An 18-kip dual tire load was applied on each side of the pipe to simulate a tandem-axle heavy-truck load on a shallow buried flexible pipe.

Since the CANDE program uses the plane-strain assumption, the circular 80 psi, 6 inch radius tire load had to be converted to an equivalent plane strain load. A procedure developed by Lytton and Kohutek (28) provided a way to estimate the reduction factor which can be applied to the 80 psi tire load in order to arrive at an equivalent uniform strip load. These factors, developed by using elastic theories of beams, plates, and shells resting on an elastic subgrade, establish the plane-strain strip load which will produce a deformation basin which is equivalent to the actual deformation basin observed under a tire load. The net result is that an 80 psi, 6 inch radius tire load can be modeled in a plane strain finite element program by simply applying a pressure equal to 16.72 psi along a 6 inch width. This value was doubled to account for each of the dual tires and applied to 6 inches of the finite element mesh at the two tire locations shown in Figure 59.

The resulting deformed shape is shown in Figure 60. The net vertical deflection of only 2% of the diameter is well below the 10%

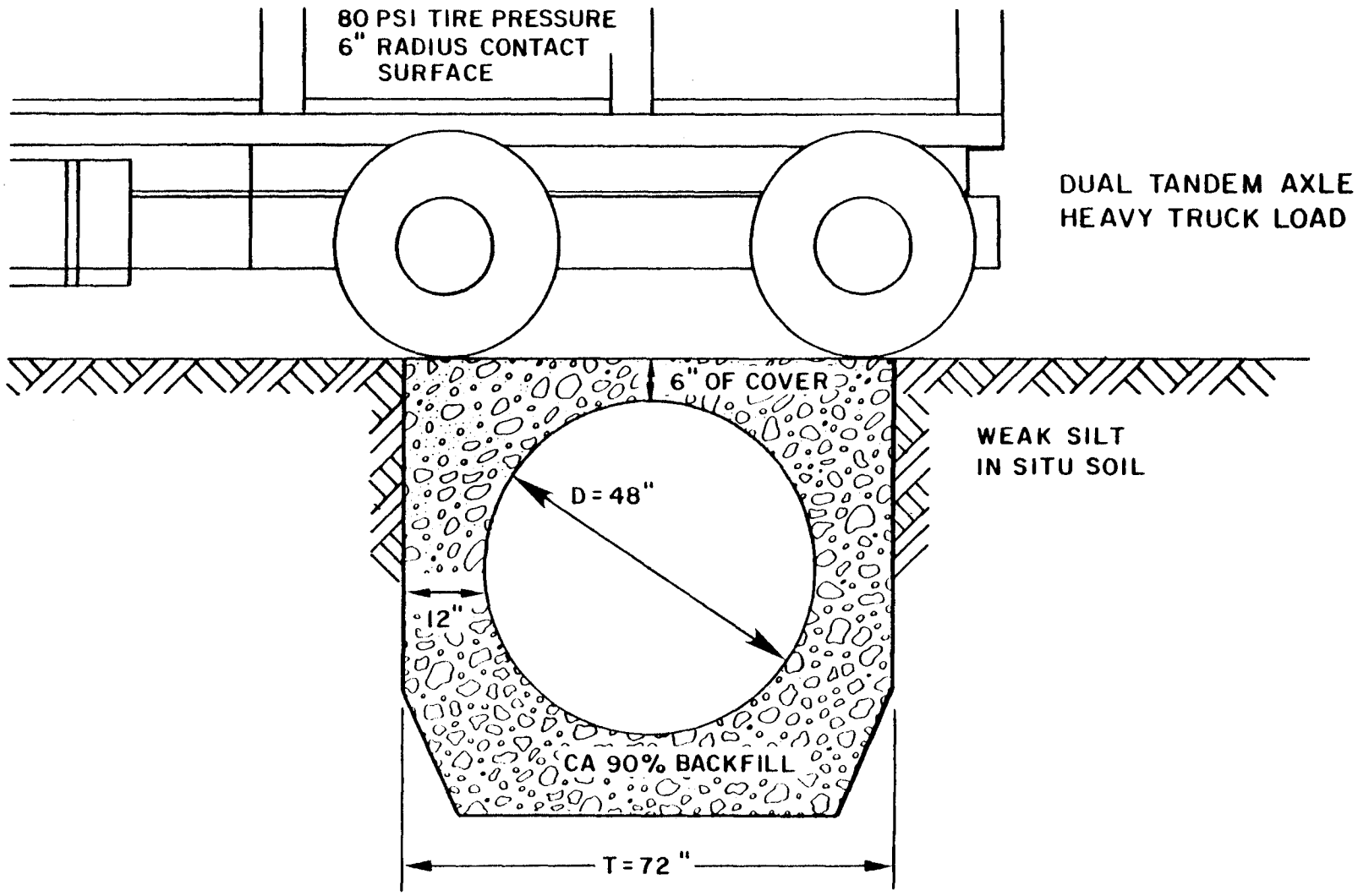

FIGURE 59. Live Load Geometric Properties

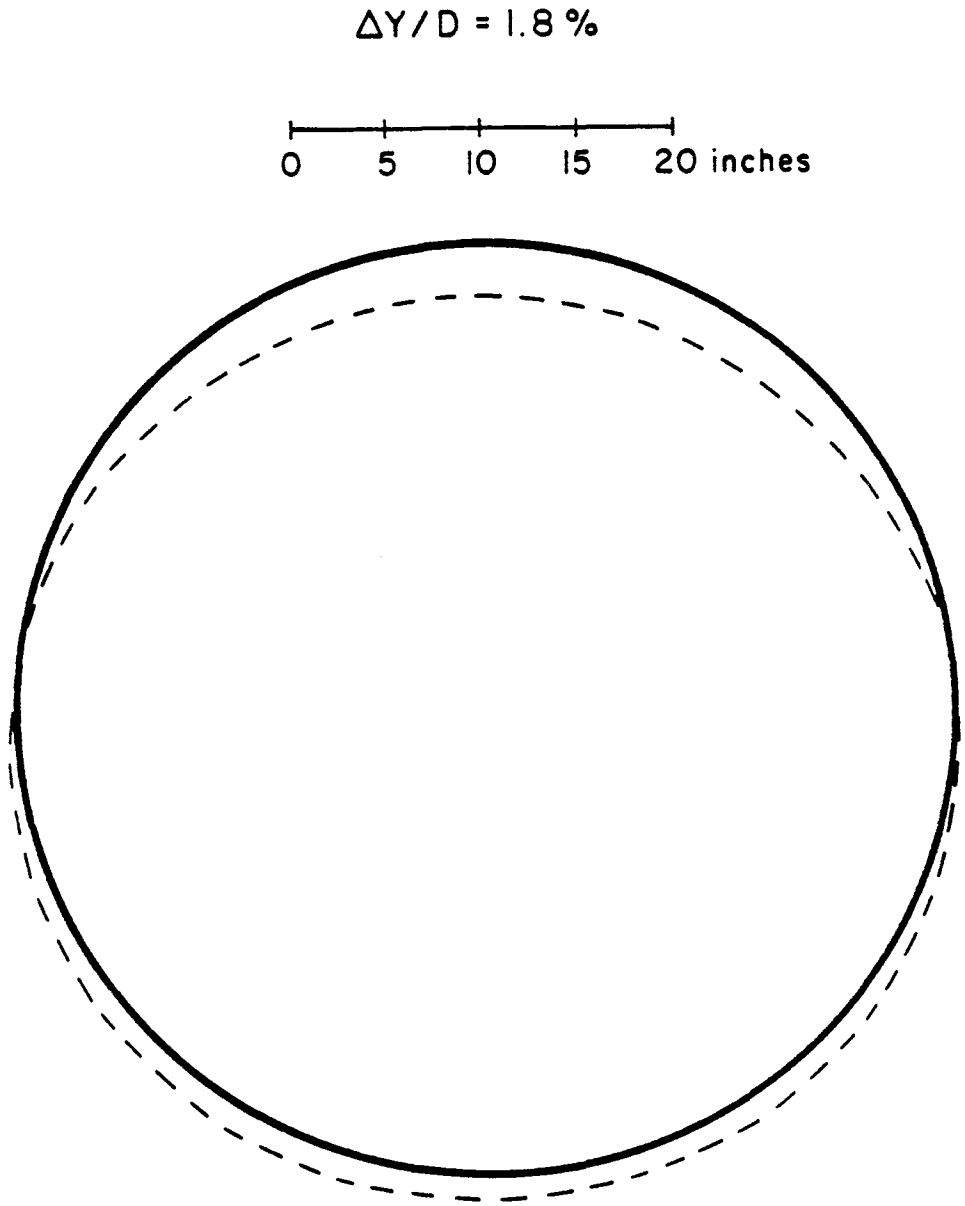

FIGURE 60. Deformed Shape for a Dual-Tire Tandem-Axle Heavy-Truck Load With 6 in. of Cover

(D=48, Weak ML, Profile #9, T=72, P=0)

allowable for most designs. Figure 61 shows the strain distribution for the outer and inner fibers of the pipe wall. The maximum wall strain of .0140 in/in is also well below the yield value of the material. Figure 62 shows the normal and shear stress distributions around the pipe. The small pressures at the pipe crown show the benefits of flexible pipe materials. The weak soil-pipe system at the top of the pipe deforms under the load, relieving the pressure which must then be transferred to other, stronger portions of the soil-pipe system.

The loading configuration was picked because it is believed (24) to produce the highest distress levels in the pipe. Further analysis using unsymmetric loads would be applicable for a large design problem.

BACKFILL DENSITY AND LOCATION

Probably the most difficult variables to determine and control in a flexible pipe installation in fine-grained soils are the backfill density and the actual amount or location of this backfill material. When installing a pipe in poor ground conditions, it is very easy to develop layers of the in-situ soil or voids in the granular backfill. In narrow trench applications, achieving adequate compaction of the material under the pipe haunches can be a problem. Unsymmetric over-compaction can also produce large initial deformations in the pipe. All of these variables are hard to determine from a design point of view since they depend, to a great extent, on the experience and

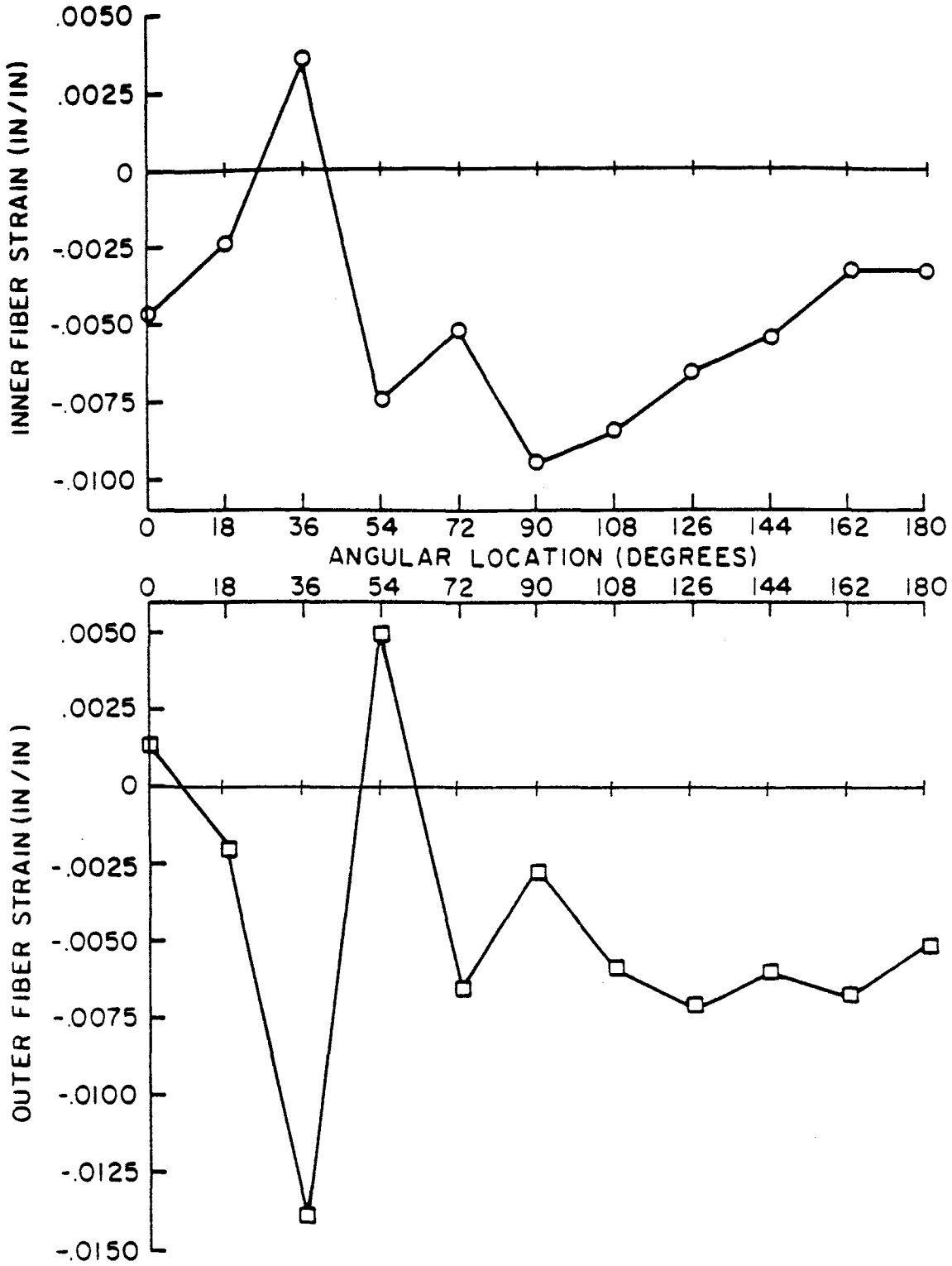

FIGURE 61. Strain Distributions for a Dual-Tire Tandem-Axle Heavy-Truck Load With 6 in. of Cover

(D=48, Weak ML, Profile #9, T=72, P=0)

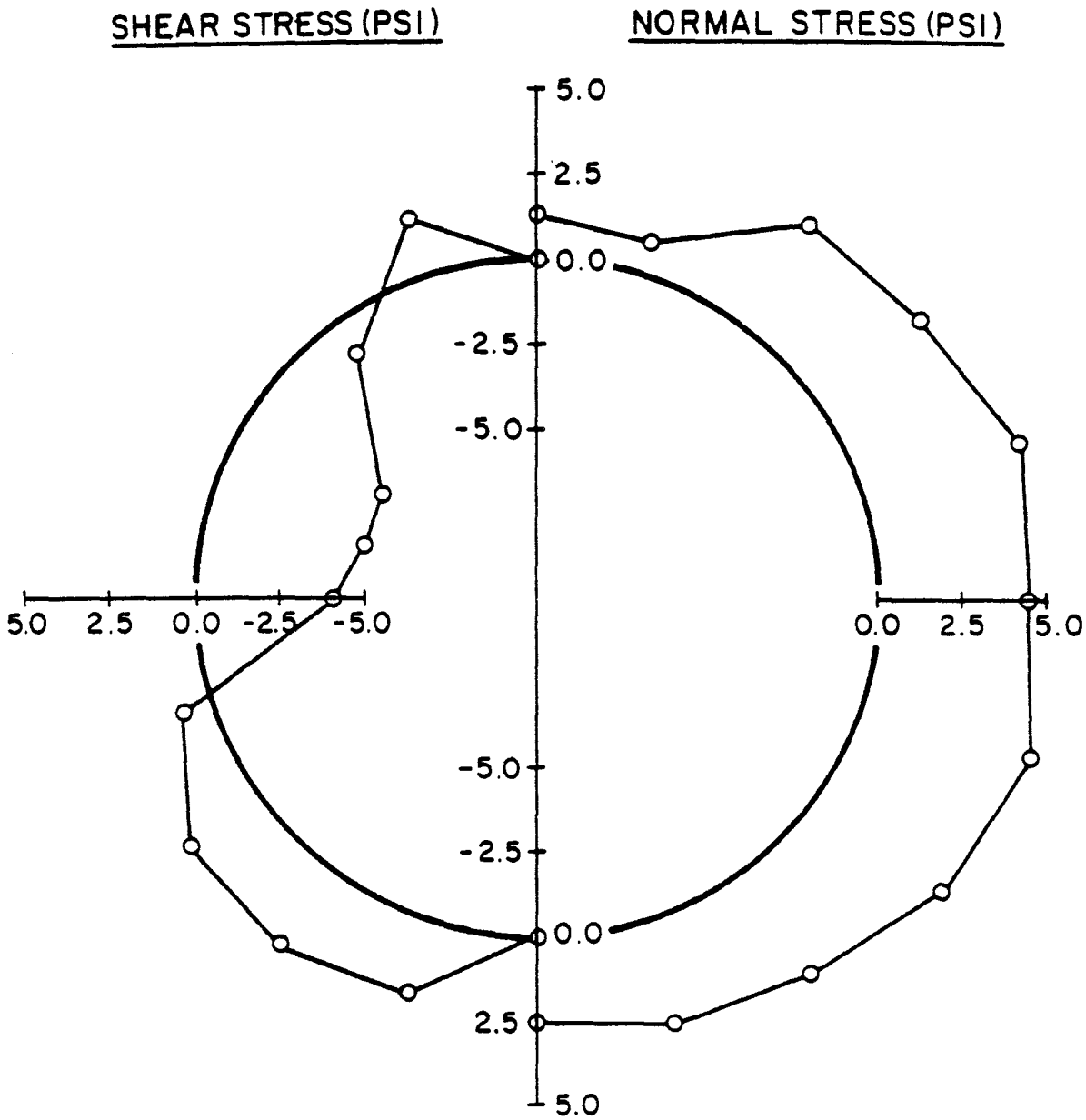

FIGURE 62. Normal and Shear Stress Distributions for a Dual-Tire Tandem-Axle Heavy-Truck Load With 6 in. of Cover

(D=48, Weak ML, Profile #9, T=72, P=0)

reliability of the contractors that install the pipe.

In a hope to successfully bridge some of the unpredictability associated with backfill strength and compaction loads, a conservative backfill material was used in the design equations. However, it is still necessary to use a factor of safety in order to ensure that the maximum levels of pipe strain and deflection due to unexpected load and improper backfill placement are above an acceptable level.

One of the inherent difficulties with the use of flexible plastic pipes is that the variables which are the most difficult to determine are also some of the most important. Backfill density, as previously stated, is an important variable when designing flexible plastic pipes in weak in-situ soils (see Figure 40 and 41). This tendency also applies in strong in-situ soil types, as can be seen in Figures 63 and 64, where the displacements and strains are compared for the different backfill types in a strong silty clay in-situ material.

To establish the range of pipe performance when different amounts of primary or granular backfill are used, several additional CANDE runs were made. The effects of changing the bedding material from the in-situ soil to granular fill material is shown in Figures 65 and 66. Bedding the pipe in granular material reduces the maximum wall strain by approximately 25% but has very little effect on displacement.

A comparison of the effects of different amounts of primary granular backfill was also investigated. A 48 in. profile #9 pipe was bedded in a #3 backfill in all cases, but the amount of additional fill was varied from 50% (#3 backfill to the springline with in-situ fill above that) to 125% (#3 backfill from the bedding zone to a

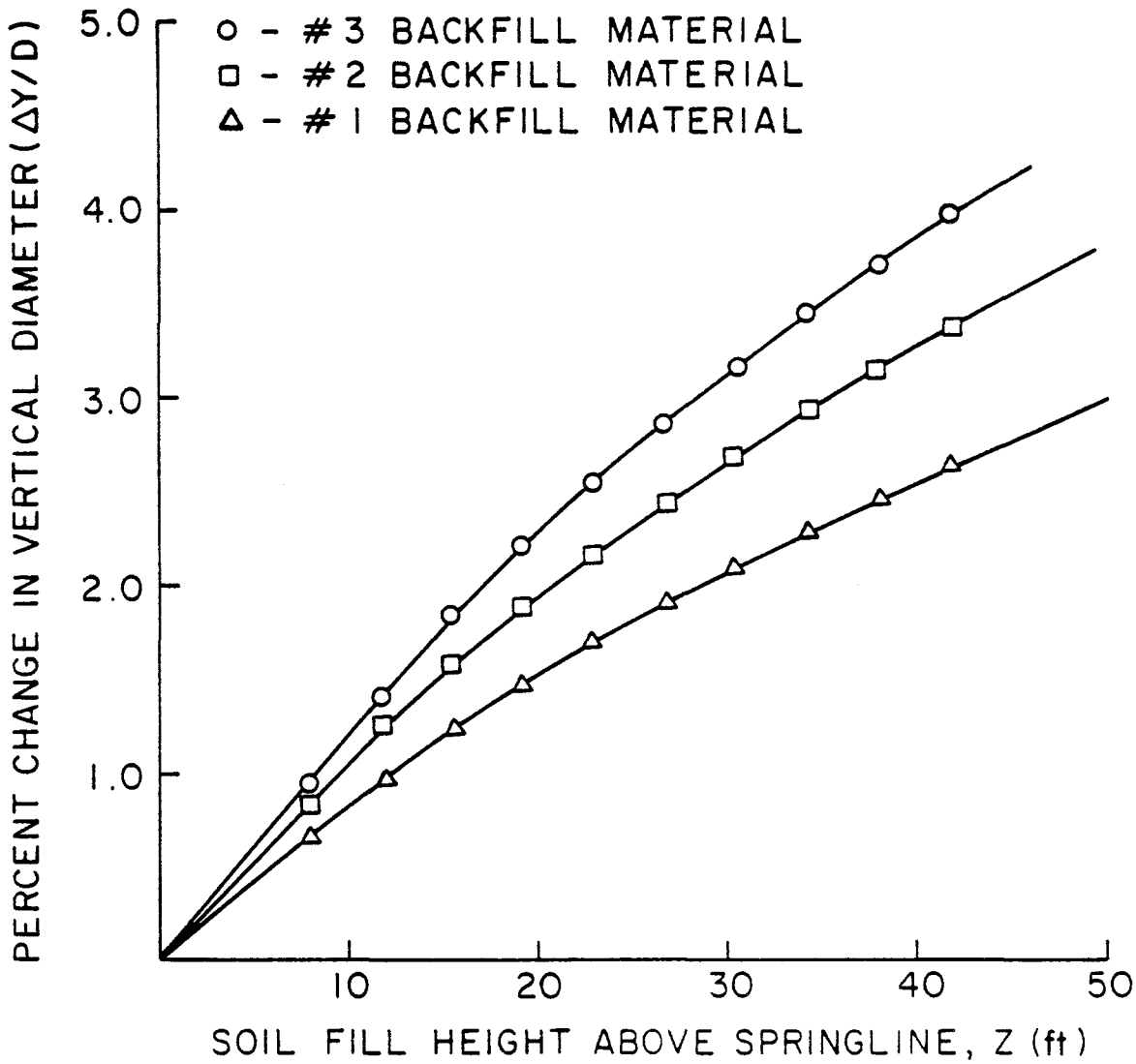

FIGURE 63. Effect of Backfill Type on Pipe Deflection With a Strong In-situ Soil

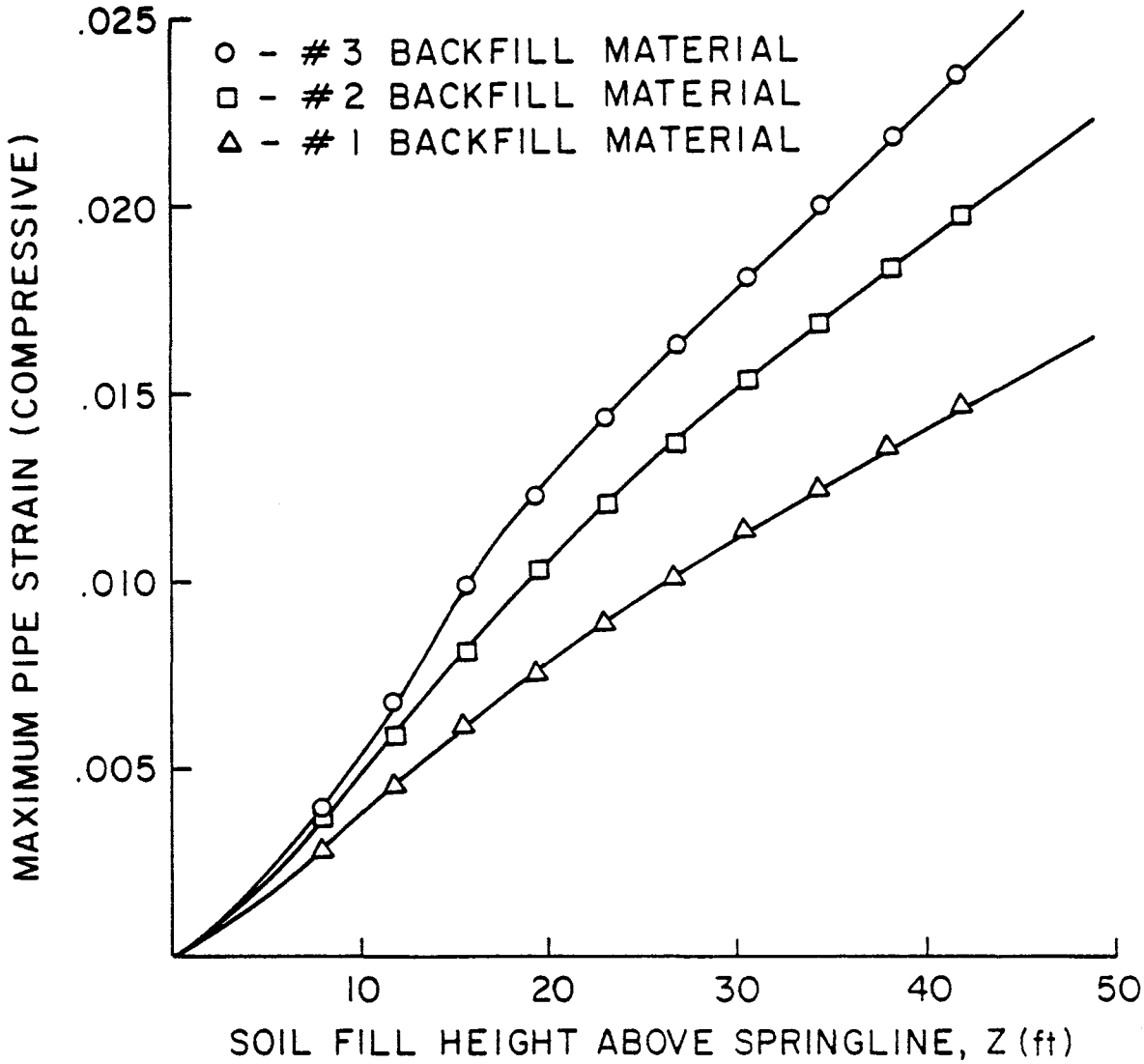

FIGURE 64. Effect of Backfill Type on Maximum Pipe-Wall Strain With a Strong In-situ Soil

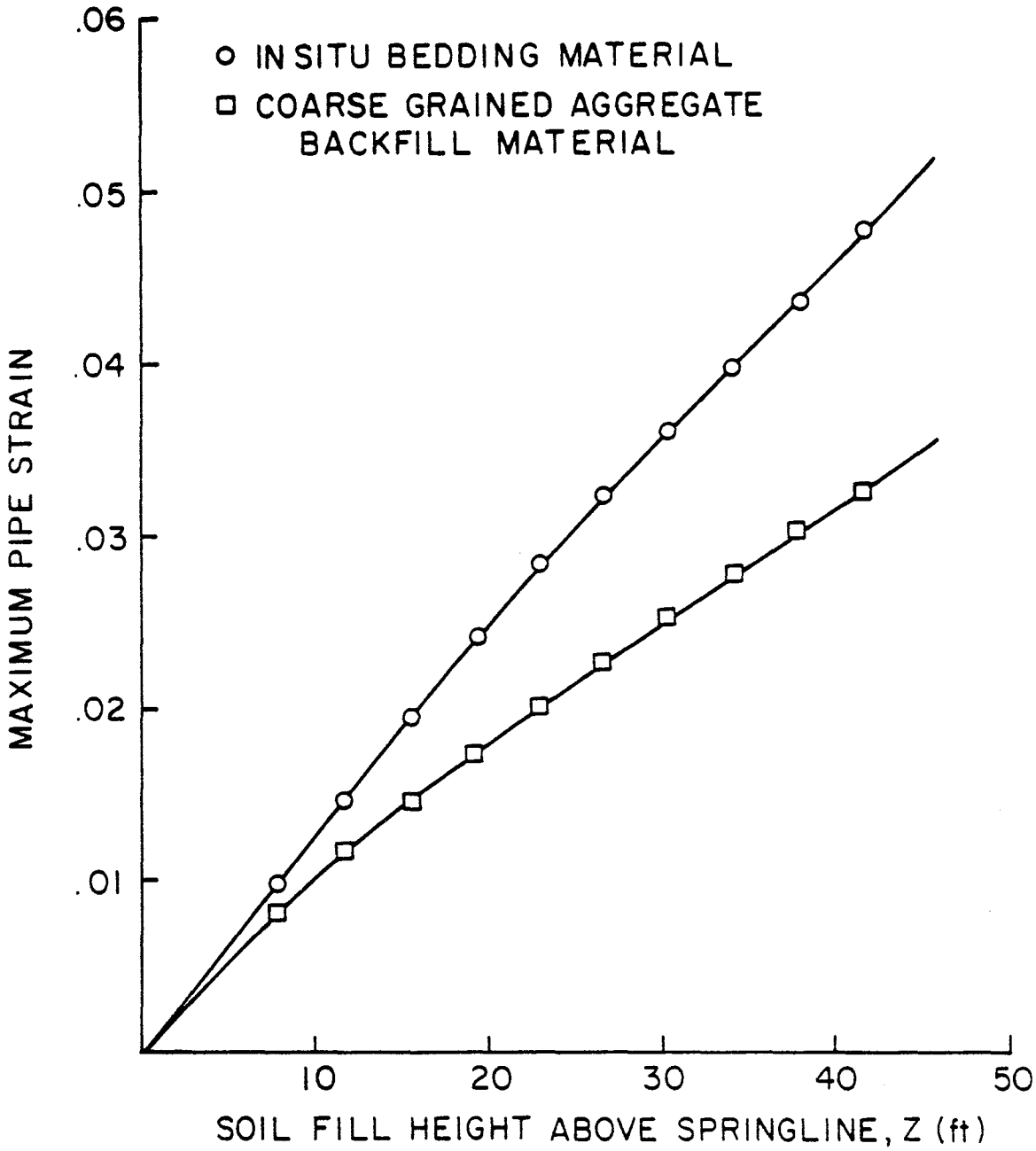

FIGURE 65. Effect of Bedding Material on Maximum Pipe Strain

(D=48, Profile #9, T=72, No Water Table, Weak Silt In-situ Soil, 105% RC Backfill)

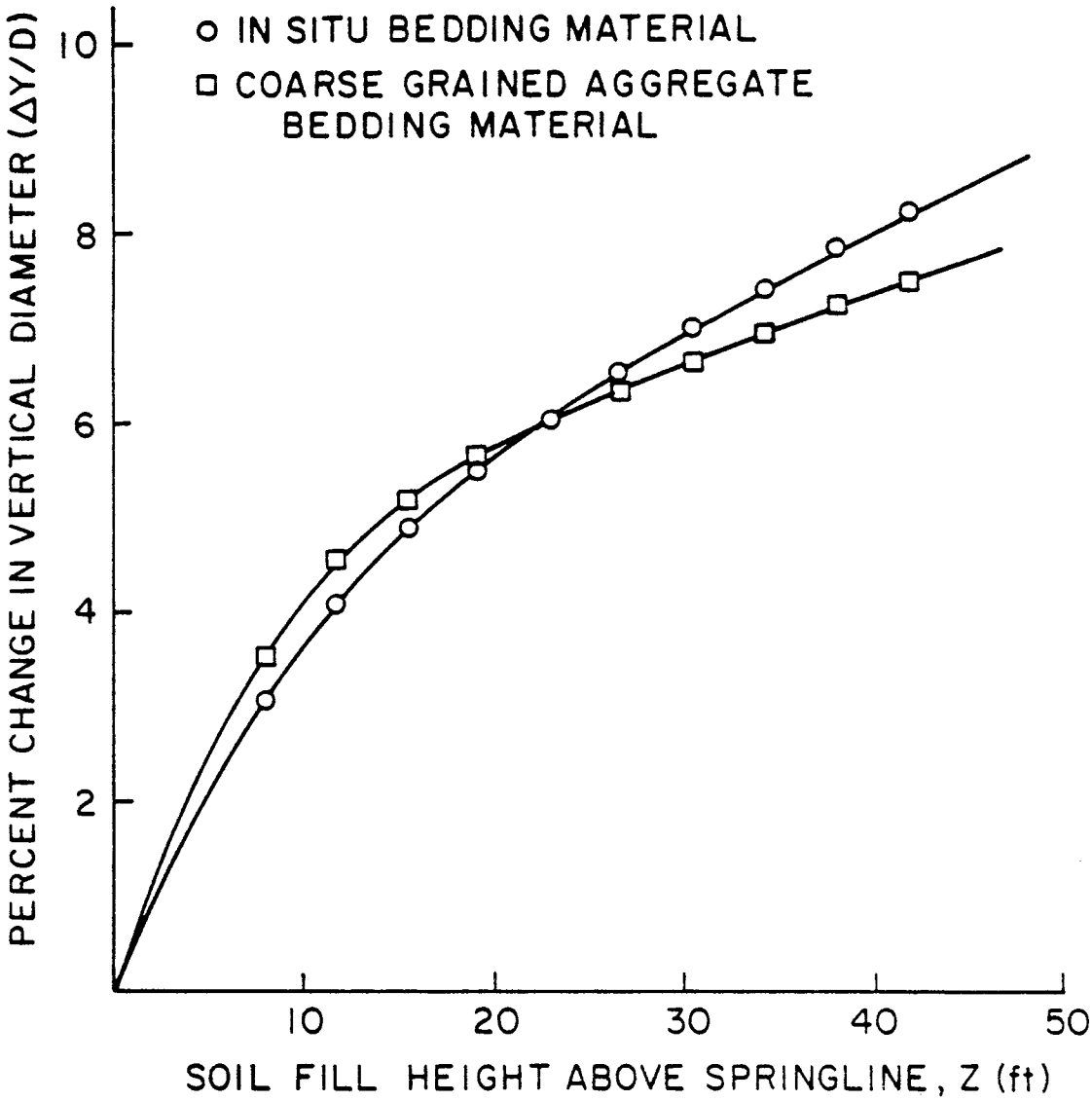

FIGURE 66. Effect of Bedding Material on Pipe Deflection

(D=48, Profile #9, T=72, No Water Table, Weak Silt In-situ Soil, 105% RC Backfill Material)

distance of 0.25D above the pipe). Placing the #3 backfill material to a distance of 0.25D above the pipe greatly reduced the maximum wall strains for large depths of cover, as can be seen in Figure 67. Contrary to what might be expected, placing the #3 backfill material just to the crown of the pipe (100% primary backfill case) creates higher strain levels than those found when placing primary backfill only up to the springline (50% primary backfill case).

This can be explained by a careful examination of the pressure distribution around the pipe (Figure 68) and the moments and thrust loads produced (Figure 69). The normal pressure at the pipe crown is very small for the 100% primary backfill case; however, at a location only 18° from the crown, the pressure is high. The reverse moment caused by this rapid variation in normal pressure produced large strains. The reverse moment does not, however, produce as large displacements as the 50% primary backfill case (see Figure 70). The large reverse moment at the springline found in the 50% primary backfill case produces a larger change in vertical diameter. It appears that the change in material properties or stiffnesses when going from the backfill material to the in-situ fill produces a reverse moment in the pipe at the location of the interface of the two materials. It is, therefore, beneficial to make the transition from backfill material to in-situ fill well above the pipe in order to prevent any stress concentrations or large moment reversals.

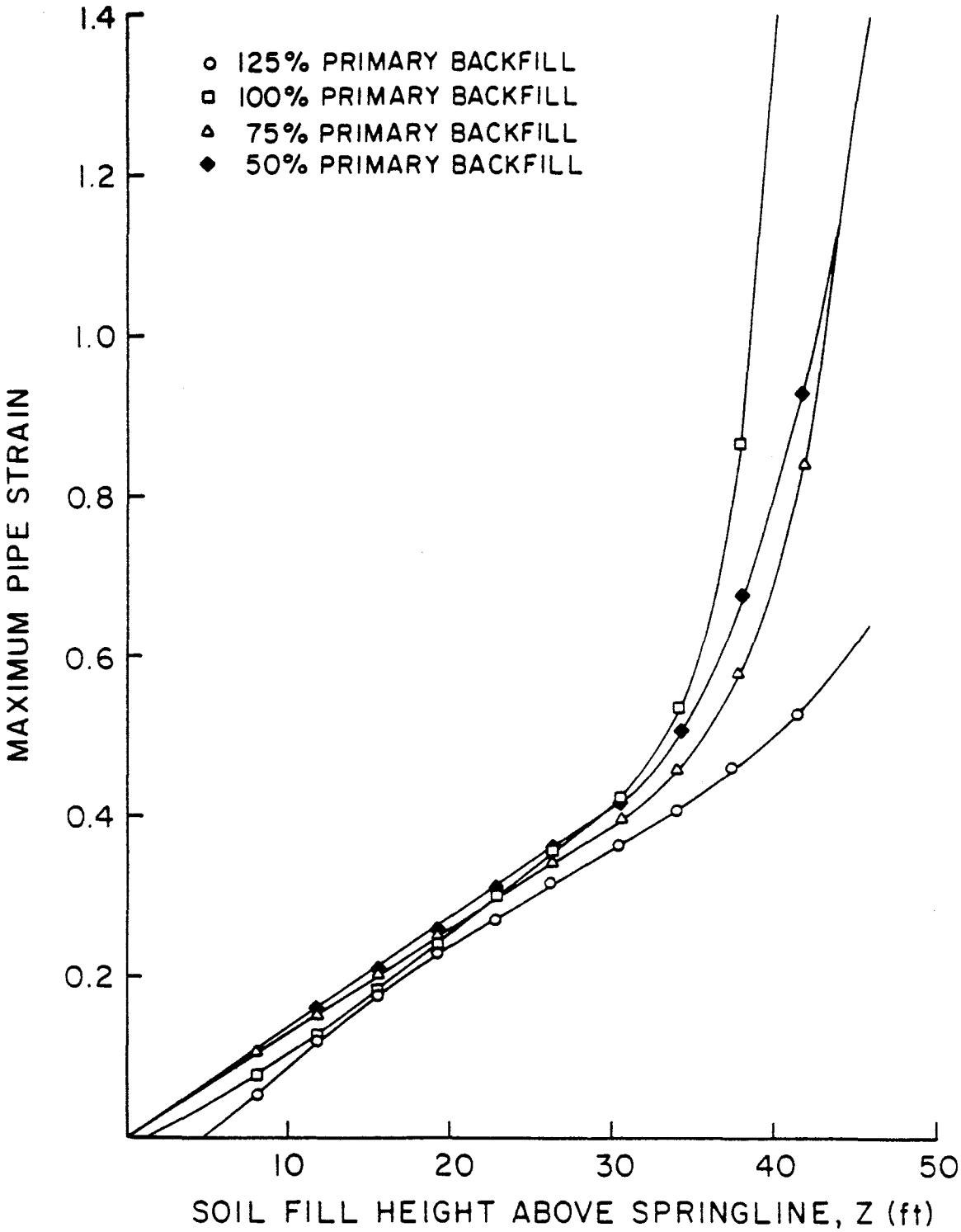

FIGURE 67. Effect of Varying the Amount of Primary Backfill on Maximum Pipe Strain

(D=48, CL*ML, Profile #9, T=72, P=0, Weak Fill)

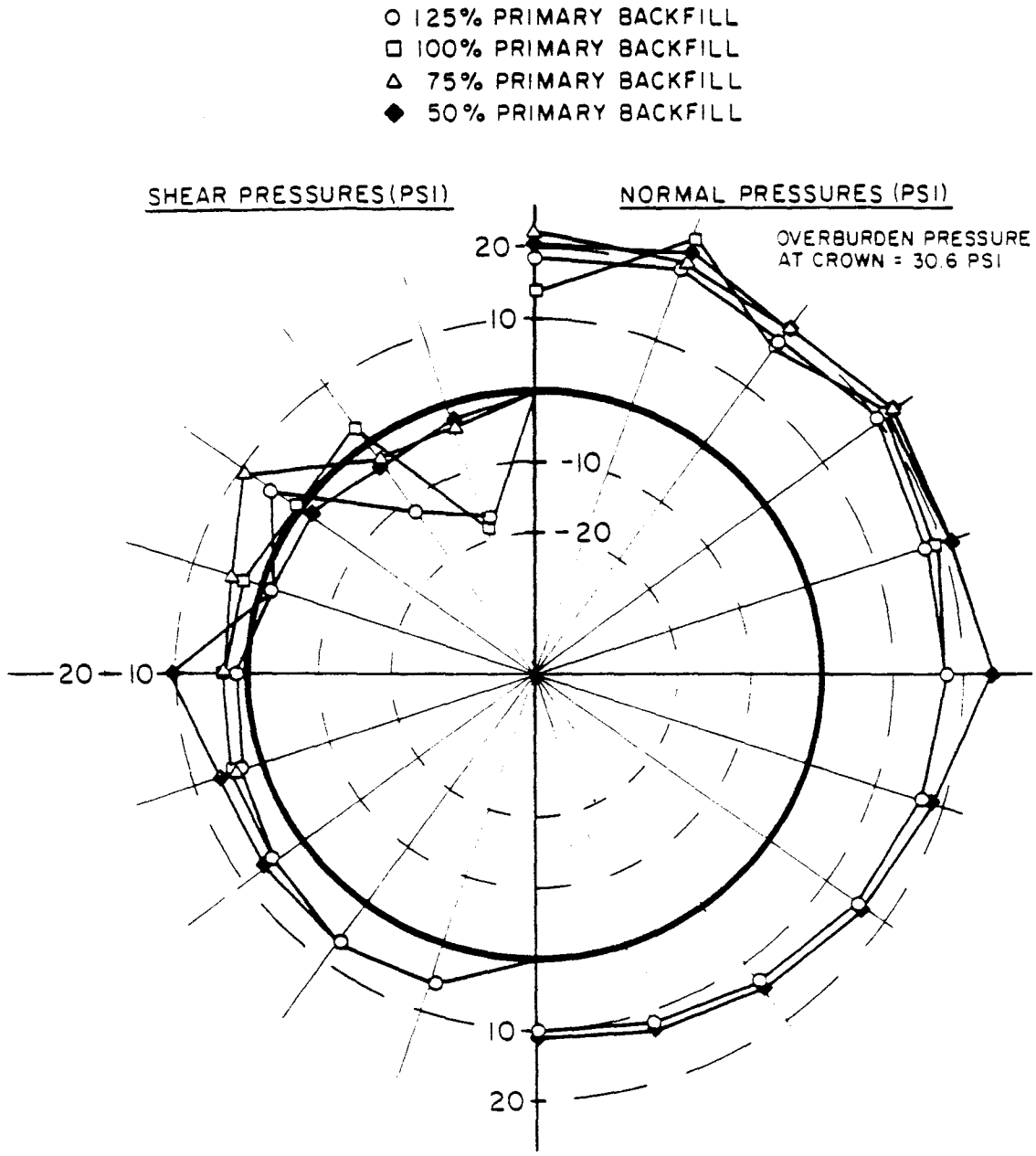

FIGURE 68. Effect of Primary Backfill Location of Normal and Shear Pressures

(D=48, CL*ML, Profile #9, T=72, P=0, Weak Fill, Z=38)

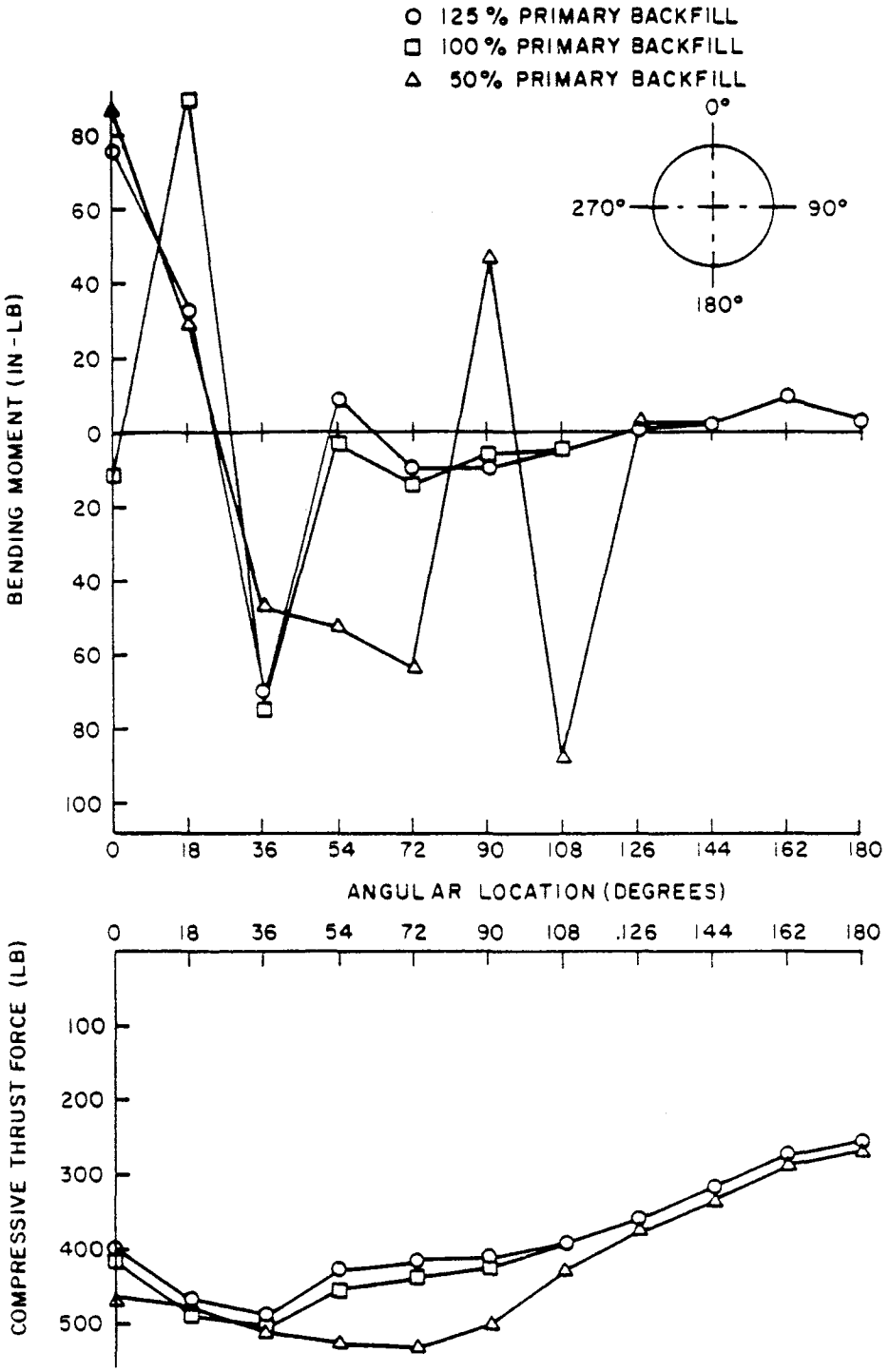

FIGURE 69. Effect of Primary Backfill Location on Maximum Pipe Moments and Thrust Loads

(D=48, CL*ML, Profile #9, T=72, P=0, Weak Fill, Z=38)

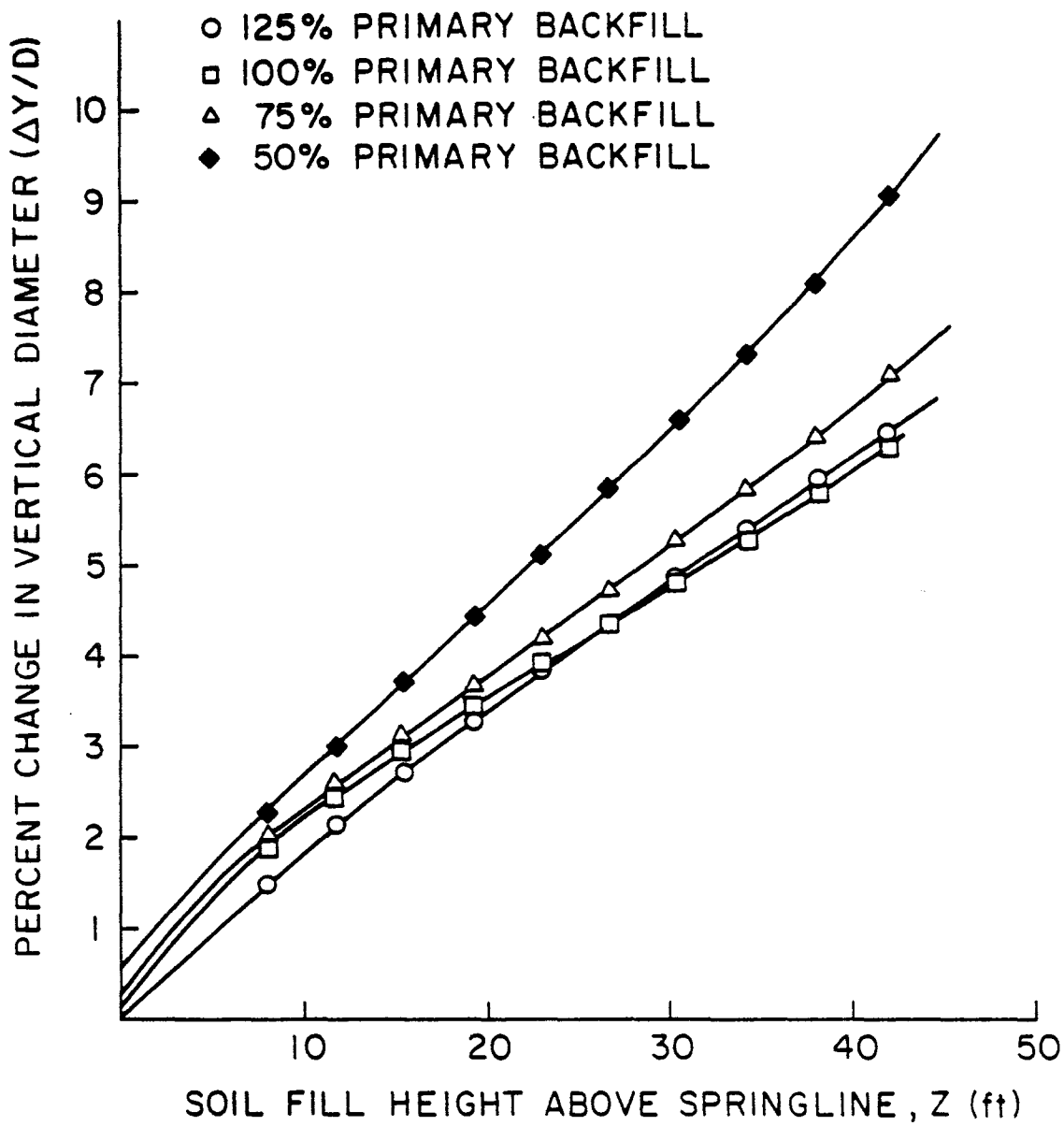

FIGURE 70. Effect of Primary Backfill Location on Maximum Pipe Displacement

(D=48, CL*ML, Profile #9, T=72, P=0, Weak Fill)

CONCLUSIONS AND RECOMMENDATIONS

CONCLUSIONS

The design of flexible high-density polyethylene profile-wall pipe is a soil-structure interaction problem. The performance of a buried polyethylene pipe is highly governed by the properties of the in-situ soil it is buried in and by the quality of backfill surrounding it. These effects are much more pronounced when analyzing flexible pipes than when considering rigid pipe types. It is, therefore, logical to conclude that the ductility and flexibility characteristics of high-density polyethylene pipe produce a soil-structure interaction system which cannot be analyzed using conventional rigid pipe formulas.

The equations for maximum fiber strain and maximum pipe deflection developed in this study represent a reliable way to calculate expected pipe performance in terms of the many governing design parameters. In-situ soil types, quality and strength of the backfill material, pipe size, pipe stiffness, trench width, burial depth, ground water, and design time are all incorporated into the design equations. These equations, when programmed on a hand-held calculator (Appendix C) or on a small micro-computer, provide a simple way to design flexible plastic pipes.

The design equations were generated using state-of-the-art methods in soil-structure interaction that incorporate both the

nonlinear and stress-dependent material properties of soils. As a result, the soil parameters needed to utilize these equations are somewhat complex. Triaxial tests are required to arrive at the hyperbolic soil parameters in these equations. However, a given soil can be classified and its hyperbolic stress-strain parameters can be determined from the presumptive soil charts developed in this study.

For elastic design of flexible pipes in wet, fine-grained soils, strain is the most important design criterion. Yield strains in the pipe wall can be produced at deflections that are both above and below the standard 5% deflection limit. However, small amounts of yielding in the outermost fibers of the pipe wall do not produce failure. In fact, the high ductility of polyethylene provides a large strain capacity. The regression equations for post-yield strains provide a way to estimate the expected size of these plastic strains.

The modified CANDE program is a realistic approach to analyzing this or other unique design problems. The post-yield behavior of nonsymmetric pipe cross sections or unusual trench geometries can be analyzed in detail with one CANDE run. Such analysis allows the utilization of the full capacity of the polyethylene material in plastic design.

Parameter studies investigating live loads, buckling, and the amount of backfill material, provide additional information about flexible pipe performance. The best backfill configuration is one in which the pipe is completely surrounded by coarse-grained material. This backfill placement produces a uniform pressure distribution which limits the amount of bending moment on the pipe wall section and

insures a full utilization of the pipe-wall material through the production of a uniform compressive thrust load. Buckling was determined not to be a controlling failure mode in dry ground applications. In the presence of large amounts of ground water, it was difficult to model the soil-pipe interface with a slip element which allowed the soil and pipe to separate. It was, therefore, difficult to determine if buckling would actually be the controlling failure mode; however, some empirical buckling equations were provided which allow the design engineer to check whether the critical buckling pressure is exceeded. Full-scale test data (24), which found that live loads were not a problem for depths of cover above the pipe greater than 1 foot, were confirmed with the CANDE program.

The design equations were extensively confirmed with additional CANDE runs (Appendix D) and found to adequately represent the performance of flexible plastic pipes even for applications that were not directly incorporated in the full factorial study. Predicted displacements were also verified with one set of full-scale field test data. This time dependent full-scale test data closely matched the design equations, adding support to the overall model used in this study and to the assumptions that were made concerning soil and pipe creep behavior.

RECOMMENDATIONS

Full-scale test data investigating the question of buckling would be most beneficial. Vacuum tests or the close monitoring of actual

pipe installations in high ground water conditions are necessary before a reliable prediction of buckling failure can be determined. A more rigorous investigation of live load placement intensities would enable the prediction of actual pipe stress, strain, and deflection values for very small or zero depths of cover.

Installation loads due to improperly placed backfill can produce large isolated displacements and strains in a buried pipe even before the trench is completely filled. A close examination of actual construction procedures and compaction loads could possibly provide a stochastic means of qualifying the variance of pipe stress, strain, and deflection levels due to installation procedures and construction crews; this would be a great asset to the design engineer.

More stringent soil and pipe creep testing coupled with a full viscoelastic solution would further verify the assumptions made regarding creep. A complete analysis of polyethylene pipe behavior in coarse-grained soils is also needed before the complete design of flexible plastic pipes can be updated with state-of-the-art soil-structure interaction theory.

REFERENCES

1. Katona, M. G., et al., "CANDE - A Modern Approach for the Structural Design and Analysis of Buried Culverts," Report No. FHWA-RD-77-5, Federal Highway Administration, Washington, D.C., October 1976.

2. Katona, M. G., Vittes, P. D., Lee, C. H., and Ho, H. T., "CANDE - 1980: Box Culverts and Soil Models," Federal Highway Administration Report No. FHWA-RD-80-172, Washington, D.C., May 1981.

3. Schapery, R. A. and Riggins, M., "Development of Cyclic Nonlinear Viscoelastic Constitutive Equations for Marine Sediments," Proceedings of the International Symposium on Numerical Models in Geomechanics, Zurich, Switzerland, September 1982.

4. Riggins, M., "The Viscoelastic Characterization of Marine Sediment in Large-Scale Simple Shear," Ph.D. Dissertation, Civil Engineering Department, Texas A&M University, May 1981.

5. Marimon, A. M., "The Effects of Suction and Temperature on the Material Characteristics of Fine-Grained Soils," Master of Engineering Report, Texas A&M University, November 1977.

6. Duncan, J. M., Byrne, P., Wong, K. S., and Mabry, P., "Strength, Stress-Strain, and Bulk Modulus Parameters for Finite Element Analyses of Stresses and Movements in Soil Masses," Report No. UCB/GT/80-G1, University of California, Berkeley, August 1980.

7. Marston, A., "The Theory of External Loads on Closed Conduits in the Light of the Latest Experiments," Proceedings HRB, Vol. 9, 1930, pp. 138-170.

8. Spangler, M. G. and Handy, R. L., Soil Engineering, Third Edition, Intext Educational Publishers, New York and London, 1973.

9. Watkins, R. K. and Spangler, M. G., "Some Characteristics of the Modulus of Pressure Resistance of Soil: A Study in Similitude," Proceedings HRB, Vol. 37, 1958, pp. 576-583.

10. White, H. L. and Layer, J. P., "The Corrugated Metal Conduit as a Compression Ring," Proceedings HRB, Vol. 39, 1960, pp. 389-397.

11. Leonards, G. A. and Stetkar, R. A., "Performance of Buried Flexible Conduits," Report No. FHWA-79-S0873.

12. Roark, R. J., Formulas for Stress and Strain, Second Edition, McGraw-Hill Book Company, New York, 1943.

13. Lee, C. H., "Evaluation of Duncan's Hyperbolic Soil Model," Master's Thesis, University of Notre Dame, May 1979.

14. Leonards, G. A., Wu, T. H., and Juang, C. H., "Predicting Performance of Buried Conduits," Report No. FHWA-IN-JHPP-81-3, Purdue University, June 1982.

15. Katona, M. G., "On the Analysis of Long Span Culverts by the Finite Element Method," Transportation Research Board, January 1978.

16. Kondner, R. L., "Hyperbolic Stress-Strain Response: Cohesive Soils," Journal of Soil Mechanics and Foundation Division, ASCE, Vol. 89, No. SM1, February 1963, p. 115.

17. Kondner, R. L. and Zelasko, J. S., "A Hyperbolic Stress-Strain Formulation of Sands," Proceedings of the 2nd PanAmerican Conference on Soil Mechanics and Foundation Engineering, Vol. 1, Brazil, 1963, p. 289.

18. Lin, T. Y. and Burns, N. H., Design of Prestressed Concrete Structures, Third Edition, John Wiley & Sons, New York, 1981.

19. Sendeckyj, G. P., Editor, Volume 2 - Mechanics of Composite Materials, Academic Press, New York, 1974, Chapter 4, "Viscoelastic Behavior and Analysis of Composite Materials," by R. A. Schapery.

20. Schapery, R. A., "On a Thermodynamic Constitutive Theory and Its Application to Various Nonlinear Materials," Proceedings of the IVTAM Symposium on Thermoinelasticity, Springer-Verlay, New York, 1969, pp. 259-285.

21. Ward, I. M., Mechanical Properties of Solid Polyners, Wiley, New York, 1971.

22. Schapery, R. A., "Wave-Sea Bottom Interaction Study (Phase One) Part 1: Theory and Results," Report No. MM 3007-74-1, Mechanics and Materials Research Center, Texas A&M University, College Station, Texas, 1974.

23. Stevenson, H. S., "Vane Shear Determination of the Viscoelastic Shear Modulus of Submarine Sediments," Thesis presented to Texas A&M University, College Station, Texas, 1973, in partial fulfillment of the requirements for the degree of Master of Science.

24. Katona, M. G., "A Simple Contact-Friction Interface Element With Applications to Buried Culverts," International Journal of Numerical Analysis Methods for Geomechanics, Vol. 7, 371-384, 1983.

25. Watkins, R. K., Reeve, R. C., and Goddard, J. B., "Effects of Heavy Loads on Buried Corrugated Pipe," Utah State University, September 1982.

26. Allgood, J. R. and Chelapati, C. V., "Buckling of Cylinders in a Confining Medium," HRR No. 413, 1972.

27. Glascock, B. and Cagle, L. L., "Recommendation of Elastic Buckling Design Requirements for Buried Flexible Pipe," a report of the C-950 Ad Hoc Committee on Buckling.

28. Lytton, R. L. and Kohutek, G. L., "Evaluation of AASHO Road Test Satellite and Environmental Studies," Final Report Phase II to the National Cooperative Highway Research Program, January 1983.

29. Katona, M. G. and Smith, J. M., "CANDE User's Manual," Report No. FHWA-RD-77-6, Federal Highway Administration, Washington, D.C., October 1976.

APPENDICES

APPENDIX A

SOLUTION FOR TRANSFORMED AREA EQUATIONS

APPENDIX A

SOLUTION FOR TRANSFORMED AREA EQUATIONS

The solution of the set of linear equations, 24, 25, 26 and 27 is shown below.

$$P2 = \frac{L - \frac{GB}{t} - \frac{(J-2G)(F-CB/t)}{(D-2C)}}{K - G - \frac{(J-2G)(E-C)}{(D-2C)}}$$

$$P3 = \frac{F - CBt}{D - 2C} - \frac{P2(E-C)}{D-2C}$$

$$P4 = B/t - P2 - 2PL$$

where

$B = A-PS$

$C = t^3/12 + t(7t/2 + S - Z)^2$

$D = \frac{8H^3}{12} + 2t\ (2t + S - Z)^2$

$E = t^3/12 + t(S + t/2 - Z)^2$

$F = I - PS3/12 - SP\ (Z - S/2)^2$

$G = Zt - t(7t/2 + S)$

$J = 2Zt - 2t\ (2t + S)$

$K = Zt - t\ (S + t/2)$

$L = PS^2/2 - ZSP$

APPENDIX B

TABLES OF DESIGN TIME FACTORS

TABLE B-1. Design Time Factors for Regression Equations With a #3 Backfill Material

Z ft	ΔY/D, %						
	10 year	30 day	30 day/ 10 yr	25 year	25/10 year	50 year	50/10 year
8	4.31	3.03	.70	4.70	1.09	4.95	1.15
11.75	6.19	4.78	.77	6.86	1.11	7.26	1.17
15.5	7.71	5.96	.77	8.53	1.11	9.01	1.17
19.25	8.85	6.84	.77	9.77	1.10	10.31	1.17
23.0	9.83	7.62	.77	10.84	1.10	11.43	1.16
26.75	10.63	8.38	.78	11.72	1.10	12.36	1.16
30.5	11.35	8.89	.78	12.50	1.10	13.19	1.16
34.25	12.03	9.47	.79	13.25	1.10	14.0	1.16
38.0	12.69	9.99	.78	13.99	1.10	14.79	1.17
41.75	13.38	10.50	.77	14.77	1.10	15.61	1.17
Average			.77		1.10		1.164

TABLE B-1. Design Time Factors for Regression Equations With a #3 Backfill Material (Cont'd)

Z ft	ε_p						
	10 year	30 day	30 day/ 10 yr	25 year	25/10 year	50 year	50/10 year
8	.0096	.0068	.70	.0111	1.156	.0117	1.219
11.75	.0212	.0213	1.00	.0237	1.118	.0250	1.179
15.5	.0330	.0307	.93	.0363	1.100	.0381	1.155
19.25	.0396	.0368	.93	.0432	1.091	.0451	1.13
23.0	.0452	.0422	.93	.0485	1.073	.0504	1.115
26.75	.0499	.0456	.91	.0566	1.134	.0618	1.239
30.5	.0601	.0573	.95	.0677	1.126	.0745	1.240
34.25	.0724	.0716	.98	.0810	1.119	.0900	1.243
38.0	.0872	.0857	.98	.0970	1.112	.1084	1.243
41.75	.1055	.1005	.98	.1169	1.108	5.48	NA
Average			.93		1.114		1.196

TABLE B-2. Design Time Factors for Regression Equations Using a Silty Clay In-situ Soil With a #1 Backfill Material

Z ft	ΔY/D, %								
	10 year	2 hour	2 hr/ 10 yr	30 day	30 day/ 10 yr	25 year	25/10 year	50 year	50/10 year
8.0	1.70	.87	.51	1.23	.72	1.86	1.09	1.96	1.15
11.75	2.17	1.16	.54	1.61	.74	2.38	1.10	2.51	1.16
15.5	2.56	1.40	.55	1.91	.74	2.80	1.09	2.95	1.15
19.25	2.87	1.60	.56	2.16	.75	3.14	1.09	3.31	1.15
23.0	3.15	1.78	.57	2.39	.76	3.45	1.09	3.62	1.15
26.75	3.41	1.95	.57	2.60	.76	3.73	1.09	3.92	1.15
30.5	3.66	2.11	.58	2.80	.77	4.00	1.09	4.20	1.15
34.25	3.90	2.27	.58	2.99	.77	4.26	1.09	4.48	1.15
38.0	4.13	2.42	.59	3.18	.77	4.52	1.09	4.74	1.15
41.75	4.36	2.56	.59	3.36	.77	4.76	1.09	5.00	1.15
Average			.57		.76		1.09		1.15

TABLE B-2. Design Time Factors for Regression Equations
Using a Silty Clay In-situ Soil With a #1 Backfill Material (Cont'd)

Z ft	ε_p								
	10 year	2 hour	2 hr/ 10 yr	30 day	30 day/ 10 yr	25 year	25/10 year	50 year	50/10 year
8.0	.0056	.0035	.63	.0044	.79	.0063	1.13	.0066	1.18
11.75	.0089	.0057	.64	.0071	.80	.0099	1.11	.0103	1.16
15.5	.0116	.0075	.65	.0093	.80	.0129	1.11	.0135	1.16
19.25	.0141	.0091	.65	.0113	.80	.0156	1.11	.0163	1.16
23.0	.0164	.0106	.65	.0132	.80	.0181	1.10	.0189	1.15
26.75	.0186	.0120	.65	.0150	.81	.0206	1.11	.0215	1.16
30.5	.0207	.0134	.65	.0167	.81	.0229	1.11	.0240	1.16
34.25	.0228	.0147	.64	.0184	.81	.0252	1.11	.0264	1.16
38.0	.0249	.0160	.64	.0200	.80	.0275	1.10	.0287	1.15
41.75	.0269	.0173	.64	.0216	.80	.0299	1.10	.0310	1.15
Average			.64		.88		1.11		1.16

APPENDIX C

DESIGN PROGRAM FOR THE HP 41CV CALCULATOR

APPENDIX C

DESIGN PROGRAM FOR THE HP 41CV CALCULATOR

In order to simplify the use of the design equations produced in this study, the following program was written for the HP 41CV hand held calculator. The program has two user friendly input options. The first, which is contained in a separate program DATIN, is called from the main program DESIN. This option prompts the user for direct input of each of the input variables. The second option allows the user to modify or change the input variables without reentering the complete set.

In the listing of the two programs, **bold** face letters indicate characters which must be input when the calculator is in alpha input mode.

LISTING OF PROGRAM

```
001  LBL DESIN
002  ENTER 1 FOR YES
003  AVIEW
004  PSE
005  0.0
006  STO 30
007  DATA INPUT?
008  PROMPT
009  X > 0?
010  XEQ DATIN
011  RCL 30
012  CHANGES TO DATA
013  PROMPT
014  X > 0?
015  XEQ 03
016  .08210739
017  ENTER
018  RCL 00
019  RCL 01
020  /
021  .2117832
022  *
023  +
024  RCL 02
025  12
026  *
027  RCL 01
028  /
029  .00295748
030  *
031  -
032  RCL 03
033  RCL 02
034  *
035  144
036  /
037  STO 28
038  14.7
039  /
040  RCL 04
041  Y^X
042  RCL 05
043  *
044  STO 18
```

```
045  .00362555
046  *
047  +
048  RCL 06
049  .42408107
050  *
051  -
052  RCL 28
053  14.7
054  /
055  RCL 07
056  Y^X
057  RCL 08
058  *
059  STO 19
060  .00037415
061  *
062  -
063  RCL 16
064  14.7
065  /
066  .77607170
067  *
068  +
069  1.8
070  X > Y?
071  X <> Y
072  STO 20
073  KO =
074  ARCL X
075  AVIEW
076  STOP
077  RAD
078  RCL 14
079  COS
080  RCL 15
081  *
082  RCL 28
083  2
084  *
085  RCL 14
086  SIN
087  *
088  +
089  1
090  ENTER
091  RCL 14
092  SIN
093  -
094  /
095  RCL 17
096  /
```

```
097  1/X
098  STO 21
099  RCL 28
100  RCL 20
101  *
102  STO 22
103  RCL 18
104  14.7
105  *
106  1/X
107  *
108  1
109  ENTER
110  RCL 21
111  RCL 22
112  *
113  -
114  /
115  STO 29
116  RCL 22
117  X <> Y
118  TAN
119  /
120  3200
121  X > Y?
122  X <> Y
123  STO 23
124  EPRIM =
125  ARCL X
126  AVIEW
127  STOP
128  23
129  RCL 08
130  X <= Y?
131  GTO 07
132  RCL 16
133  *
134  1
135  ENTER
136  RCL 06
137  SIN
138  -
139  X^2
140  /
141  STO 32
142  200
143  X > Y
144  GTO 07
145  X <> Y
146  -0.00121
147  *
148  e^X
```

```
149  1.05
150  *
151  .20
152  X <= Y?
153  X <> Y
154  STO 33
155  RCL 32
156  -0.00111
157  *
158  e^X
159  1.06
160  *
161  .22
162  X <= Y?
163  X <> Y
164  STO 34
165  LBL 06
166  RCL 18
167  299.32
168  X > Y?
169  X <> Y
170  RCL 00
171  *
172  RCL 01
173  /
174  .016214
175  *
176  CHS
177  RCL 28
178  RCL 20
179  *
180  .86732511
181  *
182  +
183  RCL 13
184  .433333
185  *
186  RCL 02
187  *
188  STO 25
189  1.2408463
190  *
191  +
192  RCL 10
193  RCL 09
194  *
195  RCL 01
196  2
197  /
198  3
199  Y^X
200  /
```

```
201  RCL 23
202  .00123
203  *
204  +
205  /
206  RCL 33
207  *
208  STO 24
209  DELY/D =
210  ARCL X
211  AVIEW
212  STOP
213  RCL 20
214  RCL 28
215  *
216  4.835
217  *
218  RCL 25
219  8.269
220  *
221  +
222  RCL 10
223  RCL 11
224  *
225  RCL 01
226  /
227  2
228  *
229  RCL 23
230  2
231  *
232  +
233  /
234  RCL 34
235  *
236  STO 26
237  EPLIN =
238  ARCL X
239  AVIEW
240  STOP
241  .0393
242  RCL 26
243  X > Y
244  XEQ 01
245  DESIGN COMPLETE
246  AVIEW
247  RTN
248  LBL 01
249  RCL 25
250  RCL 24
251  *
252  RCL 13
```

```
253  *
254  RCL 02
255  *
256  12
257  *
258  23.86
259  *
260  RCL 01
261  /
262  RCL 24
263  RCL 28
264  *
265  33.723
266  *
267  +
268  RCL 19
269  RCL 02
270  *
271  12
272  *
273  RCL 01
274  /
275  14.7
276  *
277  .1795
278  *
279  -
280  RCL 18
281  RCL 00
282  *
283  14.7
284  *
285  RCL 01
286  /
287  1.7999
288  *
289  -
290  RCL 10
291  RCL 09
292  *
293  RCL 01
294  2
295  /
296  RCL 12
297  *
298  /
299  RCL 01
300  X^2
301  RCL 23
302  *
303  4
304  /
```

```
305  RCL 12
306  /
307  .003
308  *
309  +
310  /
311  STO 27
312  EPHAT =
313  ARCL X
314  AVIEW
315  STOP
316  RCL 26
317  RCL 27
318  +
319  EPNONLIN =
320  ARCL X
321  AVIEW
322  PSE
323  RCL X
324  .0395
325  ENTER
326  5
327  *
328  X > Y?
329  GTO 04
330  STRAIN > 5 * EPY
331  AVIEW
332  PSE
333  SUGGEST NEW
334  AVIEW
335  PSE
336  DESIGN
337  AVIEW
338  PSE
339  LBL 04
340  RTN
341  LBL 03
342  AFTER LISTING
343  AVIEW
344  PSE
345  ENTER NEW VALUE
346  AVIEW
347  PSE
348  OR R/S IF NO
349  AVIEW
350  PSE
351  CHANGE
352  AVIEW
353  PSE
354  -1
355  STO 31
356  T =
```

```
357  ARCL 00
358  PROMPT
359  X > 0?
360  STO 00
361  RCL 31
362  D =
363  ARCL 01
364  PROMPT
365  X > 0?
366  STO 01
367  RCL 31
368  Z =
369  ARCL 02
370  PROMPT
371  X > 0?
372  STO 02
373  RCL 31
374  GAMAT =
375  ARCL 35
376  PROMPT
377  X > 0?
378  STO 35
379  RCL 31
380  RCL 31
381  Nb =
382  RCL 04
383  PROMPT
384  X > Y?
385  STO 04
386  RCL 31
387  Kb =
388  ARCL 05
389  PROMPT
390  X > 0?
391  STO 05
392  RCL 31
393  RCL 31
394  PHII =
395  ARCL 36
396  PROMPT
397  X > Y?
398  STO 36
399  RCL 31
400  RCL 31
401  NI =
402  ARCL 07
403  PROMPT
404  X > Y?
405  STO 07
406  RCL 31
407  KI =
408  ARCL 08
```

```
409  PROMPT
410  X > 0?
411  STO 08
412  RCL 31
413  PI =
414  ARCL 09
415  PROMPT
416  X > 0?
417  STO 09
418  RCL 31
419  PE1OY =
420  ARCL 10
421  PROMPT
422  X > 0?
423  STO 10
424  RCL 31
425  PZ =
426  ARCL 11
427  PROMPT
428  X > 0?
429  STO 11
430  RCL 31
431  PA =
432  ARCL 12
433  PROMPT
434  X > 0?
435  STO 12
436  RCL 31
437  RCL 31
438  P =
439  ARCL 13
440  PROMPT
441  X > Y?
442  STO 13
443  RCL 31
444  PHIb =
445  ARCL 37
446  PROMPT
447  X > 0?
448  STO 37
449  RCL 31
450  RCL 31
451  Cb =
452  ARCL 15
453  PROMPT
454  X > Y?
455  STO 15
456  RCL 31
457  RCL 31
458  CI =
459  ARCL 16
460  PROMPT
```

```
461  X > Y?
462  STO 16
463  RCL 31
464  RFb =
465  ARCL 17
466  PROMPT
467  X > 0?
468  STO 17
469  RCL 35
470  RCL 13
471  62.4
472  *
473  -
474  STO 03
475  RCL 36
476  .0174533
477  *
478  STO 06
479  RCL 37
480  .0174533
481  *
482  STO 14
483  RTN
484  LBL 07
485  1.0
486  STO 33
487  STO 34
488  GTO 06
489  END
```

LISTING OF INPUT PROGRAM DATIN

```
001  LBL DATIN
002  T IN. = ?
003  PROMPT
004  STO 00
005  D IN. = ?
006  PROMPT
007  STO 01
008  Z FT. = ?
009  PROMPT
010  STO 02
011  GAMAT PCF. = ?
012  PROMPT
013  STO 35
014  Nb = ?
015  PROMPT
016  STO 04
017  Kb = ?
018  PROMPT
019  STO 05
020  PHII DEG. = ?
021  PROMPT
022  STO 36
023  NI = ?
024  PROMPT
025  STO 07
026  KI = ?
027  PROMPT
028  STO 08
029  PI IN /IN = ?
030  PROMPT
031  STO 09
032  PE10Y PSI = ?
033  PROMPT
034  STO 10
035  PZ IN = ?
036  PROMPT
037  STO 11
038  PA IN /IN = ?
039  PROMPT
040  STO 12
041  P = ?
042  PROMPT
043  STO 13
044  PHIb DEG = ?
```

```
045  PROMPT
046  STO 37
047  C  PSI = ?
048  PROMPT
049  STO 15
050  CI PSI = ?
051  PROMPT
052  STO 16
053  RFb = ?
054  PROMPT
055  STO 17
056  RCL 35
057  RCL 13
058  62.4
059  *
060  -
061  STO 03
062  RCL 36
063  .0174533
064  *
065  STO 06
066  RCL 37
067  .0174533
068  *
069  STO 14
070  RTN
071  END
```

DEFINITION OF STORAGE REGISTERS

INPUT VARIABLES	REGISTER
TRENCH GEOMETRY	
Trench Width T (in.)	00
Pipe Diameter D (in.)	01
Depth of Cover to Springline Z (ft)	02
Fraction of Water Table Height p	13
IN SITU SOIL PROPERTIES	
Total Unit Weight γ_t (pcf)	35
Stiffness power n_i	07
Stiffness coefficient K_i	08
Angle of internal friction ϕ_i (deg)	36
Cohesion C_i (psi)	16
BACKFILL SOIL PROPERTIES	
Stiffness power n_b	04
Stiffness coefficient K_b	05
Angle of Internal friction ϕ_b	37
Cohesion C_b	15
Failure Ratio R_{fb}	17

INPUT VARIABLES	REGISTER
PIPE PROPERTIES	
Moment of Inertia of pipe wall PI (in^4/in)	09
Ten year Flexural Modulus PE10Y (psi)	10
Distance to the Centroid PZ (in.)	11
Pipe Wall unit area PA (in^2/in)	12
VARIABLES CALCULATED IN THE PROGRAM	
$\bar{E}_{ib}$ Initial Elastic Modulus of the Backfill	18
$\bar{E}_{ii}$ Initial Elastic Modulus of the In Situ Soil	19
Emperical pressure coefficient k_o	20
Average soil stress σ_b (psi)	22
Secant Modulus of the Backfill E'_A (psi)	23
Linear Pipe Wall strain ε_{lin} (in/in)	26
Post-yield strain $\hat{\varepsilon}$ (in/in)	27
Average effective unit weight γ'_t	03
Percent Change in Diameter ($\Delta Y/D$)	24

EXAMPLE PROBLEM

Input Variables

Trench Geometry

$T = 60$ in.

$D = 48$ in.

$Z = 18$ ft.

$p = 0.6$

In Situ Soil Properties

$\gamma_t = 125.96$ pcf

$n_i = 0.0$

$k_i = 53.76$

$\phi_i = 0.0$ deg.

$c_i = 16.67$ psi

Backfill Soil Properties

$n_b = 0.4$

$k_b = 600$

$\phi_b = 42$

$c_b = 0.0$

$R_{fb} = 0.7$

Pipe Properties

PI = .125 in^4/in

PE10Y = 29,000 psi

PZ = 0.52 in

PA = 0.492 in^2/in

DESIN PROGRAM OUTPUT

k_o = 1.8

E'_b = 3200.0 psi

$\Delta Y/D$ = 1.439%

ε_{lin} = .0075 in/in

APPENDIX D

VERIFICATION OF DESIGN EQUATIONS

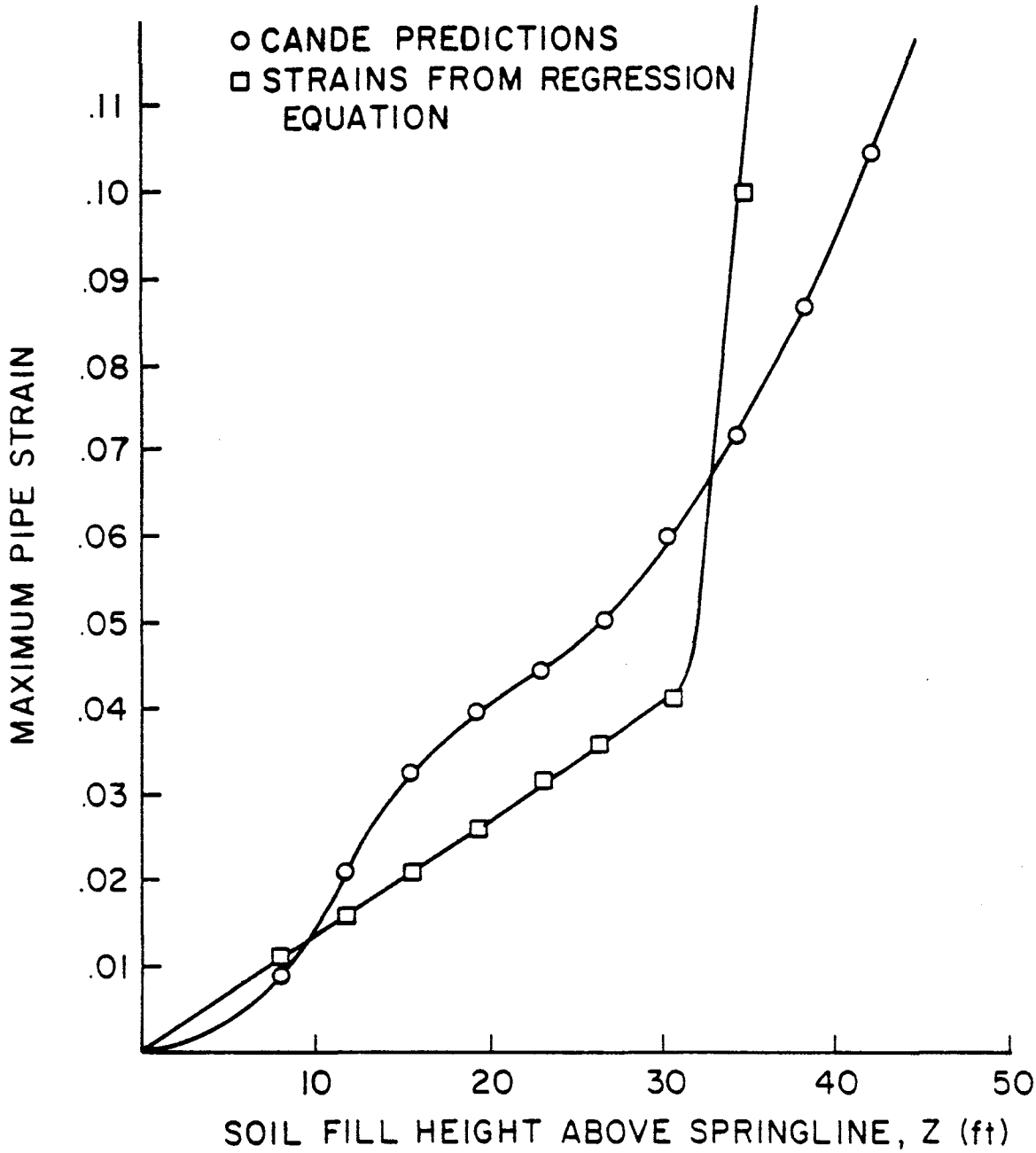

FIGURE D-1. Comparison of Regression Pipe Strain Equation
With CANDE Results
for a Standard Dry Factorial Run

(D=48, Profile #9, T=72, P=0, Weak Silt In-situ Soil)

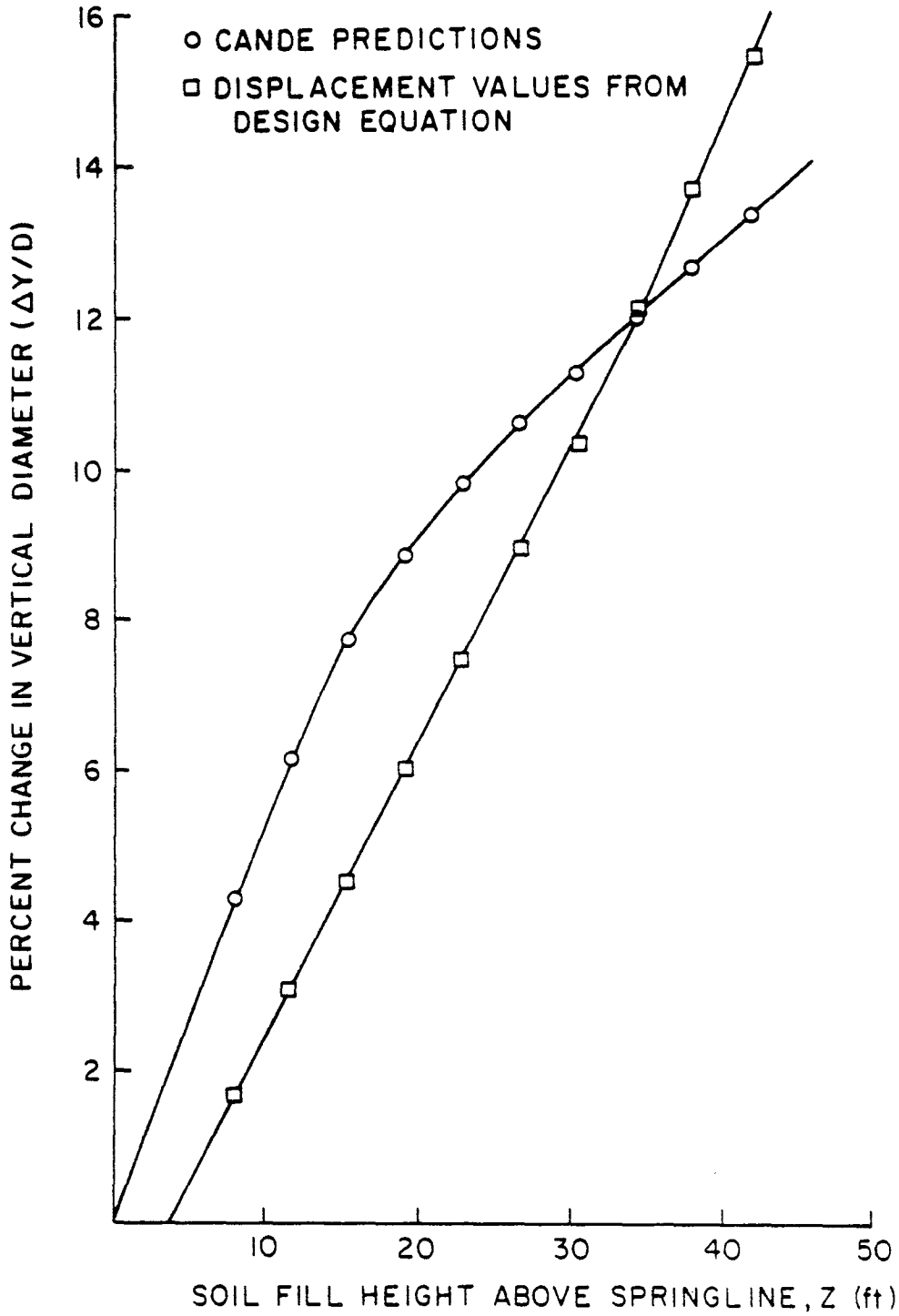

FIGURE D-2. Comparison of Regression Deflection Equation With CANDE Results for a Standard Dry Factorial Run

(D=48, Weak ML, Profile #9, T=72, P=0)

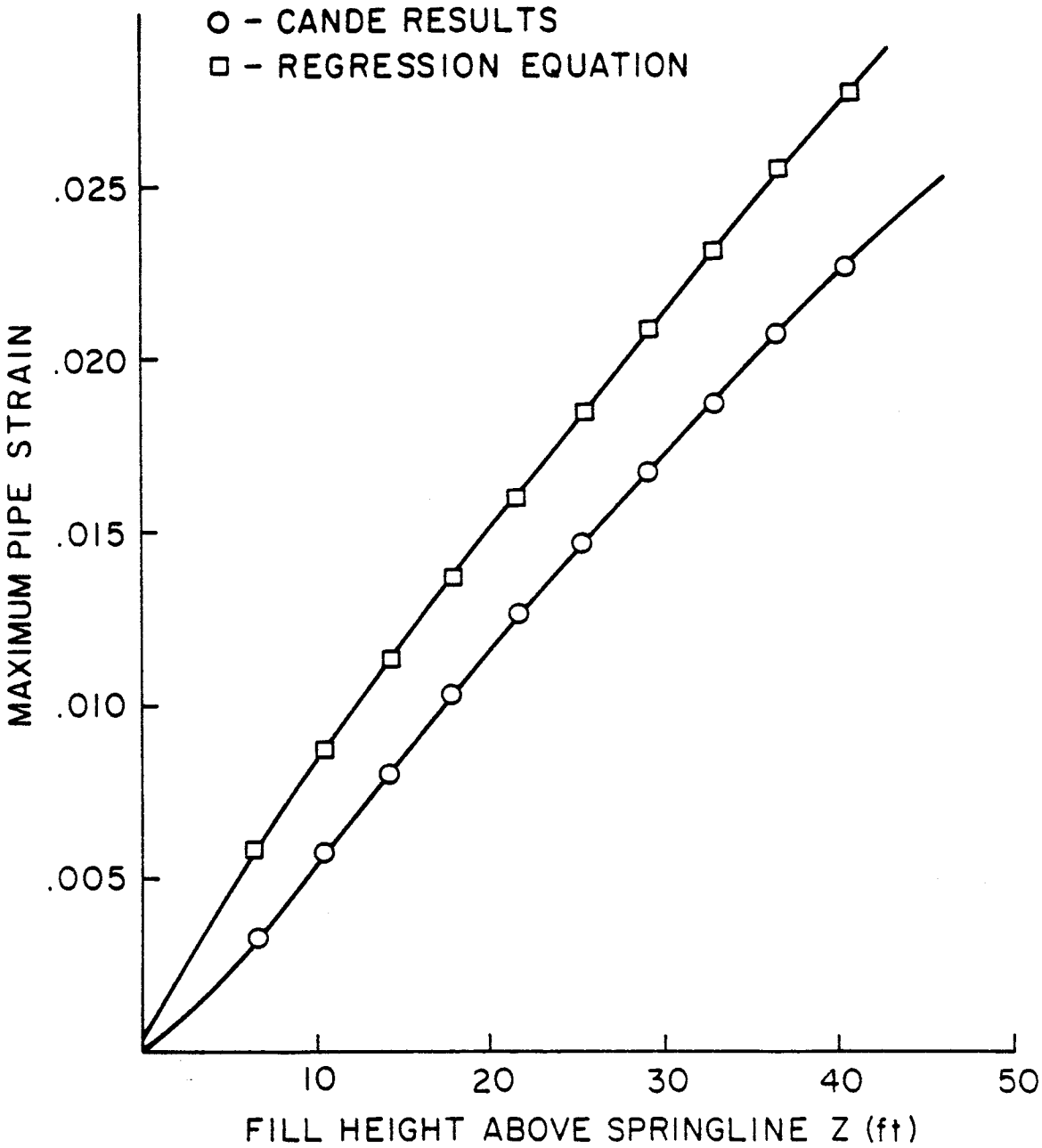

FIGURE D-3. Comparison of Regression Equation Strains
With CANDE Results
for an 18 in. #5 Profile Pipe

(T=27, P=0, Strong Silt In-situ Soil)

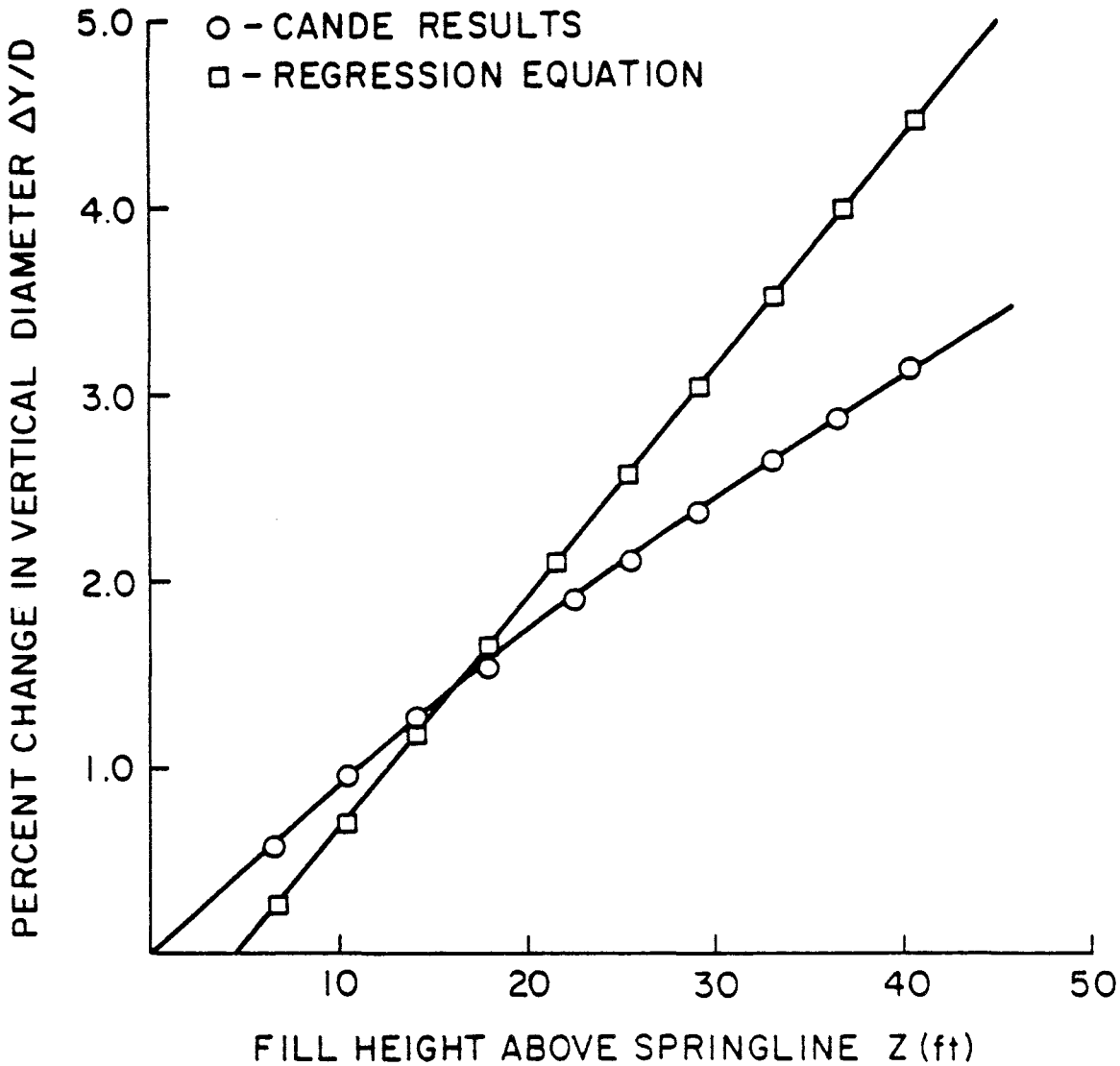

FIGURE D-4. Comparison of Regression Equation Deflections
With CANDE Results
for an 18 in. #5 Profile Pipe

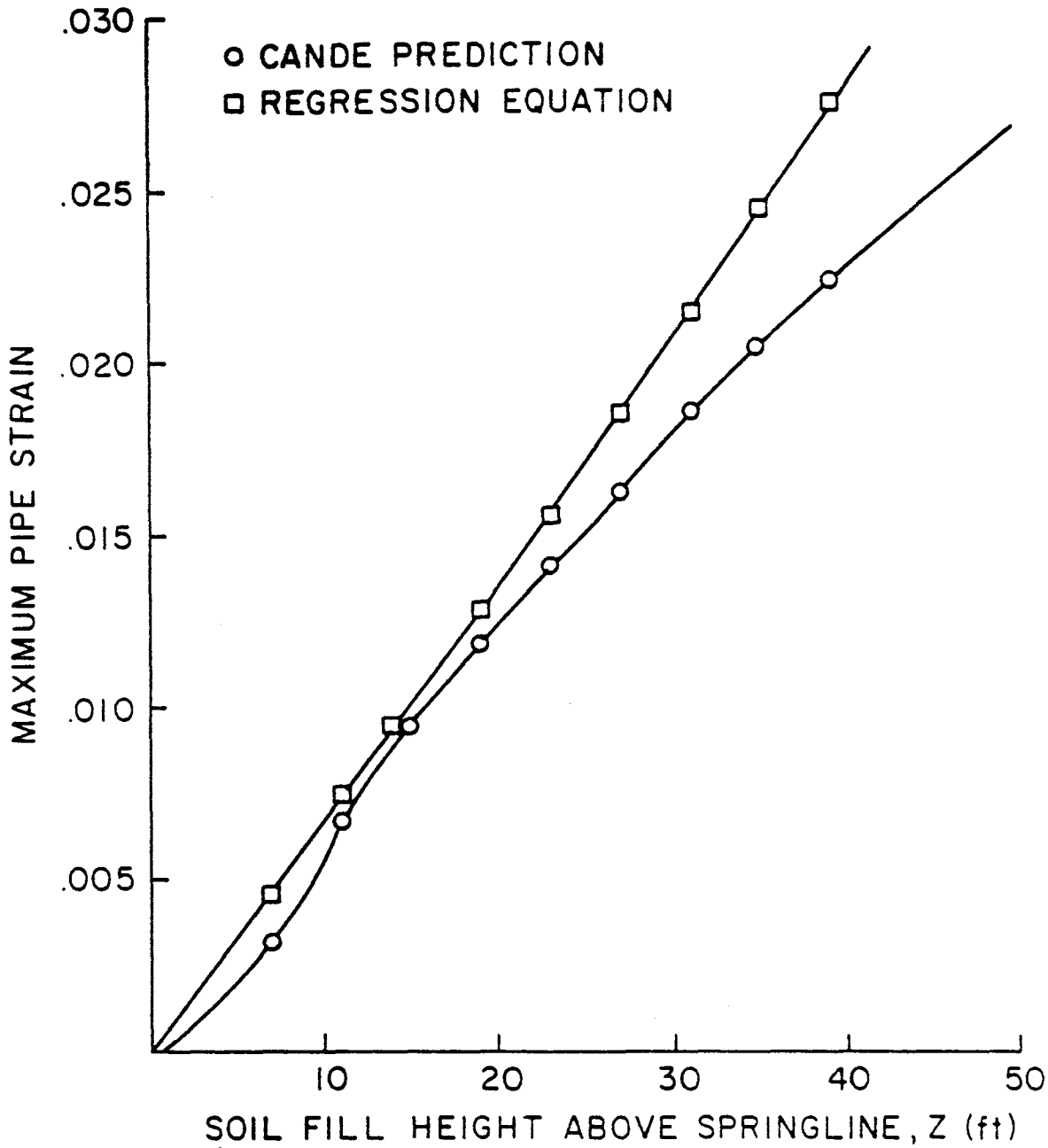

FIGURE D-5. Comparison of Regression Strain Equation
With CANDE Results
for a 42 in. #11 Profile Pipe

(T=63, P=0, Lean Clay In-situ Soil)

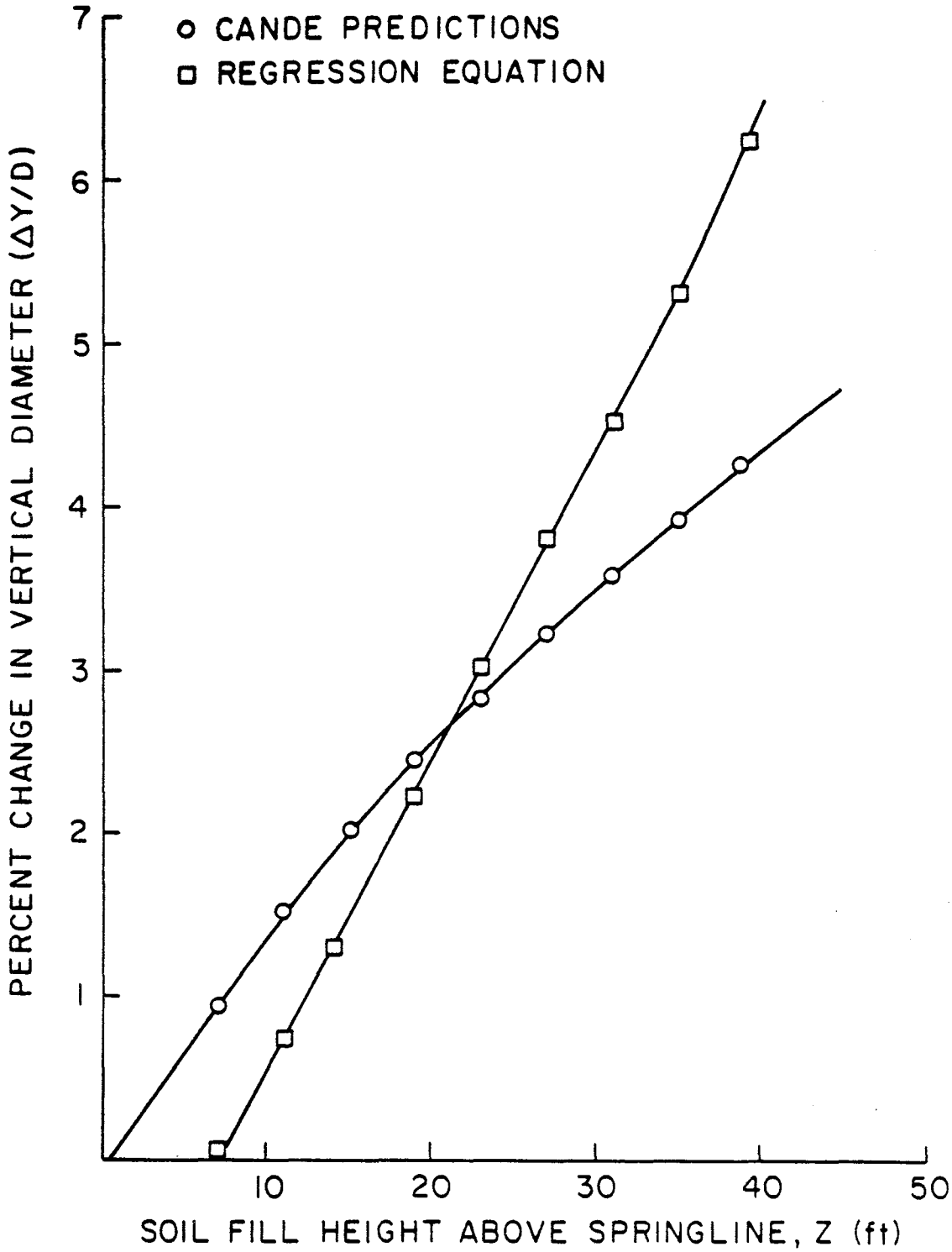

FIGURE D-6. Comparison of Regression Displacement Equation
With CANDE Results
for a 42 in. #11 Profile Pipe

(T=63, P=0, Lean Clay In-situ Soil)

APPENDIX E

CANDE MODIFICATIONS

LISTING OF MODIFIED SUBROUTINES

Changes made to the CANDE-1980 program include modifications to the main and EMOD subroutine and the addition of the new subroutine POLY. Additions to the two existing subroutines do not have card numbers.

ADDITIONAL INPUT GUIDE FOR CANDE

The input for using the nonsymmetric polyethylene pipe model follows the same form as the other pipe models given in the CANDE User Manual (29). The following input guide can be added to the existing user manual.

Profile Wall Polyethylene

Card 1B Pipe size and material properties

Columns (format)	Variable (units)	Entry Description
01-05 I5	NONLIN	= 2 for bilinear stress-strain law
06-15 F10.0	PE (in.)	Pipe Diameter, average
16-25 F10.0	PE (psi)	Elastic Youngs Modulus Default = 113,000 psi
26-35 F10.0	PNU	Poisson's ratio of pipe material Default = 0.3
36-45 F10.0	PYIELN (psi)	Yield stress of pipe material Default = 3600 psi
46-55 F10.0	PDEN (pci)	Density of pipe material Default = 0.0
56-65 F10.0	PE2 (psi)	Modulus of upper portion of the bilinear stress-strain curve. Default = 0.0

Card 2B Pipe Wall Properties

Columns (format)	Variable (units)	Entry Description
01-10 F10.0	PA (in^2/in)	Area of pipe wall section per unit length
11-20 F10.0	PI (in^4/in)	Moment of inertia of pipe wall section per unit length
21-30 F10.0	PS (in^3/in)	Section modulus of pipe wall per unit length
31-35 I5	FLAG	= 0 Spirolite cross section input = 0 General cross section
36-40 I5	ISYMM	= 1 Nonsymmetric analysis = 0 Symmetric half mesh analysis

Card 3B Spirolite Cross Section Input

Columns (format)	Variable (units)	Entry Description
01-10 F10.0	S (in.)	Pipe wall thickness
11-20 F10.0	P (in.)	Corrugation period
21-30 F10.0	HP (in.)	Total cross section height

Card 3B General Input

01-10 F10.0	H1 (in.)	Height to the top of Zone 1
11-20 F10.0	H2 (in.)	Height to the top of Zone 2
21-30 F10.0	H3 (in.)	Height to the top of Zone 3
31-40 F10.0	H (in.)	Total section height
41-50 F10.0	A1 (in^2/in)	Area per unit length of Zone 1
51-60 F10.0	A2 (in^2/in)	Area per unit length of Zone 2
61-70 F10.0	A3 (in^2/in)	Area per unit length of Zone 3
71-80 F10.0	A4 (in^2/in)	Area per unit length of Zone 4

APPENDIX F

TABLE OF PIPE PROPERTIES

	Class 40			Class 63			Class 100			Class 160		
I.D. (In.)	Profile Number	Allowable Crush Load (Lb./Ft.²)	Nominal Weight (Lb/Ft)	Profile Number	Allowable Crush Load (Lb./Ft.²)	Nominal Weight (Lb/Ft)	Profile Number	Allowable Crush Load (Lb./Ft.²)	Nominal Weight (Lb/Ft)	Profile Number	Allowable Crush Load (Lb./Ft.²)	Nominal Weight (Lb/Ft)
18							5	3188	10	7	4268	13
21				5	2789	11	6	3327	13	9	4680	18
24				5	2478	13	7	3319	17	9	4164	20
27	5	2230	14	6	2661	17	9	3751	23	11	4433	27
30	5	2027	16	7	2716	21	9	3412	25	12	4641	34
33	6	2217	21	9	3130	28	11	3700	33			
36	6	2046	23	9	2890	30	12	3935	40			
42	9	2507	35	11	2965	41				14	3931	56
48	9	2213	40	12	3018	53				14	3487	63
54	11	2272	53				14	3133	71	15	3777	87
60	12	2447	66				14	2845	79	16	3866	107
66				14	2605	87	15	3142	106	18	4011	132
72				14	2402	94	15	2899	116	20	4377	168
78				14	2229	102	16	3034	139	20	4066	182
84	14	2079	110	15	2510	134	18	3208	167			
90	14	1948	118	15	2352	144	20	3560	209			
96	14	1832	125	16	2497	170	20	3351	222			

*Minimum RSC = 90% of class designation

PIPE PROPERTIES

Profile Description		Basic Dimensions				Derived Properties*			
Shape	Profile Number	P (Period) (In.)	H (Wall Height) (In.)	S (Wall) (In.)	Ø (Core Dia.) (In.)	I (Wall Moment) ($In.^4/In.$)	S_e (Effective Wall) (In.)	A (Average Profile Area) ($In.^2/In.$)	$\bar{Z}$ (Centroid) (In.)
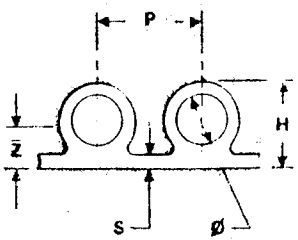	5	4.72	1.48	0.18	1.18	0.052	0.855	0.290	0.344
	6	3.15	1.48	0.18	1.18	0.070	0.944	0.346	0.409
	7	2.76	1.50	0.20	1.18	0.081	0.990	0.389	0.429
	9	3.15	1.61	0.24	1.18	0.125	1.145	0.492	0.520
	11	2.76	1.65	0.24	1.18	0.161	1.246	0.583	0.594
	12	2.76	1.73	0.28	1.18	0.202	1.343	0.674	0.640
	14	3.60	2.56	0.43	1.96	0.524	1.846	0.804	0.837
	15	3.50	2.71	0.47	1.96	0.728	2.060	0.974	0.963
	16	3.55	2.84	0.57	1.96	0.868	2.184	1.102	0.998
	18	3.55	2.99	0.72	1.96	1.014	2.300	1.253	1.019
	20	3.50	3.22	0.95	1.96	1.285	2.489	1.490	1.079

* These properties are based on the nominal dimensions presented. The effective wall is that which if the pipe had been made of solid wall would yield the same moment of inertia.

*Solid wall profiles in thicknesses from .18" up are available in all diameters.

PIPE PROPERTIES